Aus der Medizinische Klinik mit Schwerpunkt Kardiologie
der Medizinischen Fakultät Charité – Universitätsmedizin Berlin

DISSERTATION

Evaluation of mouse models of heart failure with preserved ejection fraction

zur Erlangung des akademischen Grades
Doctor medicinae (Dr. med.)

vorgelegt der Medizinischen Fakultät
Charité – Universitätsmedizin Berlin

von
Chao Ma
aus Zhengzhou, Henan, Volksrepublik China

Datum der Promotion: 4. Juni 2021

TABLE OF CONTENTS

ABBREVIATIONS

ABC	avidin-biotin complex
Acta1	actin alpha 1, skeletal muscle
AEC	3-Amino-9-Ethylcarbazole
Ang II	angiotensin II
AT1R	angiotensin II receptor type 1
BNP	B-type natriuretic peptide
BSA	bovine serum albumin
CCL	C-C Motif Chemokine Ligand
CD	cluster of differentiation
cDNA	complementary DNA
CO	cardiac output
Col1	collagen 1
Col3a1	collagen type III alpha 1 chain
CX3CL1	C-X3-C Motif Chemokine Ligand 1
DNA	deoxyribonucleic acid
DOCA	deoxycorticosterone acetate
dP/dt_{max}	maximum left ventricular pressure rise rate
dP/dt_{min}	maximum left ventricular pressure drop rate
EDTA	ethylenediaminetetraacetate
EF	ejection fraction
FEM	Forschungseinrichtungen für Experimentelle Medizin
GAPDH	glyceraldehyde 3-phosphate dehydrogenase
HF	heart failure
HFmrEF	heart failure with mid-range ejection fraction

HFpEF	heart failure with preserved ejection fraction
HFrEF	heart failure with reduced ejection fraction
IL	Interleukin
LA	left atrium
LAGeSo	Landesamt für Gesundheit und Soziales Berlin
LV	left ventricle / left ventricular
LVEDP	left ventricular end-diastolic pressure
LVEDV	left ventricular end-diastolic volume
LVEF	left ventricular ejection fraction
LVESV	left ventricular end-systolic volume
Ly6g	lymphocyte antigen 6 complex locus G6D
mRNA	message RNA
Myh7b	myosin heavy chain 7B
NaCl	sodium chloride
NOX2	nicotinamide adenine dinucleotide phosphate oxidase-2
NT-proBNP	N-terminal pro B-type natriuretic peptide
PBS	phosphate-buffered saline
PCR	polymerase chain reaction
PH	pulmonary hypertension
PHT	pressure half time
RAGE	receptor for advanced glycation end products
RAS	renin-angiotensin system
RAAS	renin–angiotensin–aldosterone system
RNA	ribonucleic acid
RV	right ventricle
RWT	relative wall thickness

s.c.	subcutaneous
S100A8	S100 calcium-binding protein A8
S100A9	S100 calcium-binding protein A9
SEM	standard error of the mean
SHR	spontaneously hypertensive rat
SPRINT	Systolic Blood Pressure Intervention Trial
SV	stroke volume
TBS	tris-buffered saline
TG	transgenic
TGF-β	transforming growth factor beta
TLR4	toll-like receptor 4
TNF-α	tumor-necrosis factor-α
VEGF	vascular endothelial growth factor
α-SMA	alpha-smooth muscle actin
τ	time of the left ventricular pressure decrease

ABSTRAKT

Hintergrund: Herzinsuffizienz mit konservierter Ejektionsfraktion (HFpEF) ist ein wichtiger Bestandteil der Herzinsuffizienz (HF). Patienten mit HFpEF weisen eine signifikante Morbidität und Mortalität auf, aber im Gegensatz zu Herzinsuffizienz mit verringerter Ejektionsfraktion (HFrEF) gibt es derzeit keine wirksamen, validierten Therapien. Die Wiederholung der klinischen Merkmale im Mausmodell kann uns dabei helfen, die dem HFpEF zugrunde liegenden Mechanismen besser zu verstehen. Angiotensin II (Ang II) -infundierte Mäuse werden als ein besseres Mittel zur Replikation des humanen HFpEF-Phänotyps angesehen. Drei veröffentlichte Studien mit unterschiedlicher Ang II-Dosis und -Dauer gaben an, dass sie eine diastolische Dysfunktion auslösen könnten. In der vorliegenden Studie wiederholten wir die Ang II-Dosis und -Dauer der obigen drei Studien und suchten nach einer, die dem HFpEF-Phänotyp nahe kommt.

Methoden: C57BL6 / j-Mäuse (Charles River, männlich, 8 Wochen alte Mäuse) wurden zufällig der Kontrolle 1,1 mg / kg 14d, Ang II 1,1 mg / kg 14d, Kontrolle 1,5 mg / kg 14d, Ang II 1,5 mg / kg 14d, Kontrolle 0,2 mg / kg 28d und Ang II 0,2 mg / kg 28d. Angiotensin II (1,1 mg / kg oder 1,5 mg / kg oder 0,2 mg / kg) wurde an 14 oder 28 aufeinanderfolgenden Tagen angewendet (Dosis und Dauer hielten sich an die Gruppennamen). An den Endpunkten der Mäuse wurde eine hämodynamische Untersuchung durchgeführt. Dann wurden die linken Ventrikel (LVs) für die folgenden molekularen und immunhistochemischen Untersuchungen entnommen.

Ergebnisse: An den Endpunkten von Mäusen wiesen die hämodynamischen Parameter darauf hin, dass alle Gruppen die normale linksventrikuläre Auswurffraktion (LVEF) aufwiesen und die globale Herzfunktion nur wenig veränderten. Im systolischen Funktionsteil, nahm der dP / dt_{max} ($P = 0,0183$) der Ang II 1,1 mg / kg 14d-Mäuse ab, während sich andere Ang II-Mäuse wenig änderten. Im Vergleich der diastolischen Funktion war der dP / dt_{min} von Ang II 1,1 mg / kg 14d-Mäusen signifikant niedriger, der Rest von Ang II-Mäusen veränderte sich geringfügig, ohne signifikant zu sein. Die Fibrosemessungen zeigten, dass die Ang II 1,1 mg / kg 14d-Mäuse eine ausgeprägtere Fibrose erhielten. Beziehen Sie sich auf die Expression von Myh7b und Acta1, es ist wahrscheinlicher, dass bei Ang II 1,1 mg / kg 14d eine Hypertrophie auftritt als bei den übrigen Ang II-Mäusen. Die Expressionsänderungen der Zytokine und des S100A8 /

A9-Signalwegs zeigten, dass Ang II 1,1 mg / kg 14d-Mäuse eine stärkere Entzündung aufwiesen, was auch durch immunhistochemische Hinweise bestätigt wurde.

Schlussfolgerungen: Die vorliegende Studie zeigte, dass Ang II 1,1 mg / kg 14d-Mäuse Eigenschaften aufweisen könnten, die dem HFpEF-Prototyp unter drei Gruppen von Mäusen mit unterschiedlichen Ang II-Dosen und -Dauern am nächsten kommen. Die Ermittlung eines idealen HFpEF-Modells und des dahinter stehenden Mechanismus bedarf jedoch noch weiterer Untersuchungen.

Background: The prevalence of heart failure with preserved ejection fraction (EF) (HFpEF), also referred to as diastolic heart failure, continues to increase in the developed world. Up to now, there are no effective, validated therapies improving survival in patients with HFpEF, indicating the need to further understand its underlying pathomechanisms. Since HFpEF is a syndrome involving different organs, mouse models can help us to better understand the mechanisms underlying HFpEF. The present research was conducted to verify which of three previously published Ang II regimens shown to induce diastolic dysfunction in mice better leads to an HFpEF phenotype.

Methods: C57BL6/j mice (Charles River, male, 8-week-old mice) were randomly assigned to control 1.1mg/kg 14d, Ang II 1.1mg/kg 14d, control 1.5mg/kg 14d, Ang II 1.5mg/kg 14d, control 0.2mg/kg 28d, and Ang II 0.2mg/kg 28d groups. During 14 or 28 consecutive days, Ang II was applied at the indicated dose via subcutaneous injection. At the day of sacrifice, hemodynamic measurements were performed to characterize left ventricular (LV) function followed by harvesting of the LVs for subsequent molecular and immunohistochemical analysis.

Results: All the Ang II groups displayed a preserved LVEF at the day of sacrifice. This was accompanied by a decreased dP/dt_{max} in the Ang II 1.1mg/kg 14d group, while the other Ang II groups remained unchanged. In addition, diastolic function, as indicated by dP/dt_{min}, was only reduced in Ang II 1.1mg/kg 14d mice compared to the corresponding controls. These changes in cardiac function in the Ang II 1.1 mg/kg 14d group were further paralleled by an increase of myocardial collagen I protein expression. Interestingly, angiogenesis was more pronounced in 1.1 mg/kg 14d Ang II versus controls, as indicated by higher density of arterioles and arteries in these mice. LV gene expression analysis of the alarmin S100A8/A9 pathway suggested an ongoing inflammation in these animals, which was confirmed by higher numbers of $CD4^+$ and $Ly6G^+$ cells in the heart of 1.1 mg/kg 14d Ang II mice compared to controls.

Conclusions: The present study demonstrated that among the 3 tested Ang II administration schemes, application of 1.1 mg/kg Ang II for 14 days was most likely to mimic the HFpEF phenotype.

1. Introduction

Heart failure (HF) is defined as a condition by which the heart cannot pump enough blood to maintain blood flow to meet the body's needs. HF is a common, expensive, potentially fatal disorder(1). In 2015, it affected about 40 million people worldwide(2). Currently, there are 5.8 million people with HF in the United States, and 550,000 new cases are diagnosed each year. The forecast is worrying because more than 8 million people are expected to develop the disease by 2030, with a 46% increase in prevalence(3). The overall prevalence rate is similar in both sexes(4). In the past, HF with reduced ejection fraction (EF) (HFrEF) was the most commonly diagnosed clinical entity in HF patients. However, with the advancement of technology, the upgrading of diagnostic equipment, especially the popularity of echocardiography, HF has recently been divided into three subtypes, namely HFrEF, HF with preserved ejection fraction (HFpEF) and heart failure with mid-range ejection fraction (HFmrEF)(5).

1.1. Epidemiology of HFpEF

HFpEF may play a leading role in driving overall HF prevalence, as the proportion of patients with HFpEF has increased over the past 20 years, whereas the proportion of patients with HFrEF has been relatively stable or even decreasing(6). It was, therefore estimated that by 2020, approximately 65% of hospitalized HF patients would be HFpEF patients(7). HFpEF is the most common form of HF in patients over 65 years of age; >80% of new HF cases in older women are HFpEF(8). Current data show that the long-term prognosis of HFrEF and HFpEF cases is still poor, especially for HFpEF, which has an increased incidence and lack of effective treatment(9).

Also, HFpEF is poorly investigated, which badly needs further exploration. To better understand the mechanisms underlying this disorder and helping scientists to explore future therapies, an optimized mouse model mimicking the clinical features of the most common form of HFpEF is particularly essential(10).

1.2. The pathophysiology of HFpEF

1.2.1. Left ventricle structure and remodeling

The structural remodeling that often occurs in HFpEF differs dramatically from that in HFrEF. A typical HFpEF phenotype is described as concentric left ventricular remodeling with normal chamber size(11). However, a number of patients with

unequivocal hemodynamic evidence of HF do not have structural remodeling of the heart but even have normal left ventricle (LV) geometry(12, 13). So the absence of structural heart disease does not exclude the diagnosis of HFpEF. Many, but not all, patients with HFpEF exhibit a concentric pattern of LV remodeling and a hypertrophic process that is characterized by the following features(14-16). 1) A normal or near-normal end-diastolic volume. 2) Increased wall thickness and/or LV mass. 3) An increased ratio of myocardial mass to cavity volume. 4) An increased relative wall thickness (RWT). The RWT is defined as either 2 X (posterior wall thickness)/(LV diastolic diameter) or as (septal wall thickness + posterior wall thickness)/(LV diastolic diameter). At the structural level, myocardial cells in HFpEF are more collagen-rich than the control population, and cardiomyocytes in HFpEF are thicker and less elongated than HFrEF(17). By comparison, patients with HFrEF typically exhibit a pattern of eccentric remodeling with an increase in end-diastolic volume, an increase in LV mass but little increase in wall thickness, and a substantial decrease in the ratio of mass to volume and thickness to radius(18).

1.2.2. Left ventricle diastolic limitations

Diastolic dysfunction is defined as the incompetency to fill the ventricle to an sufficient preload volume at an acceptable low pressure(19). Diastolic dysfunction and HFpEF are not synonymous terms(20). Diastolic dysfunction refers to the unusual mechanical properties of the ventricles. It manifests in dysfunction of diastolic relaxation, filling, or distensibility of the LV. HFpEF denotes the signs and symptoms of clinical HF in a patient with a normal LVEF and LV diastolic dysfunction. Diastolic dysfunction alone is essentially part of normal human aging and is seen in many people that do not or never will have HFpEF. However, the presence of diastolic dysfunction is a risk factor for developing HFpEF(21).

Delayed relaxation is one part of the "trouble" of the early diastolic phase of HFpEF. Healthy people have a "vacuum cleaner" effect in the LV, and prevent left atrium (LA) hypertension by increasing the suction of the LV(22). Studies have shown that the "vacuum cleaner" function of the LV in patients with HFpEF is lost, especially when the heart rate is elevated. The filling of the LV can only rely on the high pressure of the LA(22, 23).

Ventricular passive diastolic stiffness is also an essential determinant of the increase in LV filling pressures in HFpEF(24). Most, but not all, studies have shown that, on average, LV end-diastolic stiffness is increased in patients with HFpEF(16, 24). In the absence of endocardial or pericardial disease, diastolic LV dysfunction is caused by an increase in myocardial stiffness, and the increase in myocardial stiffness depends primarily on the characteristics of the cellular and extracellular structural proteins(18). According to previous studies, the increase in myocardial passive stiffness is primarily due to the deposition of extracellular collagen (fibrosis). However, there is accumulating evidence that myocardial passive stiffness can occur in the absence of cardiac fibrosis, i.e., due to differences in titin regulation. Elevated myocardial passive stiffness is also associated with changes in the giant cytoskeletal protein titin(25). Increased passive stiffness of cardiomyocytes has been reported to be particularly pronounced in patients with HFpEF as well as in patients with aortic stenosis and diabetes(26).

In ventricular tissue, fibrosis serves to impose a viscoelastic burden that compromises all of diastole, including the rate of relaxation, diastolic suction, and passive stiffness(27). Cardiac fibrosis in HFpEF is associated with impaired coronary microvascular density(28). Endothelial dysfunction can trigger cardiac fibrosis by different means(28). Primarily, NO deprivation, oxidative stress, inflammation, and age, all factors associated with endothelial dysfunction, trigger the endothelial-to-mesenchymal transition, a process by which endothelial cells transdifferentiate into fibroblasts and hereby contribute to cardiac fibrosis and diastolic dysfunction(28). Cardiac fibrosis and cardiomyocyte stiffness contribute to impaired diastolic and systolic mechanics, leading to increased LV stiffness and filling pressures, which can trigger, in a vicious circle, subendocardial ischemia, endothelial activation, and dysfunction(28) (**Figure 1**).

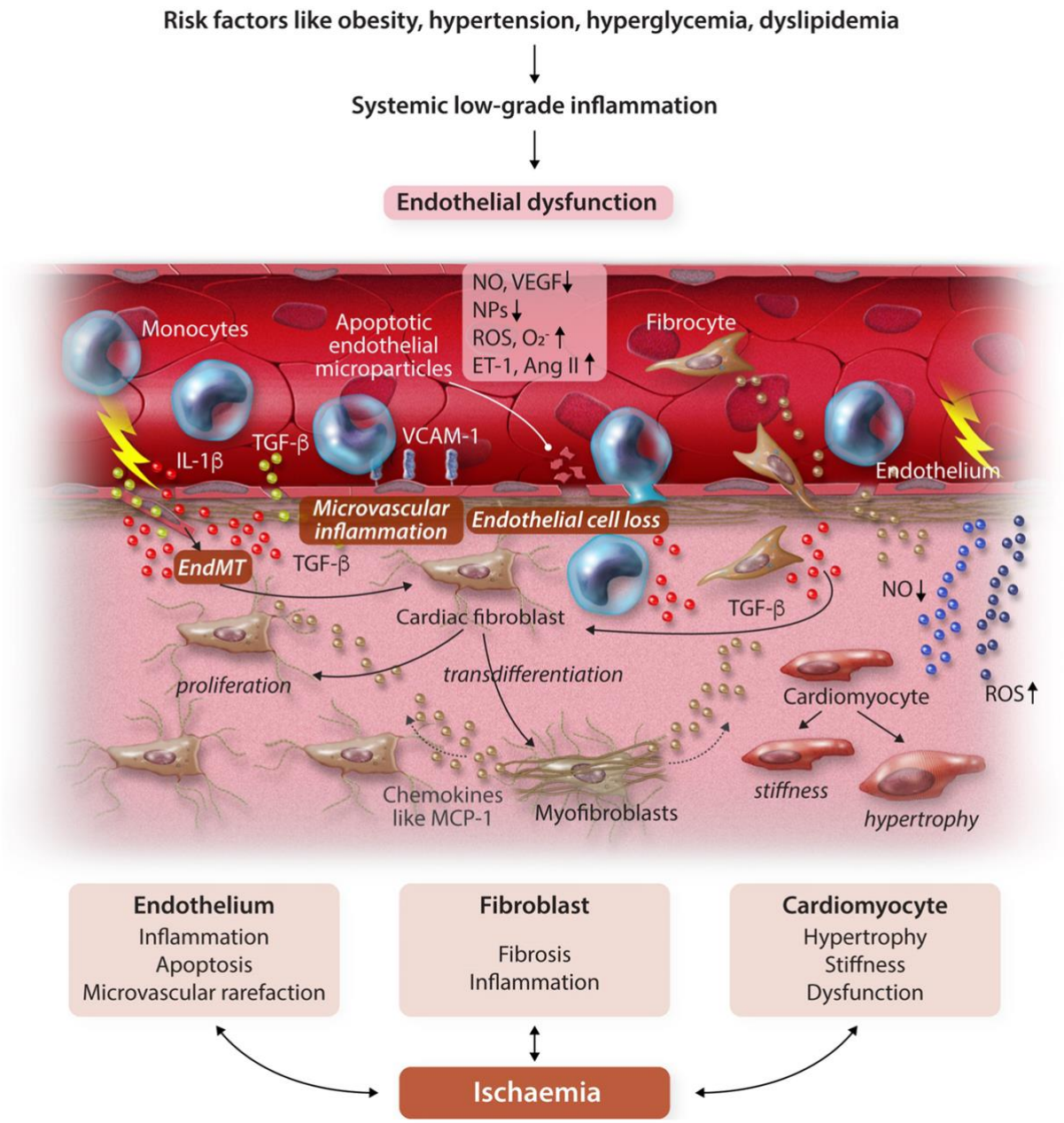

Figure 1. Endothelial dysfunction provokes cardiomyocyte stiffness/hypertrophy in the presence or absence of cardiac fibrosis. A systemic low-grade inflammatory status due to HFpEF-associated comorbidities (obesity, hypertension, hyperglycemia, and dyslipidemia) provokes endothelial dysfunction. Endothelial dysfunction is associated with microvascular inflammation, EndMT, and endothelial cell loss with release of apoptotic endothelial microparticles and promotes subendocardial ischemia. Endothelial dysfunction-associated deprivation of NO and natriuretic peptides and increase in oxidative stress (raise in reactive oxygen species, superoxide, ET-1, and Ang II) further contribute to cardiac fibrosis via stimulating proliferation and transdifferentiation of resident cardiac fibroblasts, activating EndMT, and facilitating the adhesion and transendothelial migration of inflammatory cells, including circulating fibrocytes, which trigger cardiac fibrosis via the release of TGF-ß. (Myo)fibroblasts on their turn activate the inflammatory process among others by the release of chemokines such as MCP-1. NO deprivation and oxidative stress boost cardiomyocyte stiffness and hypertrophy. Cardiac fibrosis and cardiomyocyte hypertrophy and stiffness on their turn trigger subendocardial ischemia, leading to a vicious circle. Ang II, angiotensin II; EndMT, endothelial-to-mesenchymal transition; ET-1, endothelin-1; IL, interleukin; MCP-1, monocyte chemoattractant protein-1; NO, nitric oxide; NPs, natriuretic peptides; O−2, superoxide; ROS, reactive oxygen species; TGF-ß, transforming growth factor-ß; TNF-α, tumor necrosis factor-α; VCAM-1, vascular cell adhesion molecule-1; VEGF, vascular endothelial growth factor. **Reproduced with permission from Oxford University Press.**

At rest, only two-thirds of HFpEF population can be recognized as diastolic dysfunction by echocardiography(13). Many patients with HFpEF in the early stages do not exhibit an increase in LV filling pressure at rest(29). In addition, these early HFpEF patients typically have normal B-type natriuretic peptide (BNP) plasma levels, which leads clinicians to make a diagnosis without HF(29). Besides, the level of BNP observed in patients with HFpEF is sometimes lower than usual, and studies suggest that this may be associated with obesity(30). Although studies haven't shown that diastolic dysfunction in HFpEF can impair net LV filling at the compensated stage, this semblance of peace is at the expense of abnormal LA and LV pressure elevation(18, 31, 32). Increased LA pressures can lead to dyspnoea, secondary pulmonary hypertension (PH), and atrial remodeling, which may make patients prone to right ventricular dysfunction and atrial fibrillation. A prospective trial showed that lowering LV filling pressure in HFpEF significantly reduced HF hospitalization(33). These further demonstrate that the significance of diastolic dysfunction in HFpEF should not be underestimated.

The most conspicuous and commonly present abnormalities in patients with HFpEF are related to diastolic dysfunction. This may present with impairments in relaxation, increases in chamber stiffness, or both. These abnormalities lead to an increase in LV filling pressures at rest or during exercise that causes dyspnea(15, 17).

1.2.3. Left ventricle systolic limitations

In clinical practice, EF is often used to assess systolic function, but it is better suited to value the ventricular–arterial coupling(19, 34). By definition, the LVEF and most indices of contractile function are normal or nearly normal in patients with HFpEF. However, EF is a poor and nonspecific index of contractile function. Interestingly, normal contractility can present a lower EF at the presence of very high afterload. Weak contractility can even offer a normal EF at the presence of low afterload. Therefore, we cannot simply equate the contractility and EF. Studies have shown that the systolic function of patients with HFpEF can also show subtle abnormalities(35). This finding of impaired systolic function has been confirmed in numerous studies utilizing tissue Doppler and strain imaging techniques(14, 36).

Abnormalities in LV systolic properties are strongly associated with adverse outcome in patients with HFpEF(12, 37). Inability to augment systolic function also begets and

worsens diastolic reserve in HFpEF(38). These relatively mild abnormalities in systolic function at rest become much more significant limitations during exercise, which further burden an already impaired heart. Prior studies have shown that the inability to augment cardiac output (CO) during exercise is related mainly to poor systolic reserve, where a contractile function cannot be supplemented during stress in a usual fashion. This limits the ability to augment forward stroke volume and reduces cardiac output and end-organ perfusion(31, 38).

1.3. Diagnosis of HFpEF

HFpEF is a clinical syndrome in which patients have symptoms and signs of HF, a normal or near-normal LVEF (LVEF ≥50 percent), and evidence of cardiac dysfunction as a cause of symptoms (e.g., Abnormal LV filling and elevated filling pressures). Major society HF guidelines reflect reasonable consensus on minimum criteria for the diagnosis of HFpEF, while acknowledging diagnostic challenges(5, 39).

Echocardiography is readily available in clinical practice and provides high-resolution information on cardiac anatomy and is often considered one of the most useful tests in the diagnosis of HFpEF(40). Diastolic dysfunction is a hallmark of HFpEF. The key echocardiographic measure for assessing diastolic dysfunction is E/e'. E represents the peak velocity of the transmission flow in the early diastole, and e' represents either the early diastolic septal or lateral lengthening peak velocity of the mitral annulus(40). To date, elevated E/e' (reflecting a filling pressure > 15 mmHg) has been included in the guidelines as sufficient evidence of diastolic dysfunction. In clinical practice, diastolic function can be affected by heart rate and cardiac load. Furthermore, some people have questioned the utility of E/e' because it is not sensitive enough and missed diagnosis. Therefore, the sole use of echocardiography for assessing diastolic dysfunction is questioned(40).

BNP is mainly produced by the ventricular myocardium, and its release is stimulated by ventricular wall stress. Therefore, elevated plasma levels of BNP directly reflect myocardial stretch. High BNP or N-terminal pro b-type natriuretic peptide (NT-proBNP) levels have been shown to correlate with the severity of high filling and diastolic dysfunction and are strong predictors of outcome(41). Although NT-proBNP levels are lower in HFpEF than HFrEF, it is generally considered to be of value in routine diagnostic examination of patients with an EF retention. NT-proBNP is less specific, and

its level is also affected by tachycardia, myocardial ischemia, atrial fibrillation, renal insufficiency, and obesity(40). Reduced NT-proBNP does not rule out HFpEF diagnosis, and elevated NT-proBNP does not necessarily predict diastolic dysfunction. Combination of NT-proBNP levels with other clinical manifestations of diastolic dysfunction is therefore recommended(40).

Currently, the gold standard for the diagnosis of HFpEF is right cardiac catheterization(42). If the resting intracardiac pressure is normal, an invasive exercise test is performed. Due to its invasiveness, high complexity and cost, it is impractical to perform this test routineously(42). But it can be used as a backup option for patients who have used non-invasive techniques, but whose diagnosis is still unclear or suspected. Therefore, how to use the non-invasive technology to diagnose HFpEF quickly, and accurately has always been the direction of future efforts(42).

Different algorithms have been proposed to diagnose HFpEF. The latest algorithm proposed by Pieske and colleagues(43, 44) from the Heart Failure Association (HFA) of the European Society of Cardiology (ESC) represents an accurate and straightforward algorithm to diagnose HFpEF. This algorithm includes four steps: step P, step E, step F1, and step F2. As shown in **Figure 2**: 1) Step P is meant to identify patients with the potential diagnosis of HFpEF and exclude or identify other specific causes for their HF-like symptoms; 2) The second step E should be done If step P is positive, which includes comprehensive echocardiography and brain natriuretic peptide/N-terminal natriuretic peptide levels; 3) Step F1 should be done if step E is inconclusive. An invasive or non-invasive stress test is recommended; 4) Step F2 is designed to identify a specific etiology, if appropriate when HFpEF has been diagnosed. For the very important step E of this algorithm, which is shown in **Figure 3**, simply and intuitively displays how the scoring system works.

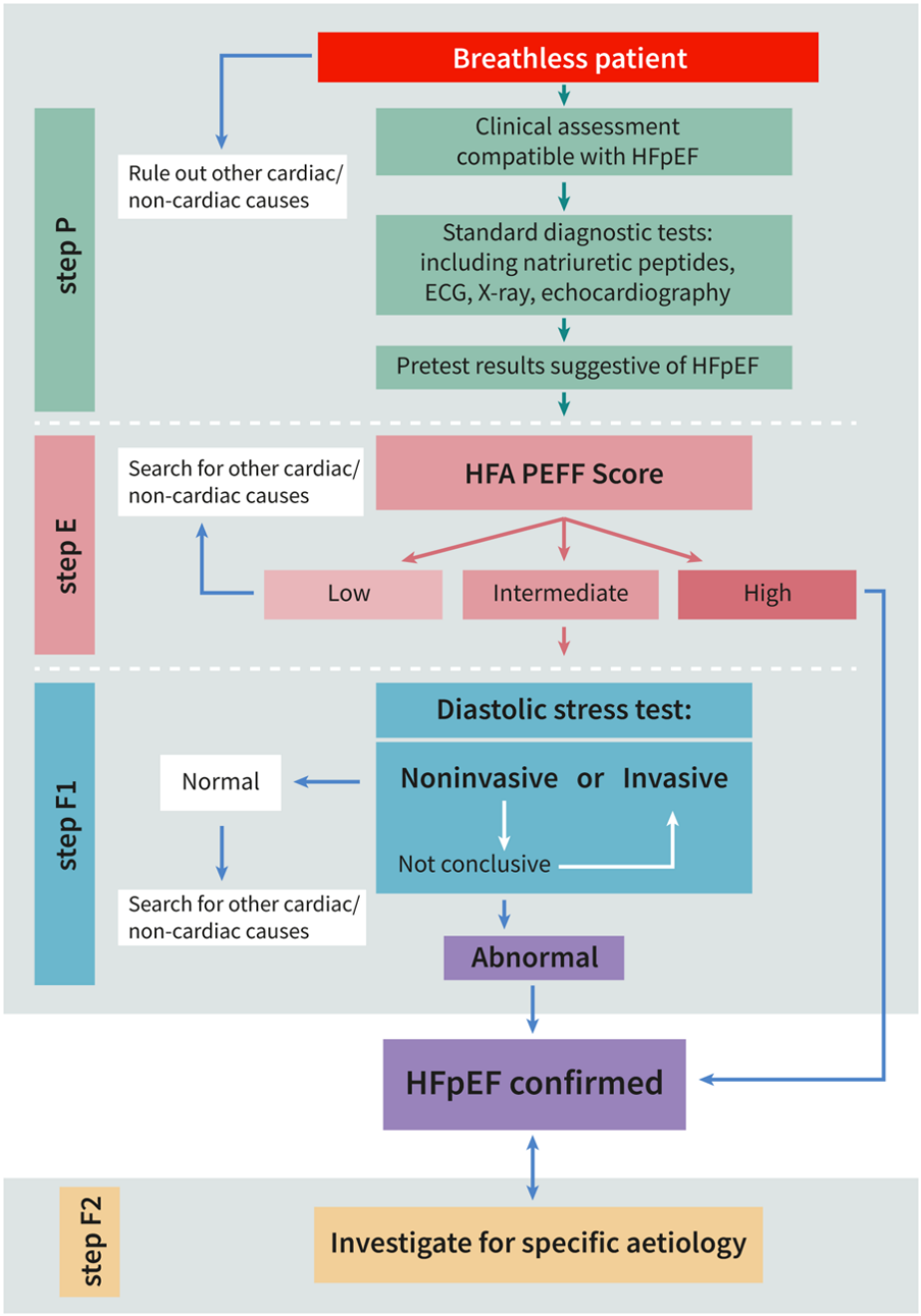

Figure 2. Flowchart of the HFA-PEFF diagnostic algorithm (proposed by Pieske)(43, 44). Step P is meant to identify patients with the potential diagnosis of heart failure with preserved ejection fraction, and exclude or identify other specific causes for their heart failure-like symptoms. Patients likely to have heart failure with preserved ejection fraction are those with typical demographics (e.g. elderly, female, and comorbidities), a preserved left ventricular ejection fraction on a standard echocardiography, and other easily detectable findings such as elevated natriuretic peptides or atrial fibrillation. Alternative causes such as coronary artery disease, significant valvular disease, pulmonary disease, and anemia should be excluded during this initial workup. If Step P is positive, the second Step E should be done, which includes a comprehensive echocardiography and brain natriuretic peptide/N-terminal natriuretic peptide levels, if not already done on Step P. Step F1 should be done, if Step E is inconclusive. Depended on clinical facilities and patient conditions an invasive or non-invasive stress test is recommended. However, the invasive stress test has a higher validity and is an option if the result of the non-invasive stress test is not conclusive. The fourth Step, Step F2 is designed to identify a specific etiology, if appropriate, when heart failure with preserved ejection fraction has been diagnosed. **Reproduced with permission from Oxford University Press.**

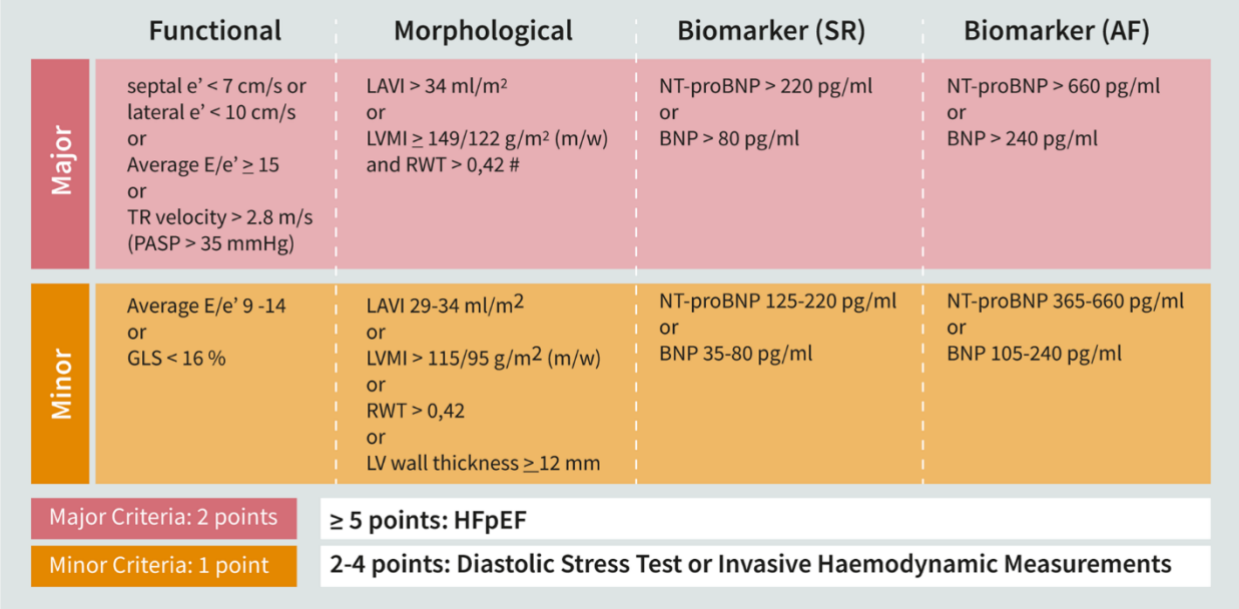

Figure 3. Scoring system for heart failure with preserved ejection fraction considering functional, morphological parameters and biomarkers with distinction of biomarker levels by sinus rhythm (SR) and atrial fibrillation (AF). (Step E of diagnostic algorithm proposed by Pieske)(43, 44). Reproduced with permission from Oxford University Press.

Currently, the use of a single diagnosis algorithm to diagnose HFpEF still has limitations(43). Future research directions should be evaluated and optimized on the existing algorithms(43). Modern imaging methods can store a large amount of high-quality and retrospective imaging data. The combination of imaging data, traditional risk factors, new biomarkers, comprehensive demographic data, proteomics, metabolomics, and genomic data can bring substantial potential driving force for the optimization of the future HFpEF diagnosis algorithm(45-47).

1.4. Treatment and prognosis of HFpEF

To date, clinical trials in HFpEF have produced neutral results, and treatment is primarily directed toward associated conditions and symptoms. Two strong recommendations are: 1) Systolic and diastolic hypertension should be controlled following published clinical practice guidelines to prevent morbidity; 2) Diuretics should be used to relieve symptoms due to volume overload. Similar recommendations were included in the 2013 American College of Cardiology Foundation/American Heart Association (ACC/AHA) HF guidelines and the 2016 European Society of Cardiology HF guidelines(5, 39).

Due to the lack of data from clinical trials, current treatment of HFpEF is mainly focused on the management of contributing factors and comorbidities, including hypertension, diabetes, kidney disease, lung disease, coronary artery disease, obesity, anemia, and sleep-disordered breathing(48). The general principle of treatment of HFpEF is to use diuretics to control pulmonary congestion and peripheral edema, to treat systolic hypertension, coronary revascularization in patients with coronary heart disease, and to prevent heart rate acceleration (especially in patients with atrial fibrillation) (48).

For patients with clear evidence of HFpEF (including increased brain natriuretic peptide) who can be carefully monitored for changes in serum potassium and renal function, treatment with a mineralocorticoid antagonist(49). Some small randomized trials have shown that exercise training can improve the function and quality of life of patients with HFpEF without any significant effect on cardiac function(50, 51). Several studies have shown that exercise training is the only intervention that can improve HFpEF exercise capacity and quality of life(50, 51). Care should be taken with the use of diuretics or intravenous dilators. If these drugs are applied to an HFpEF patient with a small and stiff LV, it can lead to insufficient left ventricular filling, decreased CO, and low blood pressure(52).

Evidence of efficacy of beta-blocker therapy in patients with HFpEF is lacking. An individual patient-level meta-analysis of 11 randomized controlled trials of beta-blockers in patients with HF found no evidence of benefit in the small subgroup of patients in sinus rhythm with LVEF ≥50 percent(53, 54). Beta-blockers for HFpEF are only recommended in the presence of an alternative indication, such as angina(53, 54). The use of organic nitrates to treat HFpEF is not recommended. Evidence of efficacy is lacking and a randomized trial found that use of isosorbide mononitrate tended to reduce daily activity levels in patients with HFpEF(55). The results of two clinical trials showed that phosphodiesterase-5 inhibitors did not have any benefit compared with placebo(56, 57). Clinical trial data indicate that digoxin does not affect mortality or hospitalization. Therefore, digoxin is not recommended to treat patients with HFpEF, except for atrial fibrillation with poorly controlled ventricular rate(58).

The incidence of HFpEF patients is almost identical to that of patients with HFrEF. Both HFpEF and HFrEF have high mortality rates. The prognosis of patients with HFpEF is less clear than that of patients with HFrEF. Population-based data from hospitalized patients showed similar mortality in patients with HFpEF and HFrEF(7). Another large

meta-analysis, including community-based research and trials, showed that HFpEF had a lower mortality rate than HFrEF(59).

1.5. Models of HFpEF

If the development of HFpEF can be simulated on animal models, it will significantly accelerate the research progress on this disease. The latest study by Valero-Muñoz proposes the "perfect" screening criteria for HFpEF animal models (**Figure 4**)(60). The most challenging problem to be solved in the HFpEF phenotype is diastolic dysfunction. This phenotype is the most crucial part of the animal model. However, other changes related to the human HFpEF phenotype including peripheral functional impairments, such as lung physiology changes, cardiac morphological changes, and exercise intolerance. Should also be taken into account in the HFpEF model. The following subparagraphs give an overview of animal models described as HFpEF models.

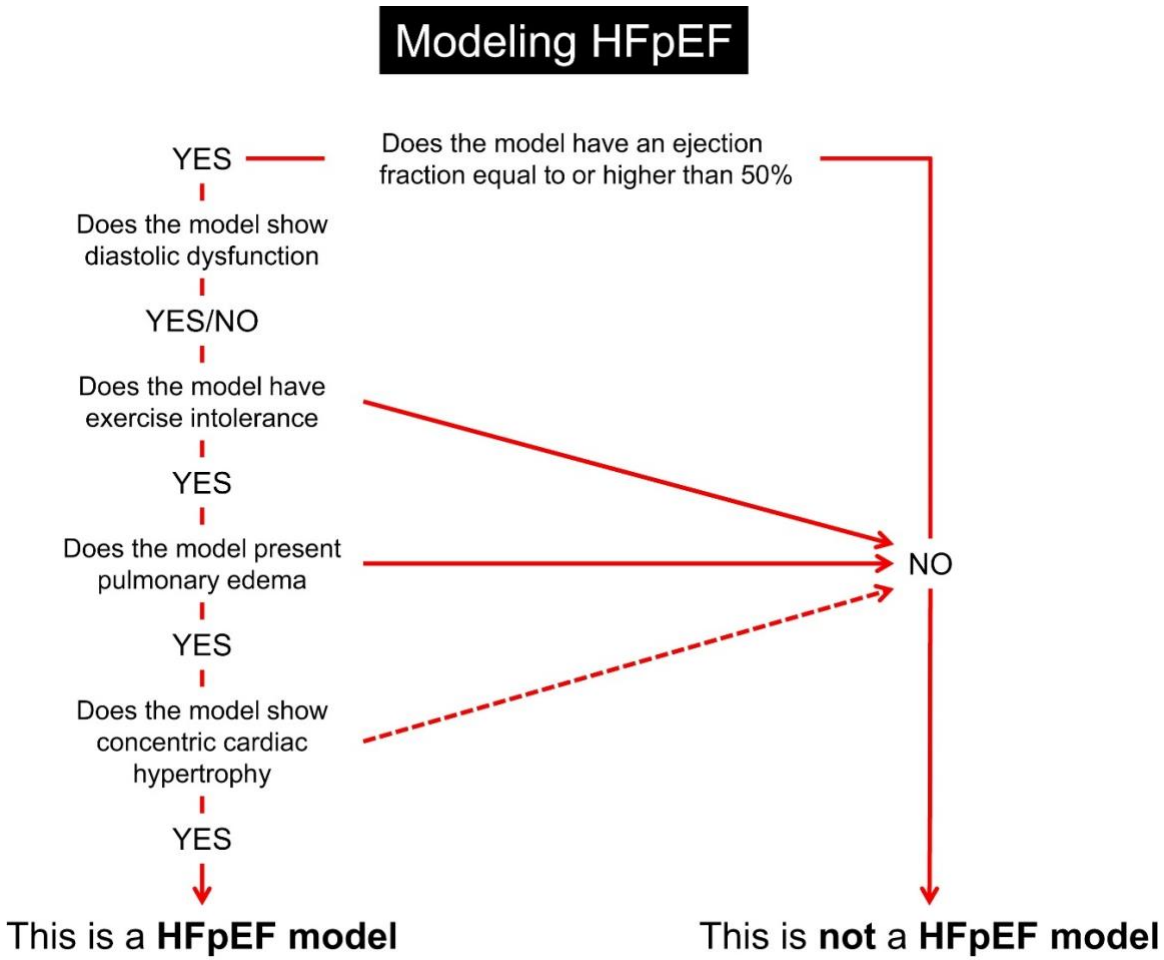

Figure 4. Flowchart Identifying Major Features to Fulfill When Modeling an "ideal" HFpEF animal model in Preclinical(60).

1.5.1. Aging HFpEF models

According to the Framingham Heart Study and the Baltimore Longitudinal Study, even in the absence of clinical hypertension, the prevalence of LV hypertrophy increases with age. This study predicts that the elderly are prone to diastolic dysfunction, and this does not cause a decrease in LVEF, even the LVEF is preserved at resting state(61). Mechanisms associated with age-related changes in myocardial structure and function include cardiomyocyte enlargement, decreased number of cardiomyocytes, compensatory cardiac remodeling, and changes in the number and function of extracellular matrix components and cardiac fibroblasts(62). Mice and rats are commonly used to study aging and age-related diseases(63). The Fischer 344 (F344) aging rat and spontaneous senescence prone mouse could example the pathophysiology of aging in several organs, including the heart(64). However, so far, no occurrence of HFpEF has been reported in such model animals(60).

1.5.2. Hypertension-induced HFpEF models

An increase in blood pressure will accelerate heart remodeling. More importantly, the continued development of hypertension leads to endothelial dysfunction, reduced coronary reserve blood flow, and reduced capillary density. All these unfavorable factors will make oxygen transport limited in the body, aggravating the condition. Also, high blood pressure can cause arterial stiffness, which will cause excessive load on the heart, further exacerbating the situation. The outcome of these changes is the impaired contraction and diastolic function, and reduced quality of life(65). According to epidemiological studies, HF registration information and large controlled trials, the prevalence of systemic hypertension in patients with HFpEF is 60% to 89%(39). Hypertension is a significant risk factor for cardiovascular events. A recent Systolic Blood Pressure Intervention Trial (SPRINT) has shown that lowering blood pressure to a lower target (compare systolic blood pressure <120 mmHg with <140 mmHg) reduces the risk of hospitalization for cardiovascular disease, death, and HF(66). However, active “blood pressure management” does not affect the incidence or prevalence of HFpEF(67). Besides, no studies have shown that patients with HFpEF can improve their prognosis by lowering blood pressure(68).

Aldosterone-infused and unilateral nephrectomized mouse. This model was initiated more than 20 years ago. Unilateral nephrectomy combined with infusion of

aldosterone and 1% sodium chloride (NaCl) can increase blood pressure, cardiac hypertrophy, and myocardial fibrosis in animal models. The model mimics the clinical HFpEF phenotype and also has clinically described molecular variation (69).

Angiotensin II–infused mouse. Administration of angiotensin II (Ang II) (1 to 8 weeks) in mice results in cardiac remodeling. However, there are still some debates. Some scholars have pointed out that cardiac remodeling under Ang II infusion is pressure-dependent(70-72), and some studies have the opposite conclusion(73). At present, there are still many different opinions on the dose of Ang II administered to animals. Previous studies have shown that the use of different doses may lead to a phenotype in animal models that is more prone to diastolic dysfunction(74) or systolic dysfunction(73) or a decrease in LVEF(75). Moreover, different strains have a great influence on the phenotype of animal models. For example, C57BL/6J mice are more prone to compensatory concentric hypertrophy and fibrosis, while Balb/c mice are more prone to LV dilatation(76). It seems that this animal model is an ideal HFpEF simulation, but optimization of the dose and the strain is still a challenge and needs further investigation (60).

Dahl salt-sensitive rat. Dahl salt-sensitive rats are highly sensitive to salt. When fed continuously on a high-salt diet at 6 weeks to 8 weeks of age, the blood pressure of such rats rises sharply, and progressive right ventricular hypertrophy occurs, precipitating HFpEF at approximately 14 to 19 weeks(77). The establishment of this model also has many drawbacks. If the high-salt diet is continued, the phenotype of such rats may be changed from HFpEF to HFrEF. Furthermore, the blood pressure of such animal models is often higher than 175 mmHg, which is inconsistent with the human phenotype(78).

Deoxycorticosterone acetate (DOCA)–salt rat and mouse. In this model, the unilateral kidney is excised at 6-10 weeks old, and 1% NaCl drinking water is administered 1 week later and treated with intraperitoneal or subcutaneous granule implantation for 4 weeks(79). This model was first mentioned in 1969(80). This model has great drawbacks, although it can well exhibit diastolic dysfunction, when HF and pulmonary congestion usually do not occur(81).

Spontaneously hypertensive rat (SHR). The phenotype of this inbred line is highly similar to human essential hypertension, and such animals are prone to

hypertension(82). This model can reproduce some of the HFpEF phenotypes in older humans. However, it must be emphasized that it takes more than two years and is expensive(64).

Thoracic aortic constriction-induced pressure overload in mouse. In 1991, the use of aortic coarctation to induce LV chronic pressure overload was first mentioned. In the following years, this method was gradually improved and was widely used in cardiac hypertrophy research (83). Usually, signs of HF (LV concentric hypertrophy, diastolic dysfunction, and pulmonary congestion) occur after 2 to 3 weeks of surgery. But it progresses soon to HFrEF, a form of progression that is not typical in humans. Moreover, the time point at which HFpEF occurs is not easily to find (78).

1.5.3. Metabolic phenotype: Obesity and diabetes models

Several studies have shown that overweight or obesity is a significant risk factor for HFpEF(84). One study reported that bariatric surgery could improve diastolic dysfunction, probably because weight loss reduces cardiac hypertrophy and LV filling pressure(85). However, this treatment strategy does not have a definite conclusion, whether it can bring any benefits to the HFpEF population remains to be studied(86). Diabetes is common in the HFpEF population, and its presence is associated with poor prognosis of HF(87). The earliest symptoms of HFpEF include changes in skeletal muscle dysfunction and capillary density, all caused by long-term hyperglycemia or hyperinsulinemia(88).

To date, five models have been associated with obesity and diabetes, namely db/db mice, ob/ob mice, streptozotocin-induced diabetic rodents, Zucker diabetic fatty (ZDF) and Zucker fatty/spontaneously hypertensive heart failure F1 hybrid (ZSF1) rats (60). Obesity and diabetes-induced animal model studies are well established, but at present, such animal models are still "imperfect" compared to the human HFpEF phenotype. The most accepted metabolic HFpEF model are the metabolic ZSF1 rats, which develop HFpEF during a 20-week time span and are characterized by cardiomyocyte hypertrophy and titin hypophosphorylation in the absence of cardiac hypertrophy(89).

1.5.4. Nitrosative stress mouse model

A new mouse model reveals that nitrosative stress is a new driving force for HFpEF. Schiattarella and colleagues(90) hypothesized a two-hit model involving cardiac mechanical and metabolic stress, which recapitulates hypertension, obesity, and

diabetes that usually coexist in HFpEF patients. According to their protocol, mice were exposed to one of four regimens: a high-fat diet, drinking water containing Nω-nitro-L-arginine methyl ester (L-NAME; an inhibitor of constitutive nitric oxide synthases), a combination of both (the two-hit model) or a standard chow diet. As a result, the two-hit model showed the most similar phenotype to human HFpEF, including cardiac hypertrophy, pulmonary congestion, exercise intolerance, and deterioration of diastolic function. This new mouse model involves mechanical stress (caused by hypertension) and metabolic stress (caused by diabetes and obesity) of HFpEF, recapitulating some of the HFpEF characteristics in humans.

1.5.5. Atrial fibrillation models

Atrial fibrillation is common in the clinic and is one of the most common arrhythmias. Its presence indicates an increased risk of HF and stroke. Epidemiological studies have also shown that AF is closely related to the occurrence of HFpEF(91). In an early study of dogs, researchers found that cardiac dysfunction caused by atrial pacing induced dilated cardiomyopathy and HFrEF in the absence of an increase in collagen(92). In the early days, no researchers believed that a mouse model of atrial fibrillation could be made because the heart quality of the mice was too small. But now the emergence of transgenic atrial fibrillation mice has broken this deadlock(93). Unfortunately, no signs of HFpEF have been found in animals with atrial fibrillation so far(60).

1.5.6. Pulmonary hypertension models

As long as a particular disease increases the LV filling pressure, it will inevitably lead to the occurrence of pulmonary hypertension(94). A small percentage of patients with HFpEF will continue to develop pulmonary hypertension(95). The severity of pulmonary hypertension in animal models is quite different from the human phenotype. The model may only reflect the lighter form of human pulmonary hypertension, which is often more severe in the human body. Therefore, based on current knowledge, we can conclude that the animal model of pulmonary hypertension does not fully represent clinical observation(96).

1.6. Angiotensin II-induced mouse models evaluation

It has been reported in many studies that the administration of Ang II in mice can lead to cardiac hypertrophy and remodeling. However, reported changes of blood pressure in mice are not the same(70-73) Obviously, the observed increase in blood pressure

depends on the dose of Ang II used(60). The use of different doses of Ang II also leads to different cardiac remodeling results.

Murdoch et al. reported that when Ang II was administered to male transgenic (TG) and wild-type mice at a dose of 1.1 mg/kg/day, Ang II induced endothelial nicotinamide adenine dinucleotide phosphate oxidase-2 activation had profound profibrotic effects on the heart, leading to a diastolic dysfunction phenotype(70). Mori et al. used an Ang II dose of 1.5 mg/kg/day for 9-week-old male C57/BL6 wild-type mice, and found that Ang II-induced hypertrophy and diastolic dysfunction was associated with decreased glucose oxidation and revealed that targeting these pathways could provide new treatments for HFpEF(97). Regan et al., they administrated eight-week-old outbred male CD1 mice Ang II dose of 0.2 mg/kg/day and found that their animal model replicated the HFpEF features of impaired LV relaxation and increased LV elastance in the absence of pressure overload, LV systolic dysfunction, LV dilatation or hypertrophy, and metabolic abnormalities(73).

1.7. Objective

Ang II infusion appears to lead to a relevant HFpEF model if the dose is optimized. Three kinds of dose regimes in the studies from Murdoch et al. (70), Mori et al. (97), and Regan et al. (73) seem to be a good catalyzer for mimicking some characteristics of HFpEF. According to the hemodynamic data provided by their research (**Table 1**), some parameters were inconsistent or still disputed, especially dP/dt_{max}, dP/dt_{min}, and τ, which are key indicators for evaluating the systolic (98, 99) and diastolic function(99-101). In these studies, researchers did not use the same mouse background, and there was no uniform external factor in the experiments they conducted, which potentially can be the reason why some hemodynamic parameters were different. From their respective studies, it is not possible to deduce which dose can better reflect the HFpEF phenotype. Therefore, the aim of this study was to compare those 3 Ang II regimes in parallel in the same mouse background: C57BL/6 mice to investigate the influence of the different doses of Ang II on the disputed hemodynamic parameters (dP/dt_{max}, dP/dt_{min}, and τ,) and molecular mechanisms, in view of identifying the potential optimal dose.

Table 1. Changes in hemodynamic parameters in three studies (70, 73, 97).

Variable	Murdoch et al. J Am Coll Cardiol. 2014	Mori et al. Circ Heart Fail. 2012	Regan et al. Am J Physiol Heart Circ Physiol. 2015
	1.1mg/kg 14d Ang II vs. control (WT mice)	1.5mg/kg 14d Ang II vs. control (C57/BL6 mice)	0.2mg/kg 28d Ang II vs. control (CD1 mice)
HR	—	NA	NA
EF	—	—	—
dP/dt_{max}	—	↓	NA
dP/dt_{min}	—	NA	NA
τ	—	NA	↑
CO	—	NA	NA
SV	↑	NA	NA
SW	—	NA	NA
E/A	NA	↓	—
E/E'	NA	↑	—
IVSD	↑	NA	NA
LVEDD	↑	NA	—
LVEDP	—	↑	↑
LVPWT	NA	↑	NA
LVESD	NA	NA	—
LVESV	—	NA	NA
LVEDV	↑	NA	NA
Ea	—	NA	NA
Ees	↑	NA	NA
EDPVR	—	NA	↑
ESPVR	NA	NA	—
TAPSE	NA	NA	—
dP/dt_{max}/ EDV	—	NA	NA
MPI	NA	NA	↑
IRT	NA	NA	↑

↑: increased compared to its corresponding control group; ↓: decreased compared to its corresponding control group; —: no change compared to its corresponding control group; NA: data unavailable; WT: wild-type; HR: heart rate; EF: ejection fraction; dP/dt_{max}: maximum left ventricular pressure rise rate; dP/dt_{min}: maximum left ventricular pressure drop rate; τ: time of the left ventricular pressure decrease; CO: cardiac output; SV: stroke volume; SW: stroke work; IVSD: interventricular septal diameter; LVEDD: left ventricular end diastolic diameter; LVEDP: end-diastolic left ventricular pressure; LVPWT: left ventricular posterior wall thickness; LVESD: left ventricular end-systolic diameter; LVESV: end-systolic left ventricular volume; LVEDV: end-diastolic left ventricular volume; Ea: arterial elastance; Ees: end-systolic elastance; EDPVR: end-diastolic pressure volume relationship; ESPVR: end-systolic pressure volume relationship; TAPSE: tricuspid annular plane systolic excursion; EDV: end-diastolic volume; MPI: myocardial perfusion imaging; IRT: isovolumetric relaxation time.

2. Materials and methods

2.1. Materials

Table 2. Consumption materials

Article	Description	Company
96-well-PCR plate		Sarstedt, Nürnbrecht, Germany
Coverslips	21 x 26 mm	R. Langenbrinck, Emmendingen, Germany
Cryotubes	1.5 ml	Carl Roth, Karlsruhe, Germany
Falcon tubes	15 ml, 50 ml	Corning, New York, USA
Folded filter	MN615 1/4·¢240 mm	Macherey-Nagel, Düren, Germany
Gloves		Sempercare, Northamptonshire, UK
Masks		Charite, Berlin, Germany
MicroAmp®Optical 384-well plate	Reaction plate with Barcode	Thermo Fisher Scientific, Waltham, Massachusetts, USA
Microtome blades	A35 type	Feather, Köln, Germany
PCR-tubes	0.2 ml, conical lid	Biozym, Hess. Oldendorf, Germany
Pipette tips	10 µl, 100 µl, 1000 µl	Biozym, Hess. Oldendorf, Germany
Pipettes		Corning, New York, USA
Plastic cannulas	18G und 20G	B.Braun, Melsungen, Germany
Plunger	2.5 ml syringe	TERUMO, Tokyo, Japan
Reaction Tubes	Safe-Lock or RNAse free	Sarstedt, Nürnbrecht, Germany
Scalpels		Feather, Köln, Germany
Slides	Super Frost Plus	R.Langenbrinck, Emmendingen, Germany

Table 3. Laboratory equipment

Equipment	Description/Type	Company
Conductance catheter	1.2 French	Scisense Inc., Ontario, Canada
Cryostat		Microm, Minnesota, USA
Homogenizer	Pellet Pestle Motor	Sigma, Taufkirchen, Germany
Horizontal shaker	SM-25	Edmund Bühler, Tübingen, Germany
Ice maker	AF-10	Scotsman, Vernon Hills, USA
Incubator	Function Line	Heraeus, Osterode, Germany
Microscope	DM2000 LED	Leica, Bensheim, Germany
pH meter	Knick Digital 646	Beyer, Düsseldorf, Germany
Pipettes		Eppendorf, Wesseling-Berzdorf, Germany
P-V Amplifier System	MPVS 300/400	Millar Instruments, Houston, USA
Spectrophotometer	NanoDrop	Thermo Scientific PEQLAB, Erlangen, Germany
Photometer	SPECTRA max 340PC384	Molecular Devices, Biberach an der Riß, Germany
Tabletop centrifuge	Centrifuge 5415 C	Eppendorf, Wesseling-Berzdorf, Germany
Thermocycler	Mastercycler gradient	Eppendorf, Wesseling-Berzdorf, Germany
Thermomixer	Comfort	Eppendorf, Wesseling-Berzdorf, Germany
Ventilator	Minutes i-Vent	Harvard Apparatus, Massachusetts, USA
Vortexer	VF2	IKA-Labortechnik, Staufen, Germany

Table 4. Chemicals, buffer reagent and kits

Article	Company
1% ß-mercaptoethanol	Sigma-Aldrich Chemie GmbH, Taufkirchen, Germany
3-Amino-9-Ethylcarbazole (AEC)	Sigma-Aldrich Chemie GmbH, Taufkirchen, Germany
Acetic acid	VWR International GmbH, Darmstadt, Germany
Acetone	VWR International GmbH, Darmstadt, Germany
Avidin-Biotin-Blocking(ABC)-Kit	Vector Labs, Burlingame, USA
Bovine serum albumin (BSA)	Carl Roth, Karlsruhe, Germany
Calcium chloride	VWR International GmbH, Darmstadt, Germany
Dianova (secondary antibody)	Dianova, Hamburg, Germany
Di-Sodium hydrogen phosphate dihydrate	VWR International GmbH, Darmstadt, Germany
Distilled water	Alleman Pharma GmbH, Rimbach, Germany
DNAse I	Qiagen, Hilden; Germany
ethylenediaminetetraacetate (EDTA)	VWR International GmbH, Darmstadt, Germany
EnVision K4003	Dako, Hamburg, Germany
Ethanol	Sigma-Aldrich Chemie GmbH, Taufkirchen, Germany
Fetal Bovine Serum (FBS)	Biochrom, Berlin, Germany
Formalin	Sigma-Aldrich Chemie GmbH, Taufkirchen, Germany
Hemalum	VWR International GmbH, Darmstadt, Germany
High Capacity cDNA Reverse Transcription Kit	Applied Biosystems, Darmstadt, Germany
Hydrogen peroxide solution	Sigma-Aldrich Chemie GmbH, Taufkirchen, Germany
Isopropanol	Sigma-Aldrich Chemie GmbH, Taufkirchen, Germany
Kaiser's glycerol gelatin	Carl Roth, Karlsruhe, Germany
Magnesium chloride	VWR International GmbH, Darmstadt, Germany
N, N-dimethylformamide	Carl Roth, Karlsruhe, Germany
Optical 96-well Reaction Plate	Applied Biosystems, Darmstadt, Germany
Optical Adhesive film	Applied Biosystems, Darmstadt, Germany
Potassium chloride	VWR International GmbH, Darmstadt, Germany

Potassium dihydrogen phosphate	VWR International GmbH, Darmstadt, Germany
RNase-free water	Thermo Fisher Scientific, Waltham, USA
RNeasy Minutes i Kit	Qiagen, Hilden; Germany
Sodium acetate	VWR International GmbH, Darmstadt, Germany
Sodium chloride	VWR International GmbH, Darmstadt, Germany
Sodium hydrogen phosphate	VWR International GmbH, Darmstadt, Germany
TaqMan®Gene Expression Master Mix (2×)	Thermo Fisher Scientific, Waltham, USA
Tissue Tek	Sakura, Zoeterwoude, Netherlands
Tris-Base	Sigma-Aldrich Chemie GmbH, Taufkirchen, Germany
Tris-HCl	VWR International GmbH, Darmstadt, Germany
TRIzol Reagent	Thermo Fisher Scientific, Waltham, USA
Universal PCR Master Mix	Applied Biosystems, Darmstadt, Germany
Angiotensin II	SIGMA-Aldrich, USA

Table 5. Real-time polymerase chain reaction reagents

Reagents	Company
Optical 384-well Reaction Plate	Applied Biosystems, Darmstadt, Germany
Optical Adhesive film	Applied Biosystems, Darmstadt, Germany
TaqMan Gene expression Master Mix (2×)	Thermo Fisher Scientific, Massachusetts, USA
Universal PCR Master Mix	Applied Biosystems, Darmstadt, Germany

Table 6. Primers for real-time polymerase chain reaction

Murine primers	Ordering number	Company, ID
Acta1	Mm00808218_g1	Applied Biosystems, Darmstadt, Germany
AT1R	Mm01166161_m1	Applied Biosystems, Darmstadt, Germany
CCL2	Mm99999056_m1	Applied Biosystems, Darmstadt, Germany
CCL5	Mm01302428_m1	Applied Biosystems, Darmstadt, Germany
CCL7	Mm00443113_m1	Applied Biosystems, Darmstadt, Germany
Col1a1	Mm01302043_g1	Applied Biosystems, Darmstadt, Germany

Col3a1	Mm00802331_m1	Applied Biosystems, Darmstadt, Germany
CX3CL1	Mm00436454_m1	Applied Biosystems, Darmstadt, Germany
IL-10	Mm00439616_m1	Applied Biosystems, Darmstadt, Germany
IL-1ß	Mm00434228_m1	Applied Biosystems, Darmstadt, Germany
IL-6	Mm00446190_m1	Applied Biosystems, Darmstadt, Germany
Myh7b	Mm01249945_m1	Applied Biosystems, Darmstadt, Germany
RAGE	Mm01134790_g1	Applied Biosystems, Darmstadt, Germany
S100A8	Mm00496696_g1	Applied Biosystems, Darmstadt, Germany
S100A9	Mm00656925_m1	Applied Biosystems, Darmstadt, Germany
TGF-ß	Mm00441724_m1	Applied Biosystems, Darmstadt, Germany
TLR4	Mm00445273_m1	Applied Biosystems, Darmstadt, Germany
TNF-α	Mm00443258_m1	Applied Biosystems, Darmstadt, Germany
VEGF	Mm01281447_m1	Applied Biosystems, Darmstadt, Germany

Table 7. Antibodies used for immunohistochemistry

Antibody	**Company**
Anti-α-SMA	Abcam, Cambridge, UK
Anti-CD4	BD Bioscience, Heidelberg, Germany
Anti-CD68	Abcam, Cambridge, Germany
Anti-CD8a	BioLegend, Koblenz, Germany
Anti-Collagen I	Merck Millipore, Darmstadt, Germany
Anti-Ly6g	GeneTex, Irvine, USA

Table 8. Software

Software	Company
GraphPad Prism 8.0	GraphPad Software, San Diego, USA
EndNote X9.1	Clarivate Analytics, Philadelphia, USA
Leica Application Suite version 4.4.0	Leica, wetzlar,Germany
Microsoft Office 2016	Microsoft, Washington, USA
Adobe Illustrator 2019	Adobe, San Jose, USA
IOX software 1.8.9	EMKA Technologies, Falls Church, USA
CircLab 2004	Leiden University, the Netherlands

2.2. Methods

2.2.1. Study design

In this experiment, 5 weeks old male C57BL6/j mice provided by Charles River (Sulzfeld, Germany) were used. Mice were randomly divided into the following groups: control 1.1mg/kg 14d group, Ang II 1.1mg/kg 14d group, control 1.5mg/kg 14d group, Ang II 1.5mg/kg 14d group, control 0.2mg/kg 28d group, and Ang II 0.2mg/kg 28d.

After acclimatization, 8 weeks old mice received Ang II (Catalog Number: A9525-10mg, SIGMA-Aldrich, United States) or sterile distilled water (control animals) via subcutaneous injection (s.c.) at different dose or duration based on the group they were in (**Table 9 and Figure 5**).

Table 9. Study design.

	Group 1		**Group 2**		**Group 3**	
Group	control 1.1mg/kg 14d	Ang II 1.1mg/kg 14d	control 1.5mg/kg 14d	Ang II 1.5mg/kg 14d	control 0.2mg/kg 28d	Ang II 0.2mg/kg 28d
Animal	male C57BL6/j mice	male C57BL6/j mice	male C57BL6/j mice	male C57BL6/j mice	male C57BL6/j mice	male C57BL6/j mice
Dose	1.1 mg / kg * d-1 water s.c.	1.1 mg / kg * d-1 Ang II s.c.	1.5 mg / kg * d-1 water s.c.	1.5 mg / kg * d-1 Ang II s.c.	0.2 mg / kg * d-1 water s.c.	0.2 mg / kg * d-1 Ang II s.c.
Duration	14 d	14 d	14 d	14 d	28 d	28 d

s.c.: subcutaneous; water: sterilized filtered water.

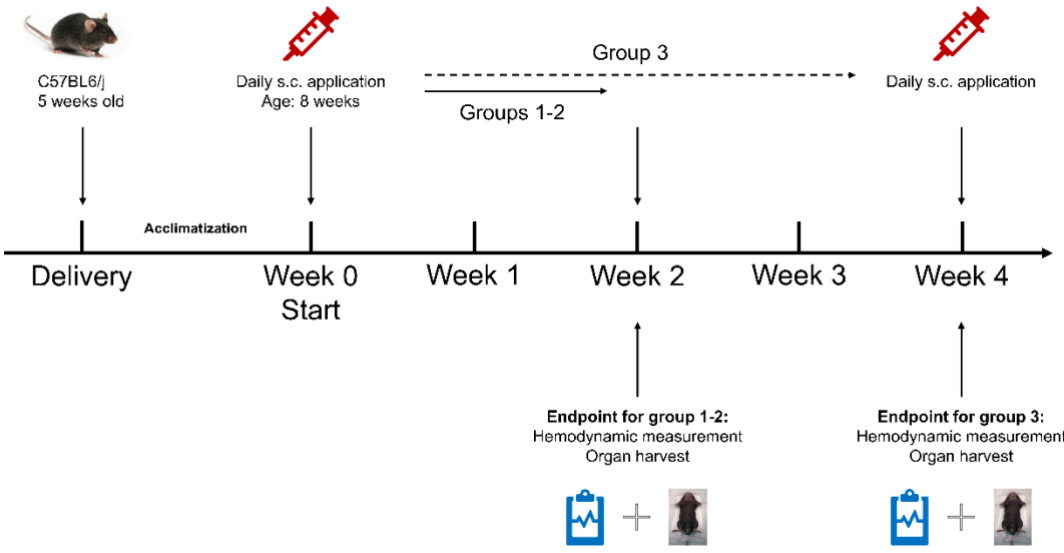

Figure 5. The time line of the study design. s.c., subcutaneous injection; Group 1, 1.1mg/kg 14d group; Group 2, 1.5mg/kg 14d group; Group 3, 0.2mg/kg 28d group.

At the end of each experiment, all surviving mice were sacrificed after hemodynamic measurements. LVs were collected and quickly frozen in liquid nitrogen and stored at -80°C for later molecular and immunohistochemical examinations. All investigations were performed in accordance with the European legislation of the Care and Use of Laboratory Animals and were approved by Landesamt für Gesundheit und Soziales Berlin (LAGeSo, Berlin, Germany; Registration code: G 0271/16).

2.2.2. Establishment of Angiotensin II-induced heart failure

2.2.2.1. Mouse strains and animal care

In this present study, C57BL6/j mice were housed in the Forschungseinrichtungen für Experimentelle Medizin (FEM, Berlin) of Charité-Universitätsklinikum Berlin with a 12-hour light/dark cycle at 19-21°C, 50-70% humidity and free access to food and water.

2.2.2.2. Angiotensin II preparation

Ang II was provided by SIGMA-Aldrich (catalog number: A9525; pack size: 10mg), as a powder and stored at −20°C. It was formulated with sterile distilled water into three solutions with different concentrations for our subsequent experiments: Solution A (110 µg / ml), Solution B (150 µg / ml), and Solution C (20 µg / ml). Then, all solutions were sterile filtered and aliquoted in 5ml Eppis, 4ml per Eppi.

2.2.2.3. Angiotensin II injection

Mice in group 1 received 10µl / g Solution A for fourteen consecutive days. Mice in group 2 received 10µl / g Solution B for fourteen consecutive days. Mice in group 3 received 10µl / g Solution C for twenty-eight consecutive days. Corresponding control mice received sterile distilled water.

2.2.3. Catheter-based hemodynamic measurements

At the day of sacrifice, pressure-volume conductance catheter measurements were performed under general anesthesia through an apical stab. The main procedure steps are shown in **Figure 6**. A combination of buprenorphine and urethane was used for anesthesia by i.p. injection at a dose of 0.05mg/kg and 0.8-1.2g/kg, respectively. Anesthesia depth was checked by pain stimulus. For intubation, a 22G cannula was used, which was connected to the ventilator (Min-Vent, Harvard Apparatus, Massachusetts, USA).

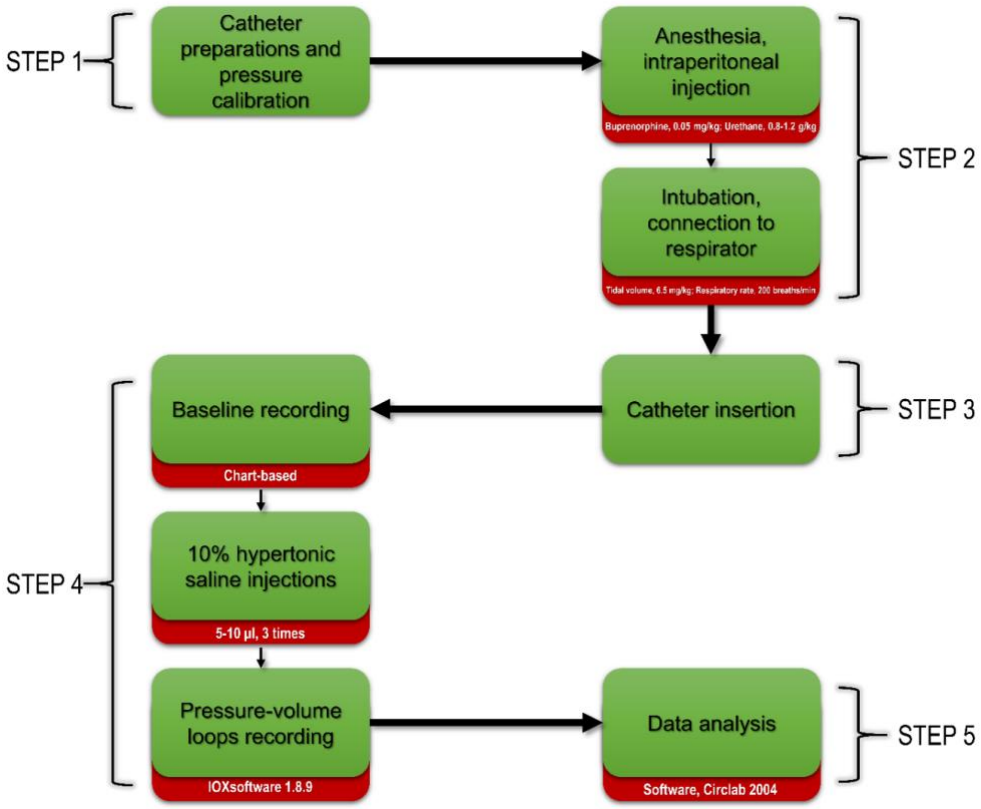

Figure 6. Main steps of hemodynamic measurement

The pressure-volume data of the LV were recorded in real-time with a conductance catheter, by which it is possible to determine both volume-dependent and volume-independent parameters that describe the heart function(102). In this procedure, a 1.2 French catheter (Scisense Inc., Ontario, Canada) was placed into the LV, which was connected to a pressure-volume-amplifier system (MPVS 300/400, Millar Instruments, Houston, USA)(103). Data were collected using the software program "IOX", 1.8.9 (EMKA Technologies, Falls Church, USA) and then analyzed using the program "CircLab 2004". PV loops were recorded, followed by volume calibration with hypertonic saline (10%) injection. All data were acquired without ventilation for 5 seconds to avoid lung motion artifacts. The mean value of three continuous measurements of hemodynamic parameters was used in final statistical analysis. Common hemodynamic parameters assessed in PV measurement are listed in **Table 10**.

Table 10. Hemodynamic parameters

Parameter	Definition
Global cardiac function	
HR, bpm	heart rate
EF, %	ejection fraction, the fraction of blood volume pumped out of the LV in each cardiac cycle
Systolic function	
dP/dt_{max}, mm Hg/s	maximum left ventricular pressure rise rate
Diastolic function	
dP/dt_{min}, mm Hg/s	maximum left ventricular pressure drop rate
τ, ms	time of the left ventricular pressure decrease

2.2.4. Tissue collection

After finishing hemodynamic measurements, mice were sacrificed and the LVs were removed and quickly frozen in liquid nitrogen and stored at -80°C for later molecular and immunohistochemical examinations.

2.2.5. Immunohistochemistry

2.2.5.1. Cryosections

LV tissue samples were transferred from the -80°C freezer to a -20 °C freezer and stored overnight before cryosection. LV samples were embedded in snap frozen Tissue-Tek (Sakura, Zoeterwoude, Netherlands). Next, the tissue block was fixed and trimmed on the specimen head in the Cryostat (Thermo Fisher Scientific, Waltham, USA). The thickness of the cryosections was 5 µm. Six cryo-slices from different transverse of tissue sample were laid on each slide. Subsequently, the sections were immersed in ice-cold acetone for 10 min. After drying, the slides were immediately used for staining or stored at -20 °C.

2.2.5.2. Immunohistochemical staining

Based on antigen-antibody reactions, immunohistochemical stainings allow to detect histological antigens on sections. The antigen-specific antibody is bound to a secondary antibody with a coupled enzyme. Further, the distribution and localization of biomarkers or differentially expressed proteins in different parts of tissue is subsequently visualized by an appropriate substrate. In this study, the Avidin-biotin complex (ABC) staining and the EnVision staining methods were used. The details of the antibodies used in this study is shown in **Table 11**.

Table 11. Antibodies for immunohistochemistry

Primary antibody	Species	Dilution	Secondary antibody	Species	Dilution	Method
α-SMA	Rabbit	1:200	EnVision Dako	Anti-Rabbit	undiluted	EnVision
Collagen I	Rabbit	1:250	EnVision Dako	Anti-Rabbit	undiluted	EnVision
CD4	Rat	1:50	Biotinylated Goat anti-rat	Anti-Rat	1:250	ABC
CD68	Rat	1:600	Biotinylated Goat anti-rat	Anti-Rat	1:250	ABC
CD8a	Rat	1:50	Biotinylated Goat anti-rat	Anti-Rat	1:250	ABC
Ly6g	Rat	1:200	Biotinylated Goat anti-rat	Anti-Rat	1:250	ABC

ABC: avidin-biotin complex

2.2.5.2.1. EnVision method

EnVision staining is a two-step staining in which the application of the primary antibody is followed by a polymeric conjugate consisting of a large number of secondary antibodies bound directly to a dextran backbone containing horseradish peroxidase. One such conjugate contains up to 100 horseradish peroxidase molecules and up to 15 antibodies. Therefore, it is suitable for a variety of antibodies. In this study, the EnVision method was used to investigate collagen I and alpha-smooth muscle actin (α-SMA) expression on the LV sections.

The detailed steps are as follows:

1). Take out the slides from -20℃.

2). Mark the slides, immerse them in 1x phosphate-buffered saline (PBS) on the shaker for 5 minutes to adapt the slices to the buffer milieu.

3). Transfer the slides to the fresh 0.075% hydrogen peroxide PBS solution. Incubate them in a lid-covered cuvette for 7 min on the shaker to block endogenous peroxidase.

4). Wash the slices with 1xPBS on a shaker for 5 minutes.

5). Add 75 ul of the primary antibody with 10% FSC and 1xPBS solution to each staining area. Then, incubate them for 1 hour in the humidifier chamber in order to bind the antibody to the target protein.

6). Wash the slices with 1xPBS twice on a shaker, each for 5 minutes.

7). Add 75 ul of the second antibody to each staining area. Then, incubate them for 30 minutes in the humidifier chamber, in order to bind the second antibody to the first antibody.

8). Wash the slices with 1xPBS twice on a shaker, each for 5 minutes.

9). Dip them into 200 ml fresh carbazol solution including 50 mg 3-Amino-9-Ethylcarbazole (AEC), 10 mL dimethylformamide, 100 ul H_2O_2, 35 mL 0.2 mol sodium acetate solution, 15 mL 0.2 mol acetic acid solution, and distilled water. Incubate for 12 minutes in the dark, in order to make the second antibody visible.

10). Wash the slices with 1xPBS twice on a shaker, each for 5 minutes.

11). Stain them with hematoxylin for 30 seconds.

12). Snap transfer them to tap water and rinse until the watercolor is clear.

13). Move them to hot tap water of circa 50-60°C and incubate for 10 minutes on a shaker.

14). Mount the slides using Kaiser Glycerol gelatin for storage.

2.2.5.2.2. Avidin-biotin complex method

ABC staining is called the immunoperoxidase method, which is based on the binding of an antibody to a suitable target antigen. The extraordinary affinity of avidin for biotin allows specific binding between biotin-containing molecules and avidin in complex mixtures. This combination of biochemistry has stable, almost irreversible properties. In this present study, the ABC method was used to determine the presence of inflammatory cells maintained by cluster of differentiation (CD) 4, CD68, CD8a, and lymphocyte antigen 6 complex locus G6D (Ly6g).

1). Take out the slides from -20℃.

2). Mark the slides, immerse them in the 1x tris-buffered saline (TBS) on the shaker for 5 minutes, adapting slices to the buffer milieu.

3). Transfer the slides to the fresh 0.075% hydrogen peroxide TBS solution. Incubate them in a lid-covered cuvette for 7 min on the shaker to block endogenous peroxidase.

4). Wash the slices with 1xTBS on a shaker for 5 minutes.

5). Add 75 ul of the serum solution with 10% goat serum, 1% bovine serum albumin (BSA), 1xTBS, and avidin to each staining area. Then, incubate them for 30 minutes in the humidifier chamber, in order to avoid electrostatic interaction and unspecific binding, and block endogenous biotin.

6). Add 75 ul of the primary antibody with 1% BSA,1xTBS, and biotin to each staining area. Then, incubate them for 60 minutes in the humidifier chamber, in order to make the first antibody and the target protein to bind, and to block the endogen avidin, avoiding unspecific bindings.

7). Wash the slices with 1xTBS twice on a shaker, each for 5 minutes.

8). Add 75 ul of the second antibody with 1% BSA and 1xTBS to each staining area. Then incubate them for 60 minutes in the humidifier chamber, in order to bind the second antibody to the first antibody, and to avoid the unspecific bindings.

9). Wash the slices with 1xTBS twice on a shaker, each for 5 minutes.

10). Wash the slices with 1xTBS and 0.01% Tween 20 on a shaker for 5 minutes to reduce the hydrophobic surface of the slides.

11). Add 75 ul of the ABC Complex solution to each staining area. Then, incubate them for 30 minutes in the humidifier chamber, in order to make the HRP-labelled avidin and the biotinylated second antibody to bind.

12). Wash the slices with 1xTBS twice on a shaker, each for 5 minutes.

13). Dip them into 200 ml fresh carbazol solution including 50 mg AEC, 10 mL dimethylformamide, 100 ul H2O2, 35 mL 0.2 mol sodium acetate solution, 15 mL 0.2 mol acetic acid solution, and distilled water. Incubate for 12 minutes in the dark, in order to make the second antibody visible.

14). Wash the slices with 1xTBS twice on a shaker, each for 5 minutes.

15). Stain them with hematoxylin for 30 seconds.

16). Snap transfer them to tap water rinsing until the watercolor is clear.

17). Move them to hot tap water of circa 50-60°C and incubate for 10 minutes on a shaker.

18). Mount the slides using Kaiser Glycerol gelatin for storage.

2.2.5.3. Digital image analysis

All tissue sections were analyzed with the color-coded digital image analysis technique through light microscopy (Leica DM2000 LED). Twenty view fields from each specimen were evaluated at a 100x magnification and digitized by a video camera. With this evaluation method, the selected fields in light microscope can be independently and accurately evaluated. The digital image processing was performed with the digital software (Leica Application Suite version 4.4.0) for which a self-programmed macro, one for areal and one for cell calculation has been developed. All microscopic images obtained for detecting the stained antigens were measured with a 100-fold microscope magnification. Quantification of collagen I is represented as positive area percentage per heart area (mm^2). To depict arterioles and arteries, an α-SMA staining was performed. α-SMA-positive arterioles and arteries were subsequently counted per high

power field (hpf). The infiltration of immune cells (CD4, CD68, CD8a, and Ly6g) is expressed in the form of positive cells/mm^2.

2.2.6. Gene expression analysis

2.2.6.1. RNA extraction

The TRIzol™ reagent (Invitrogen, Heidelberg, Germany) was used to isolate ribonucleic acid (RNA) from the LV. Frozen tissue samples in a FACS tube containing 1 ml TRIzol™ reagent were homogenized for 30 seconds, shaken for 15 seconds after adding 200 µl chloroform, and then incubated at RT for 2 minutes. Then, they were centrifuged at an accelerated speed of 10,000 rpm for 15 minutes at 4 °C and a colorless upper phase, containing the RNA, was collected. For RNA precipitation, 500µl of 100% isopropanol was added, incubated at RT for 15 minutes, and centrifuged at 10,000 rpm at 4 °C for 10 minutes. The supernatant was removed and 500 µl ethanol (70%) was added and vortexed, followed by centrifugation for 10 minutes at 4 °C and at an acceleration of 7,500 rpm. The remaining RNA pellets were dissolved in 100 µl RNase-free water and purified with the NucleoSpin® RNA mini kit (Macherey-Nagel GmbH, Düren, Germany). Samples were supplemented with 300 µl RA1 buffer and 300 µl ethanol (96%) and centrifuged at 12,000 rpm for 30 seconds followed by adding 350 µl membrane desalting buffer and a repeated centrifugation at 12,000 rpm for 1 minute. Next, 10 µl reconstituted rDNase was mixed with 90 µl reaction buffer and samples were incubated with this mixture at RT for 15 minutes. Membranes were washed 3 times with 200 µl RA2, 600 µl RA3, and 250 µl RA3, respectively, and then centrifuged for 2 minutes. Finally, 50 µl RNase-free water was used to elute the RNA and centrifuged for 1 minute. The spectrophotometer (NanoDrop 1000, Thermo Scientific, Erlangen, Germany) was used to examine the concentration of RNA with absorbance at 260 nm.

2.2.6.2. Reverse Transcription

Reverse transcription from isolated RNA to complementary DNA (cDNA) was performed by the high Capacity cDNA Reverse Transcription Kit from Applied Biosystems (Darmstadt, Germany). 1 µg RNA was completed to a total volume of 11 µl with RNase-free water. Random primers and template RNA were heated for 5 minutes at 70 °C in a thermocycler. Meanwhile, a master-mix was prepared by mixing the following components in one tube: 2 µl buffer + 3.2 µl RNase-free water + 1 µl reverse

transcriptase. The reaction tubes were directly put on ice and 6.2 µl of the master-mix was added. Then, the reverse transcription was performed in a thermocycler according to the following program: 10 minutes at 25 °C, 2 hours at 37 °C, followed by additionally 5 minutes at 85 °C and cool down to 4 °C. Finally, 30 µl RNase-free water was added to each sample to a final volume of 50 µl.

2.2.6.3. Real-time polymerase chain reaction

Real-time polymerase chain reaction (PCR) was performed by using a mixture of 5 µl PCR master-mix, 0.5 µl gene reporter assay, and 3.5 µl water.

The reporter assays obtained (Life Technologies GmbH, Darmstadt, Germany) included forward and reverse primers as well as the fluorescently 5' FAM-labelled probe, with a 3' non-fluorescent Quencher NFQ-MGB. All reporter assays used are listed in **Table 5**. The 7900HT real-time system (Applied Biosystems, Darmstadt, Germany) was used to amplify the sample according to the following steps. First, prevention of carry-over contamination by addition of Uracil N-Glycosylase for 2 minutes at 50°C. Second, denaturation and activation of the amplification-Taq deoxyribonucleic acid (DNA) polymerase for a period of 10 minutes at a temperature of 95°C, and second denaturation for 15 seconds at a temperature of 95°C. Third, annealing and elongation over 1 minute at a temperature of 60°C. Depending on the target gene, second denaturation, annealing and elongation were repeated 40 or 45 times. Analysis of the collected data was performed using the SDS program 2.2.2 (Applied Biosystems, Darmstadt, Germany).

2.2.6.4. Housekeeping gene

Housekeeping genes are typically constitutive genes required to maintain essential cell functions and are expressed in all cells of the organism under normal and pathophysiological conditions(104). In this experiment, glyceraldehyde 3-phosphate dehydrogenase (GAPDH) was chosen as the housekeeping gene and used for normalization of the target gene. The Ct-value of GAPDH of each group can be found in **Figure 7**, showing no significant differences in Ct-values among the groups. Data were further normalized against GAPDH, which served as an endogenous control using the 2^-ΔΔCt formula. To evaluate the n-fold change, message RNA (mRNA) levels in other groups were compared to each control group.

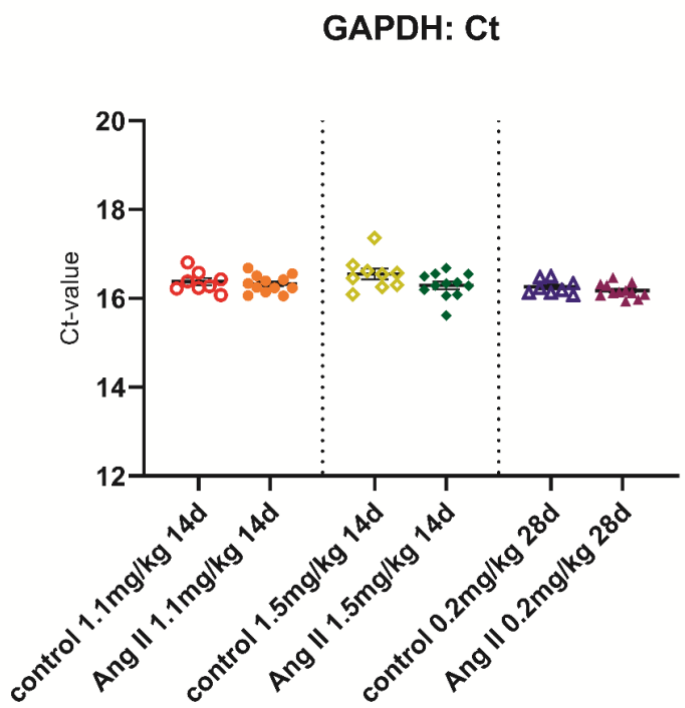

Figure 7. Ct value of housekeeping gene GAPDH of each group. Bar graphs represent the mean±SEM of Ct value, with n=8 in control 1.1 mg/kg 14d, n=12 in Ang II 1.1 mg/kg 14d, n=9 in control 1.5 mg/kg 14d, n=12 in Ang II 1.5 mg/kg 14d, n=8 in control 0.2 mg/kg 28d, n=12 in Ang II 0.2 mg/kg 28d. A nonparametric Mann–Whitney U test or a Welch's t test was performed for data comparison between each respective control vs. Ang II group. GAPDH: Glyceraldehyde 3-phosphate dehydrogenase; Ct: cycle threshold; Ang II: Angiotensin II; d: day; SEM: standard error of the mean; vs.: versus.

2.3. Statistical analysis

Statistical analysis of the experiment was performed using GraphPad Prism 8.0 software (GraphPad Software, San Diego, USA). Data are expressed as mean ± standard error of the mean (SEM). A nonparametric Mann–Whitney U test or a Welch's t test was performed for data comparison between each respective control vs. Ang II group. Differences were considered statistically significant at a value of $p<0.05$.

3. Results

3.1. Hemodynamic parameters

In global cardiac function, we found that the HR remained unchanged between all Ang II mice and their respective controls, and that the EF was higher than 70% in all six groups of mice (**Figure 8A and Figure 8B**).

Related to LV systolic function, Ang II 1.1mg/kg 14d mice had a lower maximum LV pressure rise rate (dP/dt_{max}) than control 1.1mg/kg 14d mice (19.8% drop, $p<0.05$). dP/dt_{max} was not higher in Ang II 1.5mg/kg 14d and Ang II 0.2mg/kg 28d mice compared to their respective corresponding control groups (**Figure 8C)**.

With respect to LV diastolic function, Ang II 1.1mg/kg 14d mice displayed a 20.6% ($p<0.01$) reduced maximum LV pressure drop rate (dP/dt_{min}) compared with control 1.1mg/kg 14d mice and a 5.4% higher Tau, the latter without reaching significance **(Figure 8D and Figure 8E**).

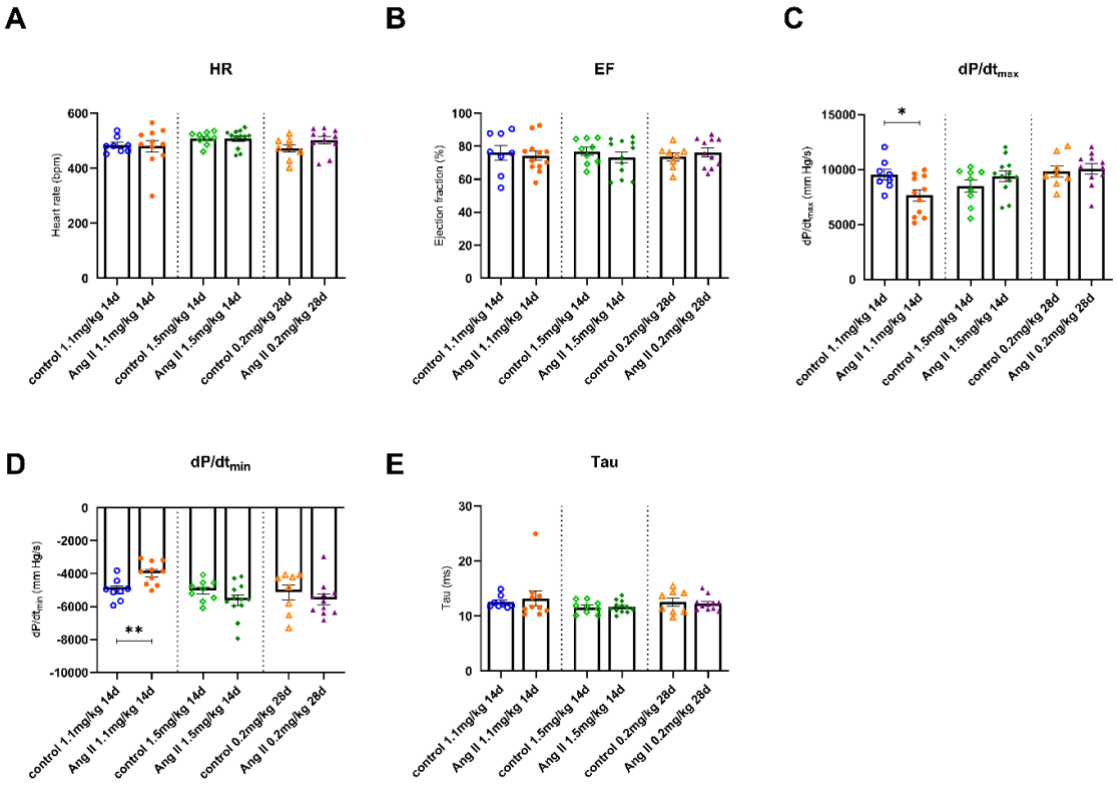

Figure 8. Impact of different doses or durations of Ang II on cardiac function in mice. All data are reported as the mean±SEM with n=8 in control 1.1 mg/kg 14d, n=12 in Ang II 1.1 mg/kg 14d, n=9 in control 1.5 mg/kg 14d, n=12 in Ang II 1.5 mg/kg 14d, n=8 in control 0.2 mg/kg 28d, n=12 in Ang II 0.2 mg/kg 28d. A nonparametric Mann–Whitney U test or a Welch's t test was performed for data comparison between each respective control vs. Ang II group. Ang II: Angiotensin II; d: day; SEM: standard error of the mean; HR: heart rate; bpm: beats per minute; EF: ejection fraction; dP/dt_{max}: maximum left ventricular pressure rise rate; dP/dt_{min}: maximum left ventricular pressure drop rate; Tau: time of the left ventricular pressure decrease; *p<0.05; **p<0.01.

3.2. Left ventricular fibrosis

3.2.1. Gene expression

In the comparison of LV Col1a1 mRNA expression, all Ang II mice had a weaker expression than the controls, but only the change in Ang II 1.1mg/kg 14d mice showed significant with 1.13-fold less than that of Control mice (P=0.0314) (**Figure 9A**). In the collagen type III alpha 1 chain (Col3a1) comparison, all Ang II mice displayed a slightly higher expression than the controls, but with no significance (**Figure 9B**).

The fibrosis-related factor, transforming growth factor beta (TGF-β), which induces fibroblast activation and differentiation of fibroblasts into myofibroblasts(105) was slightly higher expressed in Ang II 1.1mg/kg 14d mice versus controls, without reaching significance. A decreased expression of LV TGF-β was found in the rest of the examined Ang II groups versus their respective controls, but only showed significance in Ang II 1.5mg/kg 14d versus control 1.5mg/kg 14d mice(p<0.001) (**Figure 9C**).

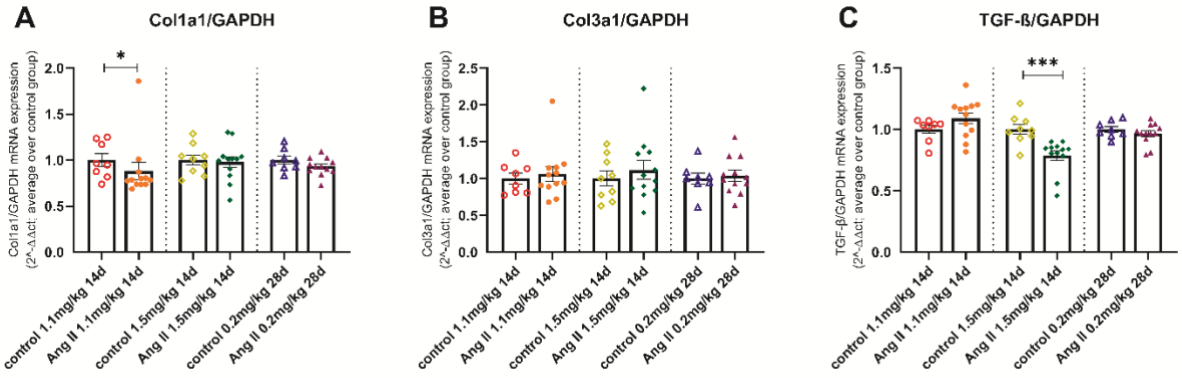

Figure 9. Impact of different doses or durations of Ang II on fibrosis-related mRNA of left ventricular in mice. The three different control and respective Ang II groups are separated with **black dotted lines**. Bar graphs represent the mean±SEM of expression, with n=8 in control 1.1 mg/kg 14d, n=12 in Ang II 1.1 mg/kg 14d, n=9 in control 1.5 mg/kg 14d, n=12 in Ang II 1.5 mg/kg 14d, n=8 in control 0.2 mg/kg 28d, n=12 in Ang II 0.2 mg/kg 28d. A nonparametric Mann–Whitney U test or a Welch's t test was performed for data comparison between each respective control vs. Ang II group. Col1a1: collagen type I alpha 1 chain; Col3a1: collagen type III alpha 1 chain; TGF-β: Transforming growth factor beta; GAPDH: Glyceraldehyde 3-phosphate dehydrogenase; Ang II: Angiotensin II; d: day; SEM: standard error of the mean; vs.: versus. For the whole graph panel with *p<0.05, ***p<0.001.

3.2.2. Immunohistological evidence

Following the evaluation of markers of cardiac fibrosis via gene expression analysis, we next analyzed LV protein collagen I expression via immunohistochemistry. The mean positive area of the extracellular matrix protein collagen I per mm^2 heart area was 3.6%,

6.7%, 5.8%, 6.8%, 6.2%, and 7.2% in the control 1.1mg/kg 14d, Ang II 1.1mg/kg 14d, control 1.5mg/kg 14d, control 1.5mg/kg 14d, control 0.2mg/kg 28d and Ang II 0.2mg/kg 28d groups, respectively (**Figure 10**).

All Ang II mice showed a stronger collagen I protein expression than their respective corresponding control mice, but only Ang II 1.1mg/kg 14d mice gained a significant difference (1.8-fold raise, $p<0.01$).

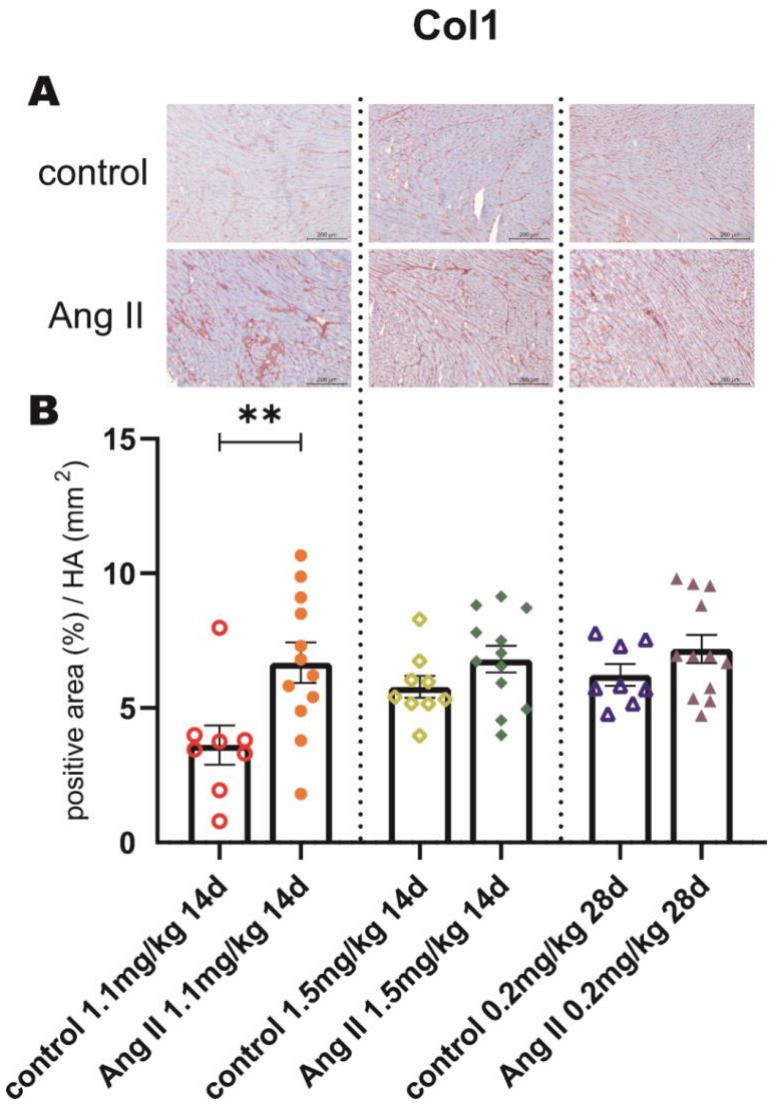

Figure 10. Impact of different doses or durations of Ang II on LV Col1 protein presence in mice. Representative Col1-stained LV sections (magnification ×100) of control (**A, upper half**) and respective Ang II groups (**A, lower half**) of 1.1 mg/kg 14d **(B, left)**, 1.5 mg/kg 14d **(B, middle**), and 0.2 mg/kg 28d **(B, right)** groups. The three different control and Ang II groups are separated with **black dotted lines**. Bar graphs represent the mean±SEM of Col1 positive area (%) per mm^2 HA with n=8 in control 1.1 mg/kg 14d, n=12 in Ang II 1.1 mg/kg 14d, n=9 in control 1.5 mg/kg 14d, n=12 in Ang II 1.5 mg/kg 14d, n=8 in control 0.2 mg/kg 28d, n=12 in Ang II 0.2 mg/kg 28d. A nonparametric Mann–Whitney U test or a Welch's t test was performed for data comparison between each respective control vs. Ang II group. Col1: Collagen 1; Ang II: Angiotensin II; LV: left ventricular; d: day; SEM: standard error of the mean; HA: heart area; vs.: versus. For the whole graph panel with **p<0.01.

3.3. Left ventricular vascular density

α-SMA is often used as a marker to identify arteries and arterioles(106). Data show that arterioles were 1.1-fold ($p<0.05$) and 1.1-fold ($p<0.005$) higher in Ang II 1.1mg/kg 14d Ang II and 1.5mg/kg 14d mice compared to their respective controls, **(Figure 11A)**. In parallel, arteries were 1.2-fold ($p<0.005$) and 1.2-fold ($p<0.005$) higher in those Ang II groups versus their respective controls **(Figure 11B)**. In contrast, LV VEGF mRNA expression was lower in the first two Ang II groups compared to their controls, reaching only significance ($p<0.005$) in Ang II 1.5mg/kg 14d versus control 1.5mg/kg 14d mice **(Figure 11C)**.

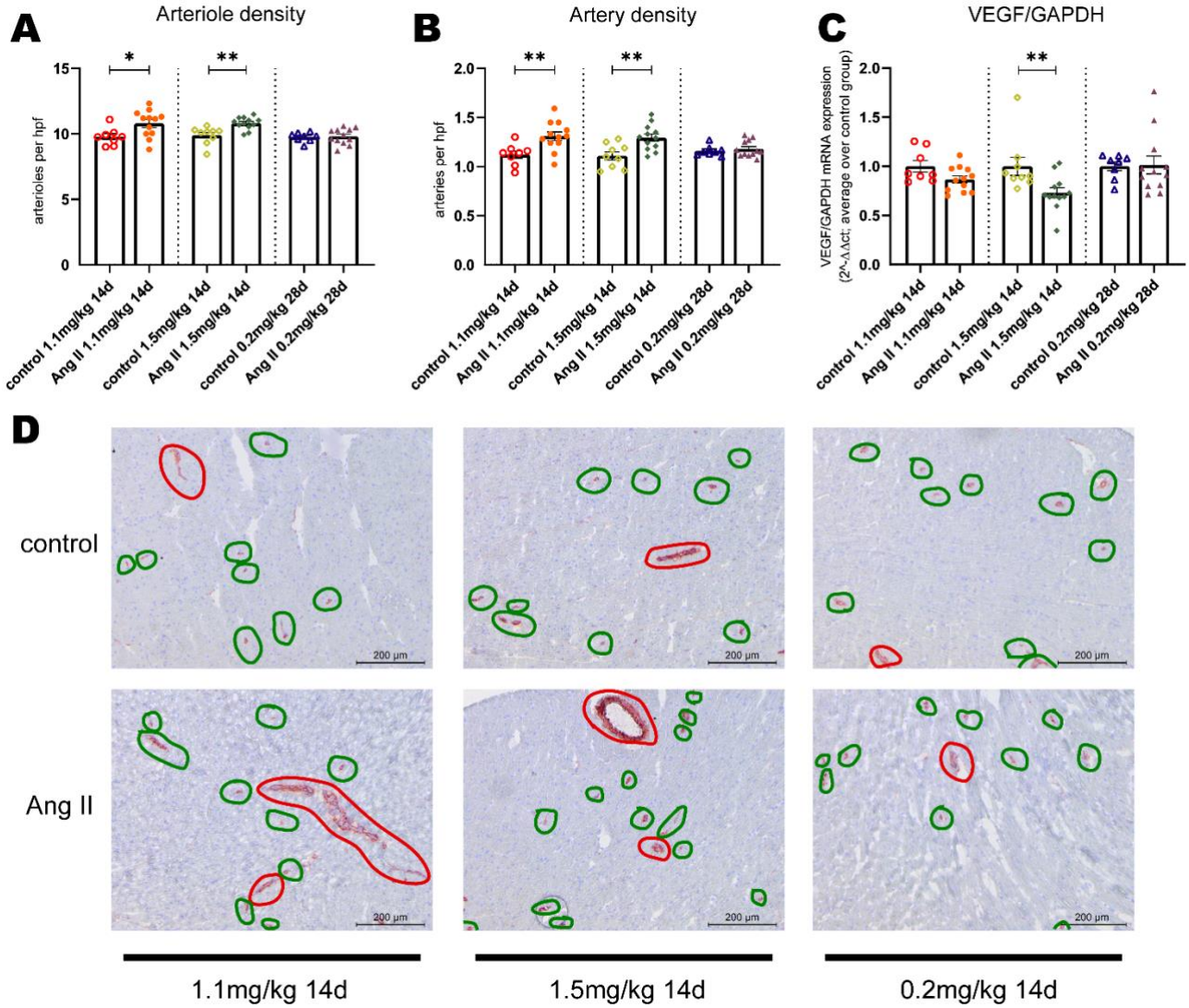

Figure 11. Impact of different doses or durations of Ang II on vascular density and VEGF mRNA expression in mice. The three different control and respective Ang II groups are separated with black dotted lines **(A, B and C)**. Representative α-SMA-stained LV sections (magnification ×100) of control (**D, upper half**) and Ang II groups (**D, lower half**) of 1.1 mg/kg 14d **(D, left)**, 1.5 mg/kg 14d **(D, middle**), and 0.2 mg/kg 28d **(D, right)** groups. Bar graphs represent the mean±SEM of expression, with n=8 in control 1.1 mg/kg 14d, n=12 in Ang II 1.1 mg/kg 14d, n=9 in control 1.5 mg/kg 14d, n=12 in Ang II 1.5 mg/kg 14d,

n=8 in control 0.2 mg/kg 28d, n=12 in Ang II 0.2 mg/kg 28d. A nonparametric Mann–Whitney U test or a Welch's t test was performed for data comparison between each respective control vs. Ang II group. Red and green circles indicate arteries and arterioles, respectively.α-SMA: Alpha-smooth muscle actin; VEGF: Vascular endothelial growth factor; GAPDH: Glyceraldehyde 3-phosphate dehydrogenase; Ang II: Angiotensin II; d: day; hpf: high power field; SEM: standard error of the mean; vs.: versus. For the whole graph panel with *p<0.05, **p<0.01.

3.4. Left ventricular hypertrophy

Since Ang II is an important inducer of LV hypertrophy (107), we next evaluated LV mRNA expression of the hypertrophy-related genes myosin heavy chain 7B (Myh7b) and actin alpha 1, skeletal muscle (Acta1). LV Myh7b mRNA expression was not different among the Ang II and respective control groups, whereas, 2.2-fold (p<0.005) and 2.0-fold (p<0.005) higher LV Acta1 mRNA expression could be observed in Ang II 1.1mg/kg 14d and Ang II 0.2mg/kg 28d mice versus their respective controls. The slight increase (1.4-fold) in LV Acta 1 mRNA expression in Ang II 1.5mg/kg 14d did not reach significance versus their controls **(Figure 12).**

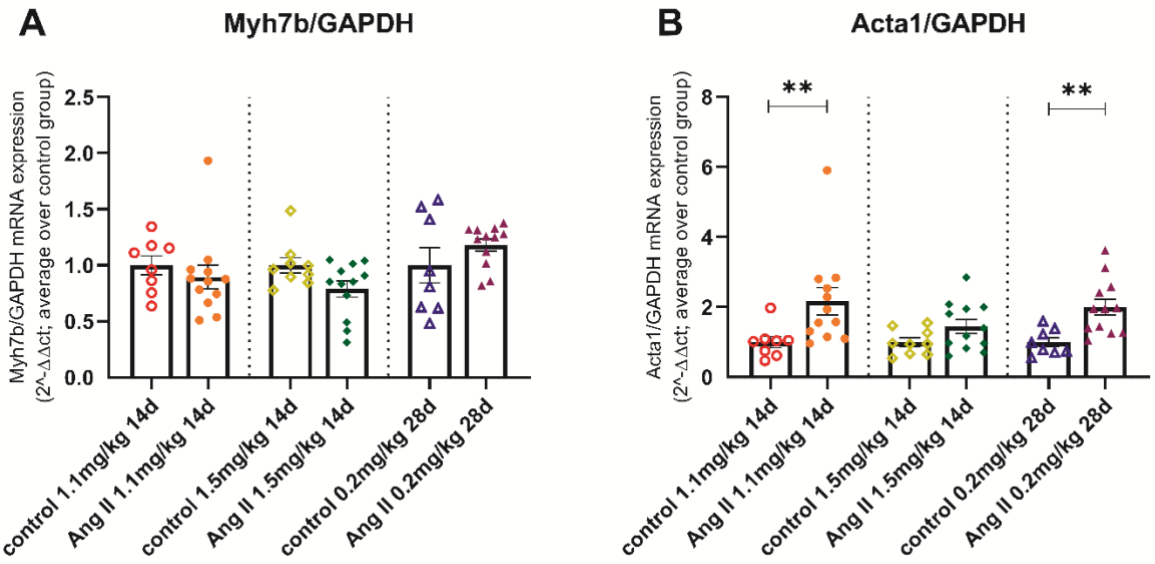

Figure 12. Impact of different doses or durations of Ang II on left ventricular mRNA expression of hypertrophy-related genes. The three different control and respective Ang II groups are separated with **black dotted lines**. Bar graphs represent the mean±SEM of expression, with n=8 in control 1.1 mg/kg 14d, n=12 in Ang II 1.1 mg/kg 14d, n=9 in control 1.5 mg/kg 14d, n=12 in Ang II 1.5 mg/kg 14d, n=8 in control 0.2 mg/kg 28d, n=12 in Ang II 0.2 mg/kg 28d. A nonparametric Mann–Whitney U test or a Welch's t test was performed for data comparison between each respective control vs. Ang II group. Myh7b: Myosin Heavy Chain 7B; Acta1: Actin Alpha 1, Skeletal Muscle; GAPDH: Glyceraldehyde 3-phosphate dehydrogenase; Ang II: Angiotensin II; d: day; SEM: standard error of the mean; vs.: versus. For the whole graph panel with **p<0.01.

3.5. Angiotensin II receptor type 1

Expression levels of the angiotensin II receptor type 1 (AT1R) define the biological efficacy of Ang II. To get first indications about the biological efficacy of Ang II in the different Ang II models, we examed the AT1R expression in each experimental group. LV AT1R mRNA expression was slightly increased (1.2-fold and 1.1-fold) in Ang II 1.1mg/kg 14d and Ang II 0.2mg/kg 28d mice compared to their respective controls, without reaching significance, whereas Ang II 1.5mg/kg 14d mice exhibited 1.3-fold ($p>0.05$) lower LV AT1R levels compared to their controls (**Figure 13**).

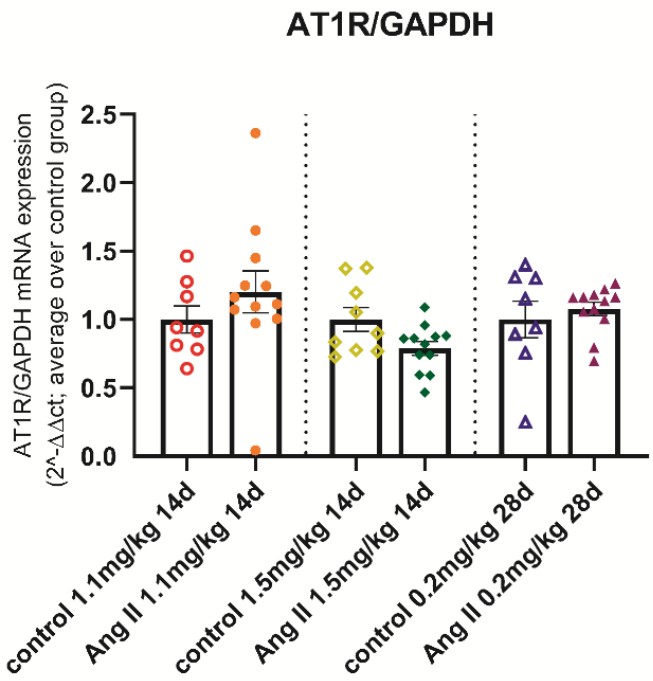

Figure 13. Impact of different doses or durations of Ang II on left ventricular AT1R mRNA expression in mice. The three different control and respective Ang II groups are separated with **black dotted lines**. Bar graphs represent the mean±SEM of expression, with n=8 in control 1.1 mg/kg 14d, n=12 in Ang II 1.1 mg/kg 14d, n=9 in control 1.5 mg/kg 14d, n=12 in Ang II 1.5 mg/kg 14d, n=8 in control 0.2 mg/kg 28d, n=12 in Ang II 0.2 mg/kg 28d. A nonparametric Mann–Whitney U test or a Welch's t test was performed for data comparison between each respective control vs. Ang II group. AT1R: Angiotensin II Receptor Type 1; GAPDH: Glyceraldehyde 3-phosphate dehydrogenase; Ang II: Angiotensin II; d: day; SEM: standard error of the mean; vs.: versus.

3.6. Left ventricular Inflammation

3.6.1. Gene expression

3.6.1.1. S100A8, S100A9, TLR4 and RAGE

S100 calcium-binding protein A8 (S100A8) and S100 calcium-binding protein A9 (S100A9) are members of the innate immunity and mediate the inflammatory response. They bind to toll-like receptor 4 (TLR4) and receptor for advanced glycosylation end products (RAGE), activating the MAP-kinase and NF-kappa-B signaling pathways and resulting in the amplification of the proinflammatory cascade. Given the relevance of S100A8 and S100A9 in different cardiac diseases (103, 108), we next evaluated their LV mRNA expression as well as of the LV mRNA expression of their receptors, TLR4 and RAGE (**Figure 14**) .

LV S100A8 and S100A9 mRNA expression tended to be increased in Ang II 1.1mg/kg versus control 1.1.mg/kg mice (2.6-fold and 3.1-fold, respectively ($P>0.05$)), whereas in the other Ang II regimens, there was clearly no regulation in LV S100A8 and S100A9 expression. LV TLR4 and RAGE expression was not changed following Ang II, under none oft he different conditions (**Figure 14**).

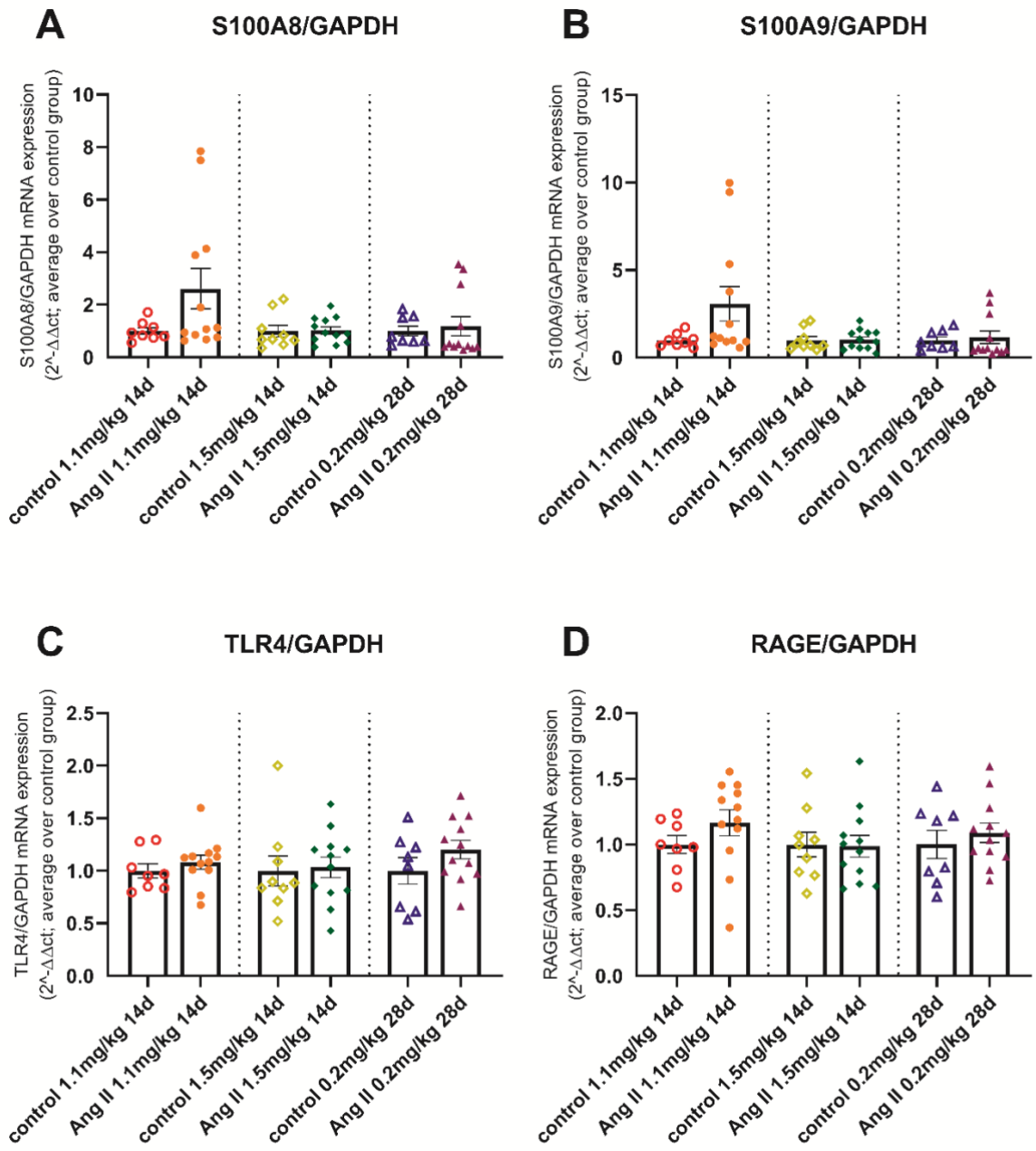

Figure 14. Impact of different doses or durations of Ang II on left ventricular S100A8, S100A9, TLR4 and RAGE mRNA expression of in mice. The three different control and respective Ang II groups are separated with **black dotted lines**. Bar graphs represent the mean±SEM of expression, with n=8 in control 1.1 mg/kg 14d, n=12 in Ang II 1.1 mg/kg 14d, n=9 in control 1.5 mg/kg 14d, n=12 in Ang II 1.5 mg/kg 14d, n=8 in control 0.2 mg/kg 28d, n=12 in Ang II 0.2 mg/kg 28d. A nonparametric Mann–Whitney U test or a Welch's t test was performed for data comparison between each respective control vs. Ang II group. S100A8: S100 Calcium Binding Protein A8; S100A9: S100 Calcium Binding Protein A9; TLR4: Toll-Like Receptor 4; RAGE: Receptor For Advanced Glycosylation End Products; GAPDH: Glyceraldehyde 3-phosphate dehydrogenase; Ang II: Angiotensin II; d: day; SEM: standard error of the mean; vs.: versus.

3.6.1.2. Cytokines

Next, the impact of Ang II on LV cytokine mRNA expression was investigated. Real-time PCR analysis revealed that LV mRNA of the anti-inflammatory cytokine interleukin (IL)-10 (**Figure 15A**), and the pro-inflammatory cytokines IL-1ß (**Figure 15B**), IL-6 (**Figure 15C**), and TNF-α (**Figure 15D**) were not altered in none of the different Ang II regimens compared to control mice.

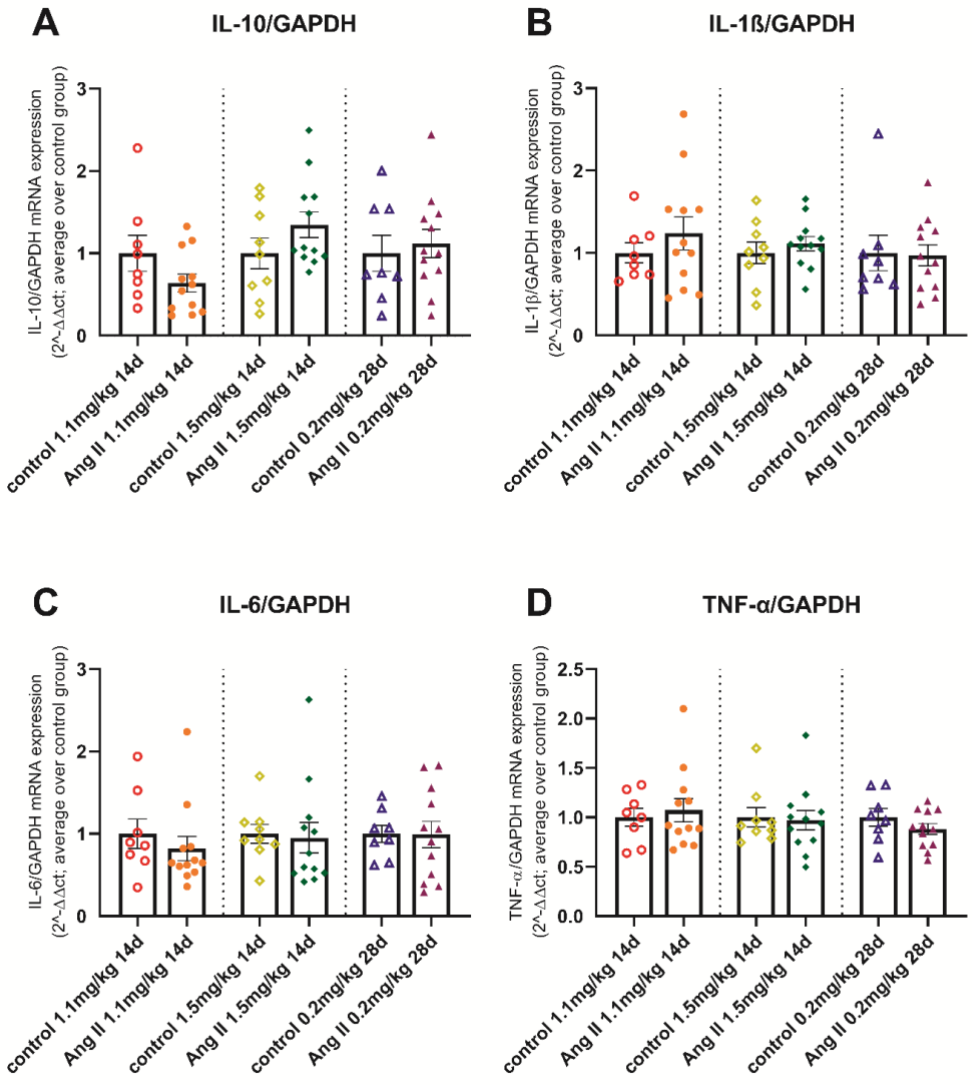

Figure 15. Impact of different doses or durations of Ang II on left ventricular cytokine mRNA expression in mice. The three different control and respective Ang II groups are separated with black dotted lines. Bar graphs represent the mean±SEM of expression, with n=8 in control 1.1 mg/kg 14d, n=12 in Ang II 1.1 mg/kg 14d, n=9 in control 1.5 mg/kg 14d, n=12 in Ang II 1.5 mg/kg 14d, n=8 in control 0.2 mg/kg 28d, n=12 in Ang II 0.2 mg/kg 28d. A nonparametric Mann–Whitney U test or a Welch's t test was performed for data comparison between each respective control vs. Ang II group. IL-10: Interleukin-10; IL-1β: Interleukin-1β; IL-6: Interleukin-6; TNF-α: Tumor-Necrosis Factor-α; GAPDH: Glyceraldehyde 3-phosphate dehydrogenase; Ang II: Angiotensin II; d: day; SEM: standard error of the mean; vs.: versus.

3.6.1.3. Chemokines

Evaluation of the LV gene expression of the chemokines C-C Motif Chemokine Ligand (CCL) 2, CCL5, CCL7 and C-X3-C Motif Chemokine Ligand 1 (CX3CL) 1 showed that CCL2 was 1.3-fold ($p<0.05$) and 1.4-fold ($p<0.05$) reduced in Ang II 1.5mg/kg 14d and Ang II 0.2mg/kg 28d compared to their respective controls (**Figure 16A**). LV CCL5 an CCL7 mRNA expression was not altered in the different Ang II groups (**Figure 16B and Figure 16C**), whereas LV CX3CL1 was 1.2-fold ($p<0.01$) and 1.3-fold ($p<0.01$) lower expressed in Ang II 1.1mg/kg 14d and Ang II 1.5mg/kg 14d mice compared to their controls, respectively (**Figure 16D**).

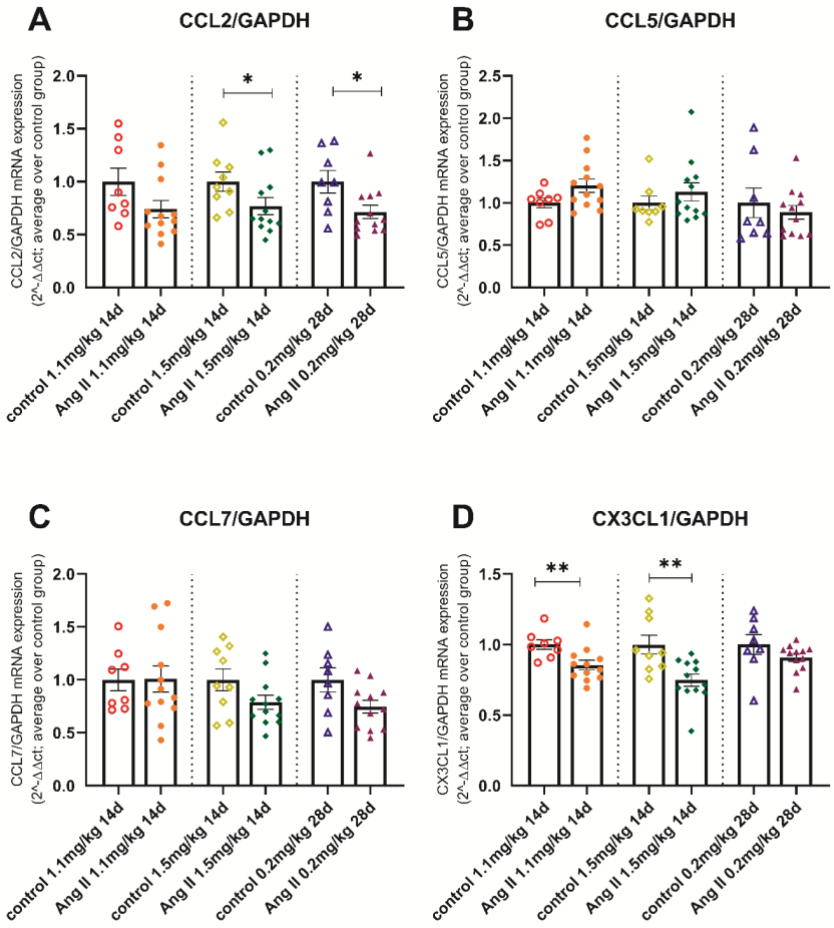

Figure 16. Impact of different doses or durations of Ang II on left ventricular chemokine expression in mice. The three different control and respective Ang II groups are separated with black dotted lines. Bar graphs represent the mean±SEM of expression, with n=8 in control 1.1 mg/kg 14d, n=12 in Ang II 1.1 mg/kg 14d, n=9 in control 1.5 mg/kg 14d, n=12 in Ang II 1.5 mg/kg 14d, n=8 in control 0.2 mg/kg 28d, n=12 in Ang II 0.2 mg/kg 28d. A nonparametric Mann–Whitney U test or a Welch's t test was performed for data comparison between each respective control vs. Ang II group. CCL2: C-C Motif Chemokine Ligand 2; CCL5: C-C Motif Chemokine Ligand 5; CCL7: C-C Motif Chemokine Ligand 7; CX3CL1: C-X3-C Motif Chemokine Ligand 1; GAPDH: Glyceraldehyde 3-phosphate dehydrogenase; Ang II: Angiotensin II; d: day; SEM: standard error of the mean; vs.: versus; For the whole graph panel with *p<0.05 and **p<0.01.

3.6.2. Left ventricle immune cell presence

Compared with control 1.1mg/kg 14d mice, Ang II 1.1mg/kg 14d displayed 1.6-fold ($p<0.05$) higher CD4 cells in the LV., whereas Ang II 1.5mg/kg 14d mice exhibited 1.7-fold ($p<0.001$) higher LV CD4 cells than control 1.5mg/kg 14d mice. LV CD4 cells were 1.3-fold ($p<0.05$) higher in Ang II 0.2mg/kg 28d mice compared to control 0.2mg/kg 28d (**Figure 17**)**.**

Related to CD8a cells, no difference in LV presence was found in Ang II 1.1mg/kg 14d versus control 1.1mg/kg 14d mice. LV CD8a cell presence was 2.3-fold ($p<0.0005$) and 1.5-fold ($p<0.05$) increased in Ang II 1.5mg/kg 14d and Ang II 0.2mg/kg 28d mice versus their respective controls (**Figure 18**)**.**

In contrast to CD4 and CD8a cells, CD68 cells were not increased in any of the Ang II groups versus their respective controls (**Figure 19**)**.**

LV Ly6g cells were only increased in, Ang II 1.1mg/kg 14d mice (1.3-fold; $p<0.05$) versus control 1.1mg/kg 14d. The other Ang II regimens did not influence LV Ly6g cell count (**Figure 20**)**.**

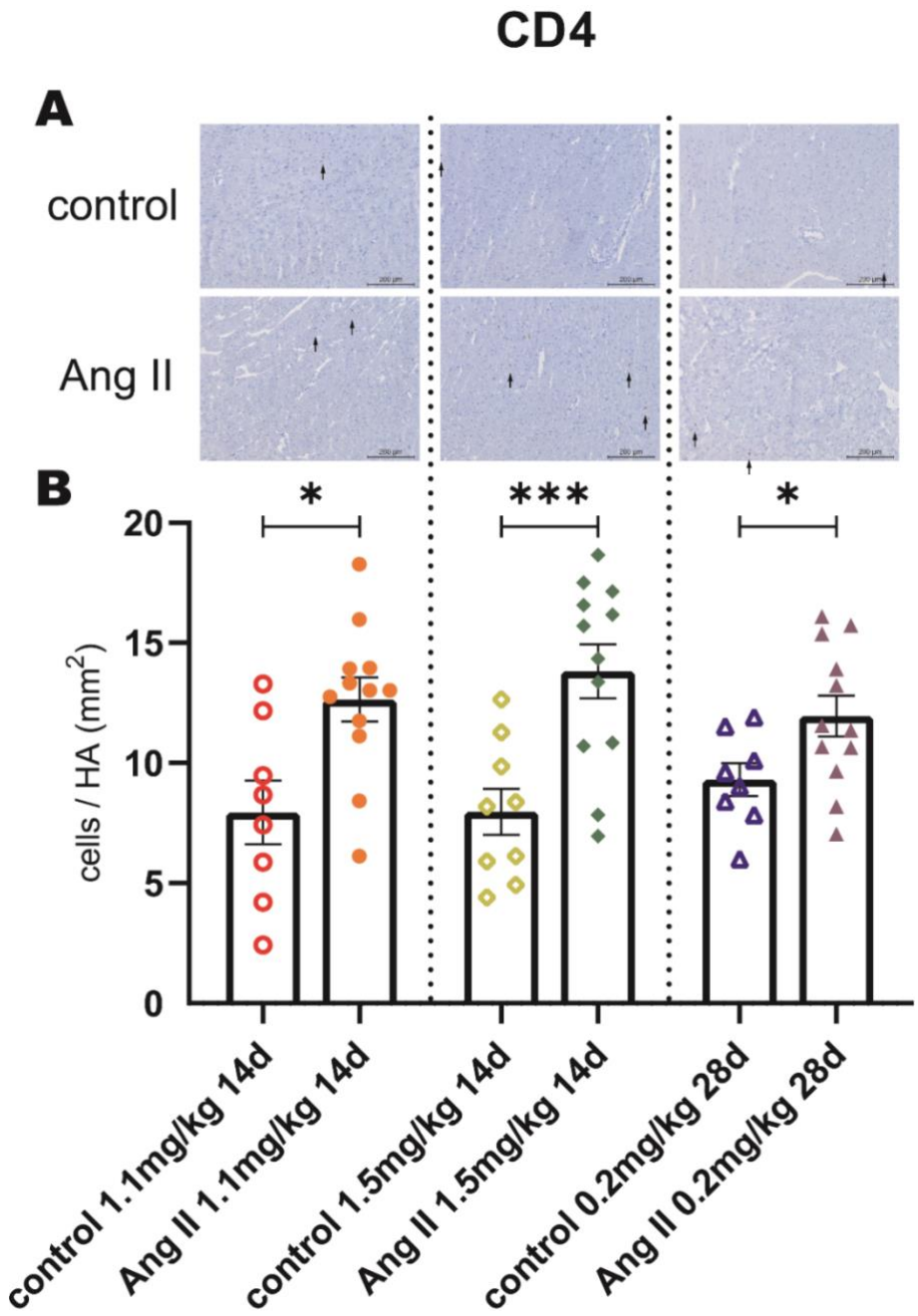

Figure 17. Impact of different doses or durations of Ang II on LV CD4⁺ cells presence in mice. Representative CD4-stained LV sections (magnification ×100) of control (**A, upper half**) and respective Ang II groups (**A, lower half**) of 1.1 mg/kg 14d **(B, left)**, 1.5 mg/kg 14d **(B, middle**), and 0.2 mg/kg 28d **(B, right)** groups. The three different control and Ang II groups are separated with black dotted lines. Bar graphs represent the mean±SEM of $CD4^+$ cells per mm^2 HA with n=8 in control 1.1 mg/kg 14d, n=12 in Ang II 1.1 mg/kg 14d, n=9 in control 1.5 mg/kg 14d, n=12 in Ang II 1.5 mg/kg 14d, n=8 in control 0.2 mg/kg 28d, n=12 in Ang II 0.2 mg/kg 28d. A nonparametric Mann–Whitney U test or a Welch's t test was performed for data comparison between each respective control vs. CD4: cluster of differentiation 4; Ang II group. Ang II: Angiotensin II; LV: left ventricular; d: day; SEM: standard error of the mean; HA: heart area; vs.: versus. For the whole graph panel with *p<0.05 and ***p<0.001.

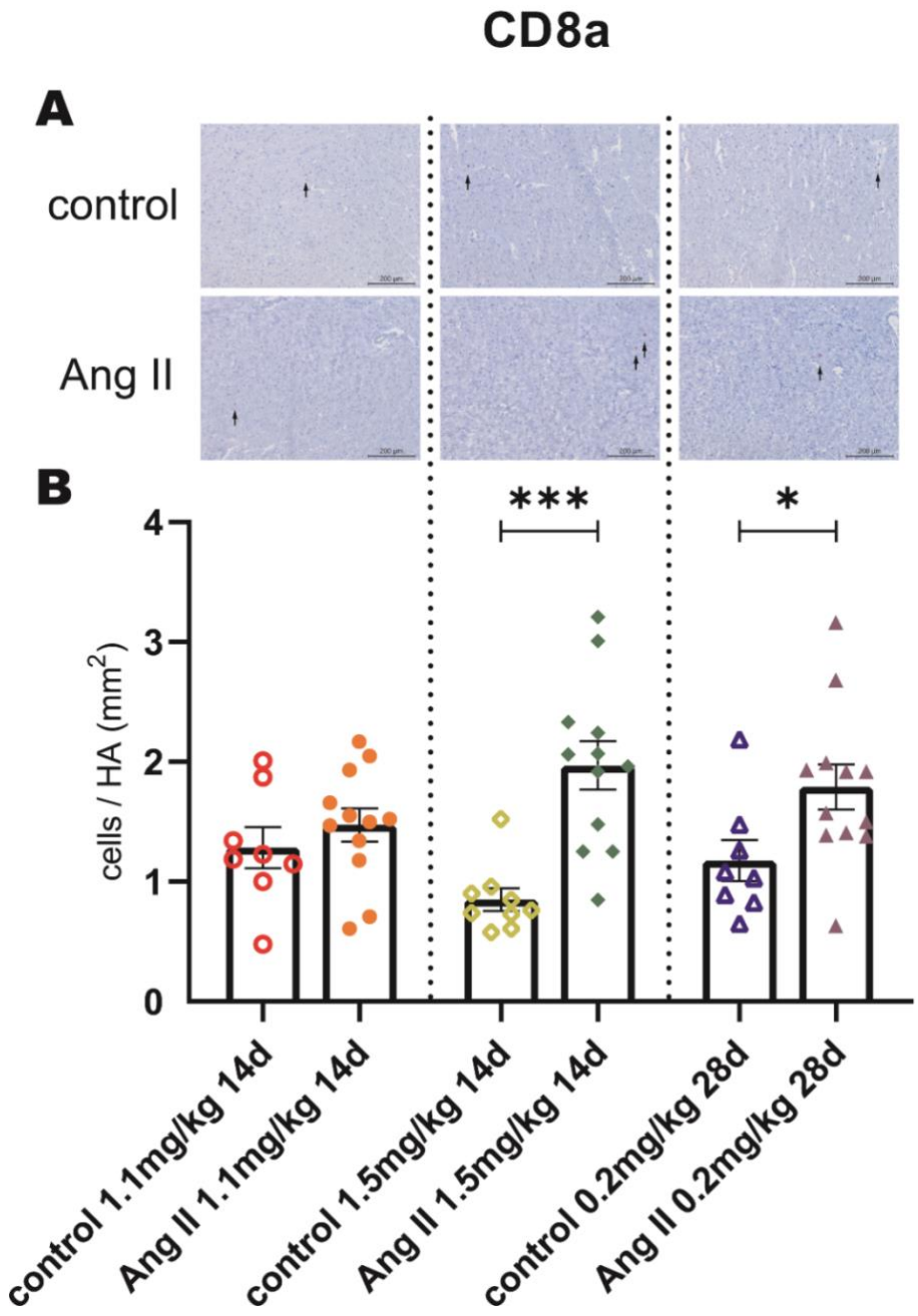

Figure 18. Impact of different doses or durations of Ang II on LV CD8a$^+$ cells presence in mice. Representative CD8a-stained LV sections (magnification ×100) of control (**A, upper half**) and respective Ang II groups (**A, lower half**) of 1.1 mg/kg 14d **(B, left)**, 1.5 mg/kg 14d **(B, middle**), and 0.2 mg/kg 28d **(B, right)** groups. The three different control and Ang II groups are separated with black dotted lines. Bar graphs represent the mean±SEM of CD8a$^+$ cells per mm^2 HA with n=8 in control 1.1 mg/kg 14d, n=12 in Ang II 1.1 mg/kg 14d, n=9 in control 1.5 mg/kg 14d, n=12 in Ang II 1.5 mg/kg 14d, n=8 in control 0.2 mg/kg 28d, n=12 in Ang II 0.2 mg/kg 28d. A nonparametric Mann–Whitney U test or a Welch's t test was performed for data comparison between each respective control vs. Ang II group. CD8a: cluster of differentiation 8a; Ang II: Angiotensin II; LV: left ventricular; d: day; SEM: standard error of the mean; HA: heart area; vs.: versus. For the whole graph panel with *p<0.05 and ***p<0.001.

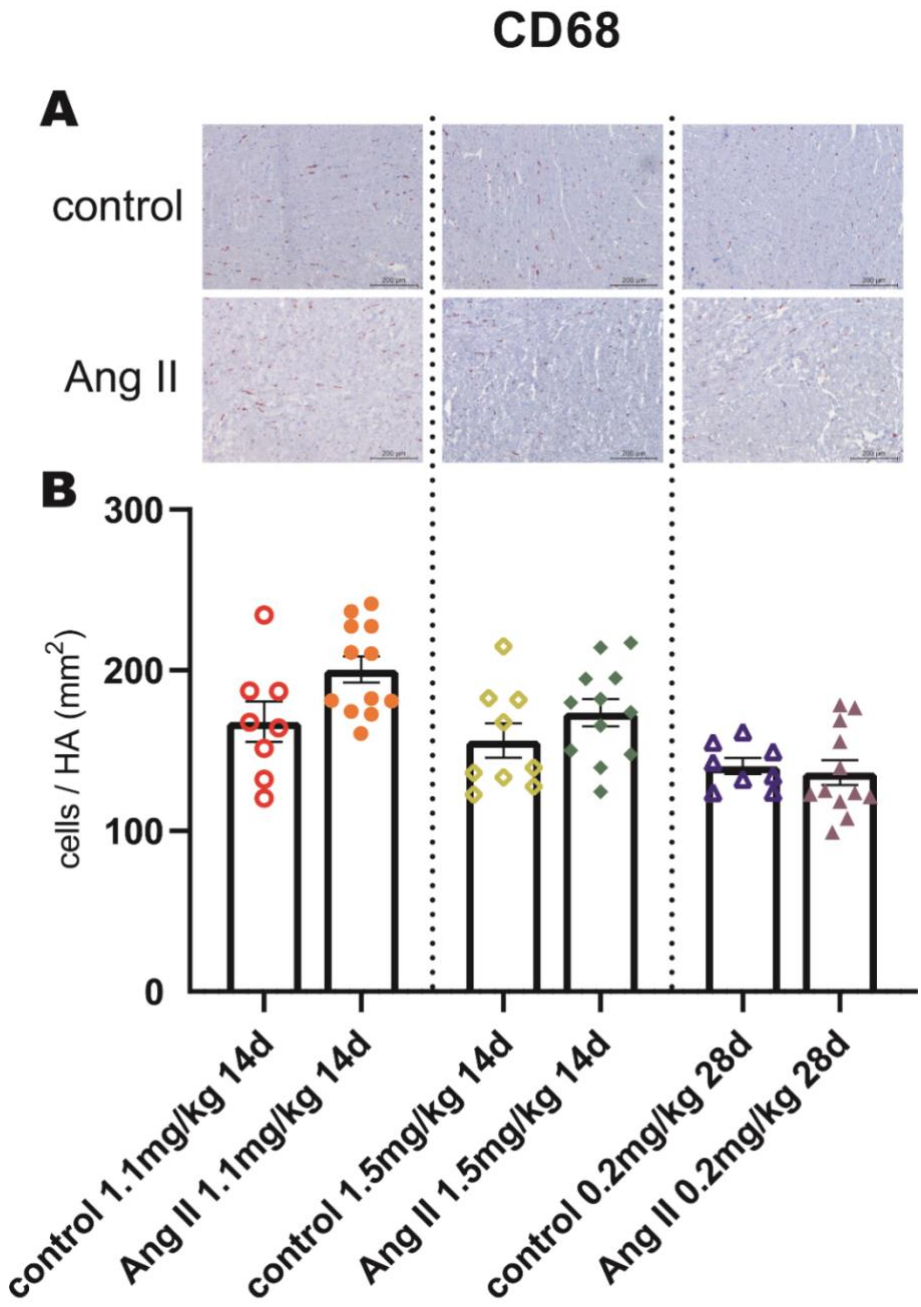

Figure 19. Impact of different doses or durations of Ang II on LV CD68⁺ cells presence in mice. Representative CD68-stained LV sections (magnification ×100) of control (**A, upper half**) and respective Ang II groups (**A, lower half**) of 1.1 mg/kg 14d **(B, left)**, 1.5 mg/kg 14d **(B, middle**), and 0.2 mg/kg 28d **(B, right)** groups. The three different control and Ang II groups are separated with black dotted lines. Bar graphs represent the mean±SEM of $CD68^+$ cells per mm^2 HA with n=8 in control 1.1 mg/kg 14d, n=12 in Ang II 1.1 mg/kg 14d, n=9 in control 1.5 mg/kg 14d, n=12 in Ang II 1.5 mg/kg 14d, n=8 in control 0.2 mg/kg 28d, n=12 in Ang II 0.2 mg/kg 28d. A nonparametric Mann–Whitney U test or a Welch's t test was performed for data comparison between each respective control vs. Ang II group. CD68: cluster of differentiation 68; Ang II: Angiotensin II; LV: left ventricular; d: day; SEM: standard error of the mean; HA: heart area; vs.: versus.

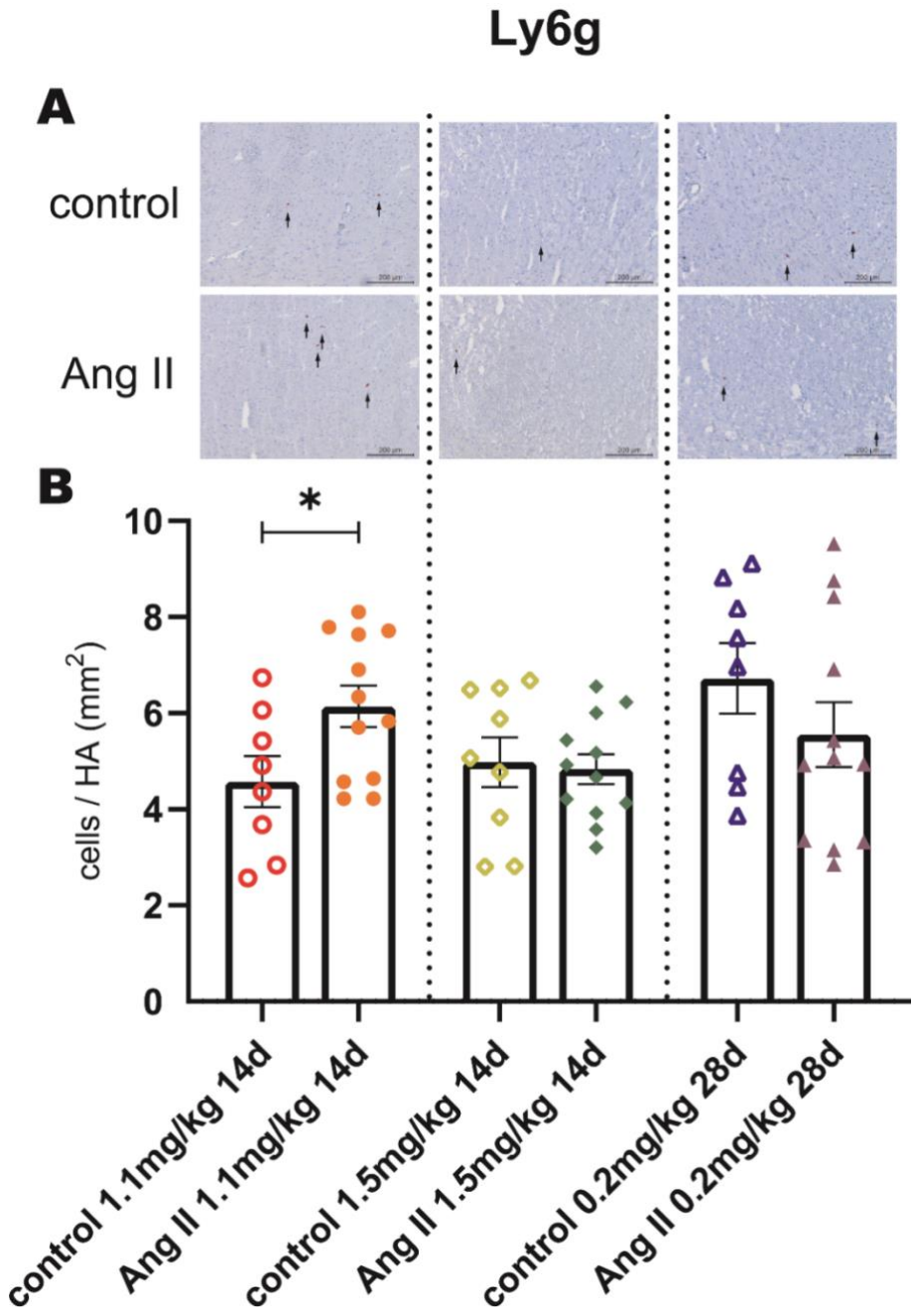

Figure 20. Impact of different doses or durations of Ang II on LV Ly6g$^+$ cells presence in mice. Representative Ly6g-stained LV sections (magnification ×100) of control (**A, upper half**) and Ang II groups (**A, lower half**) of 1.1 mg/kg 14d **(B, left)**, 1.5 mg/kg 14d **(B, middle**), and 0.2 mg/kg 28d **(B, right)** groups. The three different control and Ang II groups are separated with **black dotted lines**. Bar graphs represent the mean±SEM of Ly6g$^+$ cells per mm^2 HA with n=8 in control 1.1 mg/kg 14d, n=12 in Ang II 1.1 mg/kg 14d, n=9 in control 1.5 mg/kg 14d, n=12 in Ang II 1.5 mg/kg 14d, n=8 in control 0.2 mg/kg 28d, n=12 in Ang II 0.2 mg/kg 28d. A nonparametric Mann–Whitney U test or a Welch's t test was performed for data comparison between each respective control vs. Ang II group. Ly6g: Lymphocyte antigen 6 complex locus G6D; Ang II: Angiotensin II; LV: left ventricular; d: day; SEM: standard error of the mean; HA: heart area; vs.: versus. For the whole graph panel with *p<0.05.

4. Discussion

HFpEF is characterized by signs and symptoms of HF in the presence of a normal LVEF. Although HFpEF accounts for more than half of all clinical manifestations of HF, underlying pathomechanisms of HFpEF are still incompletely understood, and there is no effective treatment so far(109). At present, access to human samples is limited and existing HFpEF animal models imperfect, which impedes our understanding of the underlying mechanisms of HFpEF. Among the current animal model methods, Ang II-infused mice have been recognized as a model to mimic the human HFpEF phenotype(60). Though, the optimal dose and duration of Ang II application is still unknown and under intense discussion.

Murdoch et al. used an Ang II dose of 1.1 mg/kg per day for 14 days in wild-type mice. They found that this dose of Ang II can induce myocardial fibrosis and myocyte hypertrophy resulting in a diastolic dysfunction phenotype(70). Mori et al. utilized an Ang II dose of 1.5 mg/kg per day in 9-week-old male C57/BL6 wild-type mice for 14 days. Their study also showed that Ang II can induce pathological cardiac hypertrophy and LV diastolic dysfunction(97). Regan et al. implemented an Ang II dose of 0.2 mg/kg per day in 8-week-old outbred male CD1 mice for 28 days. They found that this dose and duration of Ang II can induce cardiomyocyte hypertrophy and interstitial myocardial fibrosis, and reproduce the HFpEF features of impaired LV relaxation and increased LV elastance(73). The data in their experiments were sufficient to support their conclusions. However, some hemodynamic parameter results were inconsistent or still disputed across the three studies (potentially caused by the different strains of mice), especially dP/dt_{max}, dP/dt_{min}, and τ, which are key indicators for evaluating systolic (98, 99) and diastolic function(99-101). Therefore, in this study, we compared the three Ang II dose regimens of the above studies in parallel, avoiding differences in external factors, in the same mouse background, with the aim to investigate the above-mentioned controversial parameters, and to compare markers of fibrosis, hypertrophy, and inflammation to discuss, which dose of Ang II might be of better choice to mimic HFpEF.

4.1. Hemodynamics

HFpEF denotes the signs and symptoms of clinical HF in a patient with a normal LVEF and LV diastolic dysfunction(110). Our data showed that the HR and LVEF of all Ang II

mice were at a healthy level, which were the prerequisite for the successful production of HFpEF animal models.

LVEF is a weak and nonspecific index of contractile function. Studies evaluating load-independent measures of the chamber and myocardial contractile function have shown that there are decreases in systolic function in patients with HFpEF compared with age-matched healthy controls as well as asymptomatic hypertensives(12). This finding of impaired systolic function has been confirmed in numerous studies utilizing tissue Doppler and strain imaging techniques(14, 36). Abnormalities in LV systolic properties are strongly associated with adverse outcomes in patients with HFpEF(12, 37). Inability to augment systolic function also begets and worsens diastolic reserve in HFpEF(38). These relatively mild abnormalities in systolic function at rest become much more significant during exercise, which further stresses an already-compromised heart(38).

Among the different Ang II groups, only Ang II 1.1mg/kg 14d mice established an impairment in systolic function as indicated by a reduced dP/dt_{max} compared to control 14d mice. Related to diastolic function, dP/dt_{min} was reduced in Ang II 1.1mg/kg 14d mice compared to its control group. Whereas the marker of diastolic stiffness Tau only tended to be higher ($p= 0.3154$). The diastolic function indexes of Ang II 1.5mg/kg 14d and Ang II 0.2mg/kg 28d mice were similar to their specific control groups.

The previous three studies(70, 73, 97) have proven that each of the three doses of Ang II could induce HFpEF, but the mice used and external factors were not uniform in their studies, and some of the hemodynamic results were dispute. The hemodynamics studied in this research mainly involved the controversial parameters in the previous three studies. We applied the same strain of mice, exhibited to identical external factors to allow a better horizontal comparison of three dose regimens of Ang II. Based on the parameters examined in our study, Ang II 1.1mg/kg 14d mice had a normal LVEF with characteristics of impaired systolic and diastolic function, which are necessary for a HFpEF model. It can be concluded that Ang II 1.1mg/kg 14d mice were eligible to compete for a HFpEF model.

Nevertheless, it should be addressed that Tau in our Ang II 1.1mg/kg 14d mice was consistent with Murdoch et al.(70), but inconsistent with Regan et al.(73). This might be explained due to differences in strains of mice with different genetic backgrounds we used compared to Regan et al.(111), which affect the results of Ang II-induced animal

models(112). Furthermore, differences in housing conditions may also alter the immune status of mice(113, 114) and consequently change the AngII-induced outcome.

4.2. Fibrosis

Collagen is the most abundant extracellular protein found within the myocardium(115). It is responsible for the vast majority of the mechanical strength of the matrix, while also transmitting the force generated by myocytes. More specifically, type I collagen represents 85% of the collagen content found within the myocardium(116). Kasner and colleagues(117) found correlations between LV filling index E/E' and the degree of myocardial collagen amount, collagen cross-linking, and expression of LOX in HFpEF patients, and demonstrated that cardiac fibrosis-associated LV compliance disturbances contribute to the lower cardiac performance in HFpEF. Mohammed et al. investigated 124 HFpEF patients and 104 age-appropriate control patients and confirmed that HFpEF patients had more myocardial fibrosis than controls(118). In HFpEF, an increase in the amount of collagen is observed with a corresponding increment in the width and continuity of the fibrillar components of the extracellular matrix(15, 69). While there is typically more interstitial fibrosis in HFpEF than healthy controls, the differences are not invariably striking, and many patients may not show marked evidence of fibrosis(118). TGF-β is a pleiotropic mediator with potent and diverse effects on many cell types involved in cardiac fibrosis. TGF-β can induce the transformation from fibroblasts to myofibroblasts(119, 120).

In our study, immunohistochemistry results showed that the expression of collagen 1 (Col1) protein in Ang II 1.1mg/kg 14d was higher than that in its control group, whereas Ang II 1.5 mg/kg 14d and Ang II 0.2 mg/kg 28d mice did not exhibit higher LV Col1 expression than that in their specific control group.

In parallel to the increased Col1 protein expression, Col1a1 mRNA was reduced in Ang II 1.1mg/kg 14d mice compared to the control group. This observation is in agreement with Van Linthout et al., who found that cardiac fibrosis is associated with decreased collagen type I mRNA expression under STZ-diabetic and non-LV dilatation conditions(121) and can be explained by the fact that the presence of collagen can reverse regulate the expression of collagen-related genes (negative feedback loop), LV Col3a1 mRNA expression was increased in none of the Ang II groups compared to the respective controls. LV mRNA expression of the pro-fibrotic factor TGF-β was not

increased in Ang II 1.1mg/kg 14d versus control mice, suggesting that the elevated Col1 deposition in Ang II 1.1mg/kg 14d mice might be the result of pro-fibrotic signaling which occurred within the previous 14 days or of an impaired degradation via matrix metalloproteinases.

4.3. LV hypertrophy

LV concentric remodeling or hypertrophy is one of the hallmarks of HFpEF(122). Forced expression of Myh7b protein in the mouse heart was reported causing severe dilated cardiomyopathy(123), whereas Myh7b expression is decreased in cardiac hypertrophy, (124). Chen's team demonstrated that Myh7b knockout triggered hypertrophic cardiomyopathy by activation of the CaMK-signaling pathway(125). Interestingly, LV Myh7b expression was not differently expressed in Ang II groups compared with their corresponding controls.

The Acta1 gene encodes the protein called skeletal alpha (α)-actin, which is part of the actin protein family. Actin proteins are important for cell movement and the tensing of muscle fibers (muscle contraction). Conform to our findings that Ang II 1.1mg/kg 14d represents the best HFpEF model of all Ang II investigated models, LV mRNA expression of the typical hypertrophy marker Acta1(126, 127) was increased in Ang II 1.1mg/kg 14d. Though, an increase in LV Acta1 mRNA expression could also be detected in Ang II 0.2mg/kg 28d mice versus their respective controls.

LV hypertrophy is usually accompanied by alterations in microvascular density(128). In this case, the cardiac microvasculature may undergo compensatory growth, which was also shown in our experiments. In our study, we observed that the (micro)vascular density increased in both Ang II 1.1mg/kg 14d and Ang II 1.5mg/kg 14d, versus their respective control mice. This was associated with lower LV VEGF mRNA expression compared to respective controls. This might be explained by a negative feedback loop, but the specific reasons need to be further studied.

In this section, we also measured LV mRNA expression of AT1R. This gene well represents "the biological efficacy of Ang II". Ang II binds to AT1R and initiates a signal transduction cascade that increases hypertrophy(129). In our study, LV AT1R mRNA expression was not altered in the Ang II versus control.

In summary, changes in LV Myh7b and Acta1 mRNA expression together with the alterations in (micro)vascular density indicate that hypertrophy is more likely to be present in Ang II 1.1mg/kg 14d mice than in the other Ang II groups.

4.4. Inflammation

Inflammation is an essential part of the immune response that aims to resolve the source of the disturbance (infection or injury) and to maintain tissue homeostasis. The inflammatory response requires fine-tuning and precise regulation and should be limited by an anti-inflammatory response, which is fast, reversible, localized, flexible to changes, and integrated by the nervous system(130).

Inflammation triggers HF in its different aspects. Inflammation affects pathological substrates (endothelial dysfunction, atherosclerosis)(131), and comorbidities (diabetes and obesity)(132) underlying HF, and influences the progression and outcome of acute(133, 134) and chronic HF(135). Additionally, HF causes inflammation in various peripheral tissues in a direct (inflammatory) and indirect (hemodynamic) manner, as previously studied(103). HF is a complex syndrome as the ending of virtually all forms of cardiac disease. HF induces sterile inflammation in the heart itself via wall stress and signals released by malfunctioning, stressed, or dead cells secondary to HF(130).

Increased inflammation also happens in HFpEF. There is substantial evidence that inflammation and the processes related to it, such as oxidative stress and endothelial dysfunction, are not only activated in HFpEF but that they may also play a pathophysiologically important and causative role(136). In fact, a low-grade systemic inflammation has been proposed to be the initial trigger inducing cardiac remodeling associated with HFpEF(28, 137). The microvascular HFpEF paradigm was first proposed in 2013(137). According to the paradigm, a low-grade systemic inflammation induced by comorbidities triggers coronary microvascular inflammation and dysfunction, underlying the subsequent HFpEF-specific cardiac concentric remodeling(28, 137).

S100A8 and S100A9 belong to the S100A family and are directly linked to the innate immune system(108). Their proinflammatory activity includes recruitment of leukocytes, promotion of cytokine and chemokine production, and regulation of leukocyte adhesion and migration. S100A8/A9 aggravates post-ischemic HF through activation of RAGE-dependent NF-κB signaling(103, 138). S100A8 and S100A9 are involved in inflammatory cell migration and induce reactive oxygen species (ROS) production(139).

They are abundantly expressed in neutrophils and monocytes and are released during inflammatory conditions(108). TLRs and RAGE are important pattern recognition receptors for the recognition of endogenous danger-associated molecular patterns including the intracellular S100 proteins, heat shock protein, HMGB1, matricellular proteins, and mitochondrial DNA, released by the heart during HF. Stimulation of TLRs in cardiomyocytes initiates a NF-kB-dependent inflammatory response(140). In the mouse, S100A8/A9 has been documented to signal through RAGE to promote inflammation and fibrosis after Ang II or hypoxic-induced cardiac injury(141). Clinical evidence emphasizes that high levels of plasma S100A8/A9 are risk factors for future myocardial infarction and cardiovascular death in healthy individuals(142). Müller et al. reported that S100A8 and S100A9 mRNA levels showed a 13-fold (P=0.012) and 5.1-fold (P=0.038) increase in CVB3-positive patients versus controls, respectively. Additionally, they demonstrated that S100A8 and S100A9 aggravates CVB3-induced myocarditis(103). Raphael et al found that plasma levels of S100A8 were significantly higher in patients with HFpEF than in healthy controls(143). In our study, we found a trend in increased expression of LV S100A8, S100A9, TLR4, and RAGE in Ang II 1.1 mg/kg 14d mice versus control 1.1 mg/kg 14d mice, which is in support for a potential role of S1008 and S100A9 in these Ang II mice.

Cytokines are a broad category of small proteins, which have been shown to be involved in autocrine, paracrine and endocrine signaling, as immunomodulating agents(144, 145). Their relevance in various forms of HF is well documented. In 1996, the cytokine hypothesis was proposed to define the relationship between endogenous cytokines and the progression of HF(146). IL-10 is a primary anti-inflammatory cytokine. Hulsmans et al. demonstrate that cardiac-resident $MHCII_{high}$ macrophages have a pathogenic role in HFpEF through their IL-10 production(147). In our study, no change of IL-10 was seen across the three Ang II groups. IL-1β, IL-6, and TNF-α are pro-inflammatory cytokines that are crucial for host-defense responses to infection and injury(148). However, like IL-10, no differences were found in LV IL-1β, IL-6, and TNF-α mRNA expression between all three Ang II groups and their respective controls.

Chemokines are a family of small cytokines, or signaling proteins secreted by cells, and play a central role in the development and homeostasis of the immune system. They induce inflammatory cells mobilization and migration plays a crucial role in cardiac inflammation development(149). Chemokines comprise a large family functionally

divided into inflammatory chemokines and homeostatic chemokines. CCL2, CCL5 and CCL7 are chemokines attracting pro-inflammatory monocytes(105, 150, 151), whereas CX3CL1 and its specific receptor CX3CR1 have been shown to attract anti-inflammatory monocytes(105, 152, 153). Based on the data in our research, Ang II 0.2mg / kg 28d showed a decrease in CCL2, and Ang II 1.5mg/kg 14d displayed a decrease in both CCL2 and CX3CL1, while in Ang II 1.1mg/kg 14d mice, LV CX3CL1 mRNA was reduced. Evaluation of quantitative trait loci revealed CCL2 as a prime candidate for diastolic function(154). CCL2 function is mediated through its receptor CCR2. CCR2-dependent monocyte migration has been shown to contribute to cardiac macrophage expansion in mice with diastolic dysfunction(147), whereas inhibiting monocyte recruitment alone was not sufficient to prevent congestive heart failure. LV CCL2 decreased in the Ang II 1.5 mg/kg 14d and Ang II 0.2mg/kg 28d mice, but not in Ang II 1.1mg/kg 14d versus their respective controls. This finding in Ang II 1.1mg/kg 14d mice together with the lower observed LV expression of CX3CL1, known to attract anti-inflammatory monocytes(109), in Ang II 1.1mg/kg 14d suggests a more prominent increase in pro-inflammatory response in those mice.

Immunohistochemical evidence. All three Ang II groups exhibited a higher presence of CD4 cells compared to their controls, whereas only Ang II 1.5mg/kg 14d and Ang II 0.2mg / kg 28d mice displayed higher CD8a cells versus their respective controls. No differences were found in LV presence of CD68+ cells among the AngII and respective control mice, whereas LV presence of Ly6g cells was increased in Ang II 1.1mg/kg 14d mice. CD8a plays a vital role in the LV sterile immune circuit and is crucial to ventricular remodeling caused by pathological immune changes(155). Since CD4 cells display a greater negative impact on cardiac remodeling than CD8a(156), the higher deducted CD4 to CD8 ratio in Ang II 1.1mg/kg 14d compared to Ang II 1.5mg/kg 14d and Ang II 0.2mg / kg 28d mice might be indicative for a more pronounced cardiac remodeling in those mice. Karagöz et al.(157) demonstrated that higher grades of diastolic dysfunction were associated with a higher neutrophil to lymphocyte ratio. The neutrophil marker, Ly6g, was only increased in Ang II 1.1mg/kg 14d mice versus control mice further suggesting that Ang II 1.1mg/kg 14d mice might be the best of all 3 evaluated HFpEF models.

4.5. Summary

To date, there is no universally agreed guideline for identifying HFpEF models, but most researchers agree that normal LVEF, LV diastolic dysfunction, and cardiac hypertrophy are necessary for identifying HFpEF(60, 70, 72, 73, 158). Regan et al. 's report(73) suggested that the HFpEF model should have the following characteristics, 1) normal LVEF; 2) abnormal LV diastolic function; 3) cardiomyocyte hypertrophy; and 4) myocardial fibrosis. Valero-Muñoz's group(60) reported that the “ideal” criteria for identifying HFpEF should be 1) normal LVEF; 2) diastolic dysfunction (or exercise intolerance); 3) pulmonary edema; and 4) concentric cardiac hypertrophy.

In our study, Ang II 1.1 mg/kg 14d mice displayed a normal EF. Among all three studied Ang II groups, it exhibits the most severely impaired systolic and diastolic function, the most expressed cardiac fibrosis, and the most pronounced hypertrophy, and inflammatory response. It passes the initially necessary HFpEF identification criteria. Though, following the Valero-Muñoz’s identification criteria, more experiments are needed to verify whether our model is ideal, including the investigation of exercise intolerance and pulmonary edema. An exercise test can determine whether the animal has exercise intolerance and can better elucidate the presence of diastolic dysfunction(60). In early-stage or exercise intolerance HFpEF, frequently, symptoms of diastolic dysfunction occur only during exercise, as LV filling pressure is normal at rest, but increases with exercise(159). This implies that LV filling pressures should also be measured not only at rest but also during exercise. Given that, the diastolic stress tests, during exercise, will provide insights into cardiovascular hemodynamics(159). Recently, guidelines from the American Society of Echocardiography/European Association of Cardiovascular Imaging regarding the evaluation of LV diastolic function by echocardiography(160, 161) and clinical use of stress echocardiography in nonischemic heart disease included diastolic stress echocardiography as a valuable tool for the evaluation of patients with unexplained dyspnea and subclinical LV diastolic dysfunction(162, 163). Pulmonary edema examination may insure the animal of HF. In short, Valero-Muñoz's criteria can make sure the HFpEF model is more rigorous and ideal.

HFpEF is a complex syndrome in which the etiology and pathophysiological pathways of individual patients are variable(164). Any animal model may resemble only a certain proportion of patients with HFpEF. An "ideal" animal model should meet a variety of

requirements that mimic human disease, including cardiac, hemodynamic, neurohormonal, and peripheral aberrations common in HFpEF patients(92). However, the "one size fits all" strategy is unlikely to work in animal models. In the laboratory, a more tailored approach to specific phenotypes is needed to understand the complex interactions behind this disease. HFpEF in humans is closely related to diseases such as hypertension, obesity and diabetes(84). There is a lot of overlap between these comorbidities, and a direct causal relationship between each other and HFpEF has not yet been established. However, if this causality can be elucidated, it may be an important step towards creating a more “ideal” HFpEF animal model.

In conclusion, among the three studied groups of mice with different Ang II doses and durations, Ang II 1.1 mg/kg 14d mice have properties closest to the HFpEF prototype. However, further research is needed to establish an ideal HFpEF model, to understand the underlying mechanisms of HFpEF.

5. References

1. McMurray JJ, Pfeffer MA. Heart failure. Lancet. 2005;365(9474):1877-89.

2. Disease GBD, Injury I, Prevalence C. Global, regional, and national incidence, prevalence, and years lived with disability for 310 diseases and injuries, 1990-2015: a systematic analysis for the Global Burden of Disease Study 2015. Lancet. 2016;388(10053):1545-602.

3. Writing Group M, Mozaffarian D, Benjamin EJ, Go AS, Arnett DK, Blaha MJ, Cushman M, Das SR, de Ferranti S, Despres JP, Fullerton HJ, Howard VJ, Huffman MD, Isasi CR, Jimenez MC, Judd SE, Kissela BM, Lichtman JH, Lisabeth LD, Liu S, Mackey RH, Magid DJ, McGuire DK, Mohler ER, 3rd, Moy CS, Muntner P, Mussolino ME, Nasir K, Neumar RW, Nichol G, Palaniappan L, Pandey DK, Reeves MJ, Rodriguez CJ, Rosamond W, Sorlie PD, Stein J, Towfighi A, Turan TN, Virani SS, Woo D, Yeh RW, Turner MB, American Heart Association Statistics C, Stroke Statistics S. Heart Disease and Stroke Statistics-2016 Update: A Report From the American Heart Association. Circulation. 2016;133(4):e38-360.

4. Stromberg A, Martensson J. Gender differences in patients with heart failure. Eur J Cardiovasc Nurs. 2003;2(1):7-18.

5. Ponikowski P, Voors AA, Anker SD, Bueno H, Cleland JGF, Coats AJS, Falk V, Gonzalez-Juanatey JR, Harjola VP, Jankowska EA, Jessup M, Linde C, Nihoyannopoulos P, Parissis JT, Pieske B, Riley JP, Rosano GMC, Ruilope LM, Ruschitzka F, Rutten FH, van der Meer P, Group ESCSD. 2016 ESC Guidelines for the diagnosis and treatment of acute and chronic heart failure: The Task Force for the diagnosis and treatment of acute and chronic heart failure of the European Society of Cardiology (ESC)Developed with the special contribution of the Heart Failure Association (HFA) of the ESC. Eur Heart J. 2016;37(27):2129-200.

6. Savarese G, Lund LH. Global Public Health Burden of Heart Failure. Card Fail Rev. 2017;3(1):7-11.

7. Owan TE, Hodge DO, Herges RM, Jacobsen SJ, Roger VL, Redfield MM. Trends in prevalence and outcome of heart failure with preserved ejection fraction. N Engl J Med. 2006;355(3):251-9.

8. Kitzman DW, Gardin JM, Gottdiener JS, Arnold A, Boineau R, Aurigemma G, Marino EK, Lyles M, Cushman M, Enright PL, Cardiovascular Health Study Research G. Importance of heart failure with preserved systolic function in patients > or = 65 years of age. CHS Research Group. Cardiovascular Health Study. Am J Cardiol. 2001;87(4):413-9.

9. DeBerge M, Shah SJ, Wilsbacher L, Thorp EB. Macrophages in Heart Failure with Reduced versus Preserved Ejection Fraction. Trends Mol Med. 2019;25(4):328-40.

10. Amgalan D, Kitsis RN. A mouse model for the most common form of heart failure. Nature. 2019;568(7752):324-5.

11. Zile MR, Gaasch WH, Carroll JD, Feldman MD, Aurigemma GP, Schaer GL, Ghali JK, Liebson PR. Heart failure with a normal ejection fraction: is measurement of diastolic function necessary to make the diagnosis of diastolic heart failure? Circulation. 2001;104(7):779-82.

12. Borlaug BA, Lam CS, Roger VL, Rodeheffer RJ, Redfield MM. Contractility and ventricular systolic stiffening in hypertensive heart disease insights into the pathogenesis of heart failure with preserved ejection fraction. J Am Coll Cardiol. 2009;54(5):410-8.

13. Zile MR, Gottdiener JS, Hetzel SJ, McMurray JJ, Komajda M, McKelvie R, Baicu CF, Massie BM, Carson PE, Investigators IP. Prevalence and significance of alterations in cardiac structure and function in patients with heart failure and a preserved ejection fraction. Circulation. 2011;124(23):2491-501.

14. Aurigemma GP, Zile MR, Gaasch WH. Contractile behavior of the left ventricle in diastolic heart failure: with emphasis on regional systolic function. Circulation. 2006;113(2):296-304.

15. van Heerebeek L, Borbely A, Niessen HW, Bronzwaer JG, van der Velden J, Stienen GJ, Linke WA, Laarman GJ, Paulus WJ. Myocardial structure and function differ in systolic and diastolic heart failure. Circulation. 2006;113(16):1966-73.

16. Lam CS, Roger VL, Rodeheffer RJ, Bursi F, Borlaug BA, Ommen SR, Kass DA, Redfield MM. Cardiac structure and ventricular-vascular function in persons with heart failure and preserved ejection fraction from Olmsted County, Minnesota. Circulation. 2007;115(15):1982-90.

17. Borbely A, van der Velden J, Papp Z, Bronzwaer JG, Edes I, Stienen GJ, Paulus WJ. Cardiomyocyte stiffness in diastolic heart failure. Circulation. 2005;111(6):774-81.

18. Borlaug BA. The pathophysiology of heart failure with preserved ejection fraction. Nat Rev Cardiol. 2014;11(9):507-15.

19. Borlaug BA, Kass DA. Invasive hemodynamic assessment in heart failure. Cardiol Clin. 2011;29(2):269-80.

20. Zile MR, Baicu CF, Bonnema DD. Diastolic heart failure: definitions and terminology. Prog Cardiovasc Dis. 2005;47(5):307-13.

21. Borlaug BA, Redfield MM, Melenovsky V, Kane GC, Karon BL, Jacobsen SJ, Rodeheffer RJ. Longitudinal changes in left ventricular stiffness: a community-based study. Circ Heart Fail. 2013;6(5):944-52.

22. Ohara T, Niebel CL, Stewart KC, Charonko JJ, Pu M, Vlachos PP, Little WC. Loss of adrenergic augmentation of diastolic intra-LV pressure difference in patients with diastolic dysfunction: evaluation by color M-mode echocardiography. JACC Cardiovasc Imaging. 2012;5(9):861-70.

23. Borlaug BA, Jaber WA, Ommen SR, Lam CS, Redfield MM, Nishimura RA. Diastolic relaxation and compliance reserve during dynamic exercise in heart failure with preserved ejection fraction. Heart. 2011;97(12):964-9.

24. Westermann D, Kasner M, Steendijk P, Spillmann F, Riad A, Weitmann K, Hoffmann W, Poller W, Pauschinger M, Schultheiss HP, Tschope C. Role of left ventricular stiffness in heart failure with normal ejection fraction. Circulation. 2008;117(16):2051-60.

25. Linke WA, Hamdani N. Gigantic business: titin properties and function through thick and thin. Circ Res. 2014;114(6):1052-68.

26. Falcao-Pires I, Hamdani N, Borbely A, Gavina C, Schalkwijk CG, van der Velden J, van Heerebeek L, Stienen GJ, Niessen HW, Leite-Moreira AF, Paulus WJ. Diabetes mellitus worsens diastolic left ventricular dysfunction in aortic stenosis through altered myocardial structure and cardiomyocyte stiffness. Circulation. 2011;124(10):1151-9.

27. Tschope C, Van Linthout S. New insights in (inter)cellular mechanisms by heart failure with preserved ejection fraction. Curr Heart Fail Rep. 2014;11(4):436-44.

28. Camici PG, Tschope C, Di Carli MF, Rimoldi O, Van Linthout S. Coronary microvascular dysfunction in hypertrophy and heart failure. Cardiovasc Res. 2020;116(4):806-16.

29. Borlaug BA, Nishimura RA, Sorajja P, Lam CS, Redfield MM. Exercise hemodynamics enhance diagnosis of early heart failure with preserved ejection fraction. Circ Heart Fail. 2010;3(5):588-95.

30. Anjan VY, Loftus TM, Burke MA, Akhter N, Fonarow GC, Gheorghiade M, Shah SJ. Prevalence, clinical phenotype, and outcomes associated with normal B-type natriuretic peptide levels in heart failure with preserved ejection fraction. Am J Cardiol. 2012;110(6):870-6.

31. Abudiab MM, Redfield MM, Melenovsky V, Olson TP, Kass DA, Johnson BD, Borlaug BA. Cardiac output response to exercise in relation to metabolic demand in heart failure with preserved ejection fraction. Eur J Heart Fail. 2013;15(7):776-85.

32. Borlaug BA, Olson TP, Lam CS, Flood KS, Lerman A, Johnson BD, Redfield MM. Global cardiovascular reserve dysfunction in heart failure with preserved ejection fraction. J Am Coll Cardiol. 2010;56(11):845-54.

33. Abraham WT, Adamson PB, Bourge RC, Aaron MF, Costanzo MR, Stevenson LW, Strickland W, Neelagaru S, Raval N, Krueger S, Weiner S, Shavelle D, Jeffries B, Yadav JS, Group CTS. Wireless pulmonary artery haemodynamic monitoring in chronic heart failure: a randomised controlled trial. Lancet. 2011;377(9766):658-66.

34. Lam CS, Roger VL, Rodeheffer RJ, Borlaug BA, Enders FT, Redfield MM. Pulmonary hypertension in heart failure with preserved ejection fraction: a community-based study. J Am Coll Cardiol. 2009;53(13):1119-26.

35. Zile MR. Treating diastolic heart failure with statins: "phat" chance for pleiotropic benefits. Circulation. 2005;112(3):300-3.

36. Nikitin NP, Witte KK, Clark AL, Cleland JG. Color tissue Doppler-derived long-axis left ventricular function in heart failure with preserved global systolic function. Am J Cardiol. 2002;90(10):1174-7.

37. Shah AM, Claggett B, Folsom AR, Lutsey PL, Ballantyne CM, Heiss G, Solomon SD. Ideal Cardiovascular Health During Adult Life and Cardiovascular Structure and Function Among the Elderly. Circulation. 2015;132(21):1979-89.

38. Borlaug BA, Kane GC, Melenovsky V, Olson TP. Abnormal right ventricular-pulmonary artery coupling with exercise in heart failure with preserved ejection fraction. Eur Heart J. 2016;37(43):3293-302.

39. Yancy CW, Jessup M, Bozkurt B, Butler J, Casey DE, Jr., Drazner MH, Fonarow GC, Geraci SA, Horwich T, Januzzi JL, Johnson MR, Kasper EK, Levy WC, Masoudi FA, McBride PE, McMurray JJ, Mitchell JE, Peterson PN, Riegel B, Sam F, Stevenson LW, Tang WH, Tsai EJ, Wilkoff BL, American College of Cardiology F, American Heart Association Task Force on Practice G. 2013 ACCF/AHA guideline for the management of heart failure: a report of the American College of Cardiology Foundation/American Heart Association Task Force on Practice Guidelines. J Am Coll Cardiol. 2013;62(16):e147-239.

40. Huis In 't Veld AE, de Man FS, van Rossum AC, Handoko ML. How to diagnose heart failure with preserved ejection fraction: the value of invasive stress testing. Neth Heart J. 2016;24(4):244-51.

41. van Veldhuisen DJ, Linssen GC, Jaarsma T, van Gilst WH, Hoes AW, Tijssen JG, Paulus WJ, Voors AA, Hillege HL. B-type natriuretic peptide and prognosis in heart failure patients with preserved and reduced ejection fraction. J Am Coll Cardiol. 2013;61(14):1498-506.

42. Reddy YNV, Carter RE, Obokata M, Redfield MM, Borlaug BA. A Simple, Evidence-Based Approach to Help Guide Diagnosis of Heart Failure With Preserved Ejection Fraction. Circulation. 2018;138(9):861-70.

43. Pieske B, Tschope C, de Boer RA, Fraser AG, Anker SD, Donal E, Edelmann F, Fu M, Guazzi M, Lam CSP, Lancellotti P, Melenovsky V, Morris DA, Nagel E, Pieske-Kraigher E, Ponikowski P, Solomon SD, Vasan RS, Rutten FH, Voors AA, Ruschitzka F, Paulus WJ, Seferovic P, Filippatos G. How to diagnose heart failure with preserved ejection fraction: the HFA-PEFF diagnostic algorithm: a consensus recommendation from the Heart Failure Association (HFA) of the European Society of Cardiology (ESC). Eur Heart J. 2019;40(40):3297-317.

44. Pieske B, Tschope C, de Boer RA, Fraser AG, Anker SD, Donal E, Edelmann F, Fu M, Guazzi M, Lam CSP, Lancellotti P, Melenovsky V, Morris DA, Nagel E, Pieske-Kraigher E, Ponikowski P, Solomon SD, Vasan RS, Rutten FH, Voors AA, Ruschitzka F, Paulus WJ, Seferovic P, Filippatos G. How to diagnose heart failure with preserved ejection fraction: the HFA-PEFF diagnostic algorithm: a consensus recommendation from the Heart Failure Association (HFA) of the European Society of Cardiology (ESC). Eur J Heart Fail. 2020;22(3):391-412.

45. Sanchez-Martinez S, Duchateau N, Erdei T, Kunszt G, Aakhus S, Degiovanni A, Marino P, Carluccio E, Piella G, Fraser AG, Bijnens BH. Machine Learning Analysis of Left Ventricular Function to Characterize Heart Failure With Preserved Ejection Fraction. Circ Cardiovasc Imaging. 2018;11(4):e007138.

46. Omar AMS, Narula S, Abdel Rahman MA, Pedrizzetti G, Raslan H, Rifaie O, Narula J, Sengupta PP. Precision Phenotyping in Heart Failure and Pattern Clustering of Ultrasound Data for the Assessment of Diastolic Dysfunction. JACC Cardiovasc Imaging. 2017;10(11):1291-303.

47. Shah SJ, Katz DH, Selvaraj S, Burke MA, Yancy CW, Gheorghiade M, Bonow RO, Huang CC, Deo RC. Phenomapping for novel classification of heart failure with preserved ejection fraction. Circulation. 2015;131(3):269-79.

48. Mentz RJ, Kelly JP, von Lueder TG, Voors AA, Lam CS, Cowie MR, Kjeldsen K, Jankowska EA, Atar D, Butler J, Fiuzat M, Zannad F, Pitt B, O'Connor CM. Noncardiac comorbidities in heart failure with reduced versus preserved ejection fraction. J Am Coll Cardiol. 2014;64(21):2281-93.

49. Pitt B, Pfeffer MA, Assmann SF, Boineau R, Anand IS, Claggett B, Clausell N, Desai AS, Diaz R, Fleg JL, Gordeev I, Harty B, Heitner JF, Kenwood CT, Lewis EF, O'Meara E, Probstfield JL, Shaburishvili T, Shah SJ, Solomon SD, Sweitzer NK, Yang S, McKinlay SM, Investigators T. Spironolactone for heart failure with preserved ejection fraction. N Engl J Med. 2014;370(15):1383-92.

50. Kitzman DW, Brubaker PH, Morgan TM, Stewart KP, Little WC. Exercise training in older patients with heart failure and preserved ejection fraction: a randomized, controlled, single-blind trial. Circ Heart Fail. 2010;3(6):659-67.

51. Kitzman DW, Brubaker P, Morgan T, Haykowsky M, Hundley G, Kraus WE, Eggebeen J, Nicklas BJ. Effect of Caloric Restriction or Aerobic Exercise Training on Peak Oxygen Consumption and Quality of Life in Obese Older Patients With Heart Failure With Preserved Ejection Fraction: A Randomized Clinical Trial. JAMA. 2016;315(1):36-46.

52. Schwartzenberg S, Redfield MM, From AM, Sorajja P, Nishimura RA, Borlaug BA. Effects of vasodilation in heart failure with preserved or reduced ejection fraction implications of distinct pathophysiologies on response to therapy. J Am Coll Cardiol. 2012;59(5):442-51.

53. Cleland JGF, Bunting KV, Flather MD, Altman DG, Holmes J, Coats AJS, Manzano L, McMurray JJV, Ruschitzka F, van Veldhuisen DJ, von Lueder TG, Bohm M, Andersson B, Kjekshus J, Packer M, Rigby AS, Rosano G, Wedel H, Hjalmarson A, Wikstrand J, Kotecha D, Beta-blockers in Heart Failure Collaborative G. Beta-blockers for heart failure with reduced, mid-range, and preserved ejection fraction: an individual patient-level analysis of double-blind randomized trials. Eur Heart J. 2018;39(1):26-35.

54. Wassertheil-Smoller S, Oberman A, Blaufox MD, Davis B, Langford H. The Trial of Antihypertensive Interventions and Management (TAIM) Study. Final results with regard to blood pressure, cardiovascular risk, and quality of life. Am J Hypertens. 1992;5(1):37-44.

55. Redfield MM, Anstrom KJ, Levine JA, Koepp GA, Borlaug BA, Chen HH, LeWinter MM, Joseph SM, Shah SJ, Semigran MJ, Felker GM, Cole RT, Reeves GR, Tedford RJ, Tang WH, McNulty SE, Velazquez EJ, Shah MR, Braunwald E, Network NHFCR. Isosorbide Mononitrate in Heart Failure with Preserved Ejection Fraction. N Engl J Med. 2015;373(24):2314-24.

56. Redfield MM, Chen HH, Borlaug BA, Semigran MJ, Lee KL, Lewis G, LeWinter MM, Rouleau JL, Bull DA, Mann DL, Deswal A, Stevenson LW, Givertz MM, Ofili EO, O'Connor CM, Felker GM, Goldsmith SR, Bart BA, McNulty SE, Ibarra JC, Lin G, Oh JK, Patel MR, Kim RJ, Tracy RP, Velazquez EJ, Anstrom KJ, Hernandez AF, Mascette AM, Braunwald E, Trial R. Effect of phosphodiesterase-5 inhibition on exercise capacity and clinical status in heart failure with preserved ejection fraction: a randomized clinical trial. JAMA. 2013;309(12):1268-77.

57. Hoendermis ES, Liu LC, Hummel YM, van der Meer P, de Boer RA, Berger RM, van Veldhuisen DJ, Voors AA. Effects of sildenafil on invasive haemodynamics and exercise capacity in heart failure patients with preserved ejection fraction and pulmonary hypertension: a randomized controlled trial. Eur Heart J. 2015;36(38):2565-73.

58. Ahmed A, Rich MW, Fleg JL, Zile MR, Young JB, Kitzman DW, Love TE, Aronow WS, Adams KF, Jr., Gheorghiade M. Effects of digoxin on morbidity and mortality in diastolic heart failure: the ancillary digitalis investigation group trial. Circulation. 2006;114(5):397-403.

59. Meta-analysis Global Group in Chronic Heart F. The survival of patients with heart failure with preserved or reduced left ventricular ejection fraction: an individual patient data meta-analysis. Eur Heart J. 2012;33(14):1750-7.

60. Valero-Munoz M, Backman W, Sam F. Murine Models of Heart Failure with Preserved Ejection Fraction: a "Fishing Expedition". JACC Basic Transl Sci. 2017;2(6):770-89.

61. Dai DF, Rabinovitch PS. Cardiac aging in mice and humans: the role of mitochondrial oxidative stress. Trends Cardiovasc Med. 2009;19(7):213-20.

62. Lakatta EG. Arterial and cardiac aging: major shareholders in cardiovascular disease enterprises: Part III: cellular and molecular clues to heart and arterial aging. Circulation. 2003;107(3):490-7.

63. Mitchell SJ, Scheibye-Knudsen M, Longo DL, de Cabo R. Animal models of aging research: implications for human aging and age-related diseases. Annu Rev Anim Biosci. 2015;3:283-303.

64. Horgan S, Watson C, Glezeva N, Baugh J. Murine models of diastolic dysfunction and heart failure with preserved ejection fraction. J Card Fail. 2014;20(12):984-95.

65. Samson R, Jaiswal A, Ennezat PV, Cassidy M, Le Jemtel TH. Clinical Phenotypes in Heart Failure With Preserved Ejection Fraction. J Am Heart Assoc. 2016;5(1).

66. Group SR, Wright JT, Jr., Williamson JD, Whelton PK, Snyder JK, Sink KM, Rocco MV, Reboussin DM, Rahman M, Oparil S, Lewis CE, Kimmel PL, Johnson KC, Goff DC, Jr., Fine LJ, Cutler JA, Cushman WC, Cheung AK, Ambrosius WT. A Randomized Trial of Intensive versus Standard Blood-Pressure Control. N Engl J Med. 2015;373(22):2103-16.

67. Benjamin EJ, Blaha MJ, Chiuve SE, Cushman M, Das SR, Deo R, de Ferranti SD, Floyd J, Fornage M, Gillespie C, Isasi CR, Jimenez MC, Jordan LC, Judd SE, Lackland D, Lichtman JH, Lisabeth L, Liu S, Longenecker CT, Mackey RH, Matsushita K, Mozaffarian D, Mussolino ME, Nasir K, Neumar RW, Palaniappan L, Pandey DK, Thiagarajan RR, Reeves MJ, Ritchey M, Rodriguez CJ, Roth GA, Rosamond WD, Sasson C, Towfighi A, Tsao CW, Turner MB, Virani SS, Voeks JH, Willey JZ, Wilkins JT, Wu JH, Alger HM, Wong SS, Muntner P, American Heart Association Statistics C, Stroke Statistics S. Heart Disease and Stroke Statistics-2017 Update: A Report From the American Heart Association. Circulation. 2017;135(10):e146-e603.

68. Adams V, Alves M, Fischer T, Rolim N, Werner S, Schutt N, Bowen TS, Linke A, Schuler G, Wisloff U. High-intensity interval training attenuates endothelial dysfunction in a Dahl salt-sensitive rat model of heart failure with preserved ejection fraction. J Appl Physiol (1985). 2015;119(6):745-52.

69. Zile MR, Baicu CF, Ikonomidis JS, Stroud RE, Nietert PJ, Bradshaw AD, Slater R, Palmer BM, Van Buren P, Meyer M, Redfield MM, Bull DA, Granzier HL, LeWinter MM. Myocardial stiffness in patients with heart failure and a preserved ejection fraction: contributions of collagen and titin. Circulation. 2015;131(14):1247-59.

70. Murdoch CE, Chaubey S, Zeng L, Yu B, Ivetic A, Walker SJ, Vanhoutte D, Heymans S, Grieve DJ, Cave AC, Brewer AC, Zhang M, Shah AM. Endothelial NADPH oxidase-2 promotes interstitial cardiac fibrosis and diastolic dysfunction through proinflammatory effects and endothelial-mesenchymal transition. J Am Coll Cardiol. 2014;63(24):2734-41.

71. Glenn DJ, Cardema MC, Ni W, Zhang Y, Yeghiazarians Y, Grapov D, Fiehn O, Gardner DG. Cardiac steatosis potentiates angiotensin II effects in the heart. Am J Physiol Heart Circ Physiol. 2015;308(4):H339-50.

72. Shen Y, Cheng F, Sharma M, Merkulova Y, Raithatha SA, Parkinson LG, Zhao H, Westendorf K, Bohunek L, Bozin T, Hsu I, Ang LS, Williams SJ, Bleackley RC, Eriksson JE, Seidman MA, McManus BM, Granville DJ. Granzyme B Deficiency Protects against Angiotensin II-Induced Cardiac Fibrosis. Am J Pathol. 2016;186(1):87-100.

73. Regan JA, Mauro AG, Carbone S, Marchetti C, Gill R, Mezzaroma E, Valle Raleigh J, Salloum FN, Van Tassell BW, Abbate A, Toldo S. A mouse model of heart failure with preserved ejection fraction due to chronic infusion of a low subpressor dose of angiotensin II. Am J Physiol Heart Circ Physiol. 2015;309(5):H771-8.

74. Mori J, Alrob OA, Wagg CS, Harris RA, Lopaschuk GD, Oudit GY. ANG II causes insulin resistance and induces cardiac metabolic switch and inefficiency: a critical role of PDK4. Am J Physiol Heart Circ Physiol. 2013;304(8):H1103-13.

75. Westermann D, Becher PM, Lindner D, Savvatis K, Xia Y, Frohlich M, Hoffmann S, Schultheiss HP, Tschope C. Selective PDE5A inhibition with sildenafil rescues left ventricular dysfunction, inflammatory immune response and cardiac remodeling in angiotensin II-induced heart failure in vivo. Basic Res Cardiol. 2012;107(6):308.

76. Essick EE, Wilson RM, Pimentel DR, Shimano M, Baid S, Ouchi N, Sam F. Adiponectin modulates oxidative stress-induced autophagy in cardiomyocytes. PLoS One. 2013;8(7):e68697.

77. Kamimura D, Ohtani T, Sakata Y, Mano T, Takeda Y, Tamaki S, Omori Y, Tsukamoto Y, Furutani K, Komiyama Y, Yoshika M, Takahashi H, Matsuda T, Baba A, Umemura S, Miwa T,

Komuro I, Yamamoto K. Ca2+ entry mode of Na+/Ca2+ exchanger as a new therapeutic target for heart failure with preserved ejection fraction. Eur Heart J. 2012;33(11):1408-16.

78. Conceicao G, Heinonen I, Lourenco AP, Duncker DJ, Falcao-Pires I. Animal models of heart failure with preserved ejection fraction. Neth Heart J. 2016;24(4):275-86.

79. Ogata T, Miyauchi T, Sakai S, Takanashi M, Irukayama-Tomobe Y, Yamaguchi I. Myocardial fibrosis and diastolic dysfunction in deoxycorticosterone acetate-salt hypertensive rats is ameliorated by the peroxisome proliferator-activated receptor-alpha activator fenofibrate, partly by suppressing inflammatory responses associated with the nuclear factor-kappa-B pathway. J Am Coll Cardiol. 2004;43(8):1481-8.

80. Willard PW. A model for evaluation of thiazide-induced hypotension. J Pharm Pharmacol. 1969;21(6):406-8.

81. Bowen TS, Eisenkolb S, Drobner J, Fischer T, Werner S, Linke A, Mangner N, Schuler G, Adams V. High-intensity interval training prevents oxidant-mediated diaphragm muscle weakness in hypertensive mice. FASEB J. 2017;31(1):60-71.

82. Folkow B. Early structural changes in hypertension: pathophysiology and clinical consequences. J Cardiovasc Pharmacol. 1993;22 Suppl 1:S1-6.

83. Rockman HA, Ross RS, Harris AN, Knowlton KU, Steinhelper ME, Field LJ, Ross J, Jr., Chien KR. Segregation of atrial-specific and inducible expression of an atrial natriuretic factor transgene in an in vivo murine model of cardiac hypertrophy. Proc Natl Acad Sci U S A. 1991;88(18):8277-81.

84. Shah SJ, Kitzman DW, Borlaug BA, van Heerebeek L, Zile MR, Kass DA, Paulus WJ. Phenotype-Specific Treatment of Heart Failure With Preserved Ejection Fraction: A Multiorgan Roadmap. Circulation. 2016;134(1):73-90.

85. de las Fuentes L, Waggoner AD, Mohammed BS, Stein RI, Miller BV, 3rd, Foster GD, Wyatt HR, Klein S, Davila-Roman VG. Effect of moderate diet-induced weight loss and weight regain on cardiovascular structure and function. J Am Coll Cardiol. 2009;54(25):2376-81.

86. Nanayakkara S, Kaye DM. Management of heart failure with preserved ejection fraction: a review. Clin Ther. 2015;37(10):2186-98.

87. Triposkiadis F, Giamouzis G, Parissis J, Starling RC, Boudoulas H, Skoularigis J, Butler J, Filippatos G. Reframing the association and significance of co-morbidities in heart failure. Eur J Heart Fail. 2016;18(7):744-58.

88. Scherbakov N, Bauer M, Sandek A, Szabo T, Topper A, Jankowska EA, Springer J, von Haehling S, Anker SD, Lainscak M, Engeli S, Dungen HD, Doehner W. Insulin resistance in

heart failure: differences between patients with reduced and preserved left ventricular ejection fraction. Eur J Heart Fail. 2015;17(10):1015-21.

89. Hamdani N, Franssen C, Lourenco A, Falcao-Pires I, Fontoura D, Leite S, Plettig L, Lopez B, Ottenheijm CA, Becher PM, Gonzalez A, Tschope C, Diez J, Linke WA, Leite-Moreira AF, Paulus WJ. Myocardial titin hypophosphorylation importantly contributes to heart failure with preserved ejection fraction in a rat metabolic risk model. Circ Heart Fail. 2013;6(6):1239-49.

90. Schiattarella GG, Altamirano F, Tong D, French KM, Villalobos E, Kim SY, Luo X, Jiang N, May HI, Wang ZV, Hill TM, Mammen PPA, Huang J, Lee DI, Hahn VS, Sharma K, Kass DA, Lavandero S, Gillette TG, Hill JA. Nitrosative stress drives heart failure with preserved ejection fraction. Nature. 2019;568(7752):351-6.

91. Vermond RA, Geelhoed B, Verweij N, Tieleman RG, Van der Harst P, Hillege HL, Van Gilst WH, Van Gelder IC, Rienstra M. Incidence of Atrial Fibrillation and Relationship With Cardiovascular Events, Heart Failure, and Mortality: A Community-Based Study From the Netherlands. J Am Coll Cardiol. 2015;66(9):1000-7.

92. Halapas A, Papalois A, Stauropoulou A, Philippou A, Pissimissis N, Chatzigeorgiou A, Kamper E, Koutsilieris M. In vivo models for heart failure research. In Vivo. 2008;22(6):767-80.

93. Riley G, Syeda F, Kirchhof P, Fabritz L. An introduction to murine models of atrial fibrillation. Front Physiol. 2012;3:296.

94. Thenappan T, Shah SJ, Gomberg-Maitland M, Collander B, Vallakati A, Shroff P, Rich S. Clinical characteristics of pulmonary hypertension in patients with heart failure and preserved ejection fraction. Circ Heart Fail. 2011;4(3):257-65.

95. Waxman AB. Pulmonary hypertension in heart failure with preserved ejection fraction: a target for therapy? Circulation. 2011;124(2):133-5.

96. Maarman G, Lecour S, Butrous G, Thienemann F, Sliwa K. A comprehensive review: the evolution of animal models in pulmonary hypertension research; are we there yet? Pulm Circ. 2013;3(4):739-56.

97. Mori J, Basu R, McLean BA, Das SK, Zhang L, Patel VB, Wagg CS, Kassiri Z, Lopaschuk GD, Oudit GY. Agonist-induced hypertrophy and diastolic dysfunction are associated with selective reduction in glucose oxidation: a metabolic contribution to heart failure with normal ejection fraction. Circ Heart Fail. 2012;5(4):493-503.

98. Curl CL, Danes VR, Bell JR, Raaijmakers AJA, Ip WTK, Chandramouli C, Harding TW, Porrello ER, Erickson JR, Charchar FJ, Kompa AR, Edgley AJ, Crossman DJ, Soeller C, Mellor KM, Kalman JM, Harrap SB, Delbridge LMD. Cardiomyocyte Functional Etiology in Heart

Failure With Preserved Ejection Fraction Is Distinctive-A New Preclinical Model. J Am Heart Assoc. 2018;7(11).

99. Penicka M, Bartunek J, Trakalova H, Hrabakova H, Maruskova M, Karasek J, Kocka V. Heart failure with preserved ejection fraction in outpatients with unexplained dyspnea: a pressure-volume loop analysis. J Am Coll Cardiol. 2010;55(16):1701-10.

100. Plitt GD, Spring JT, Moulton MJ, Agrawal DK. Mechanisms, diagnosis, and treatment of heart failure with preserved ejection fraction and diastolic dysfunction. Expert Rev Cardiovasc Ther. 2018;16(8):579-89.

101. Bai X, Wang Q. Time constants of cardiac function and their calculations. Open Cardiovasc Med J. 2010;4:168-72.

102. Pacher P, Nagayama T, Mukhopadhyay P, Batkai S, Kass DA. Measurement of cardiac function using pressure-volume conductance catheter technique in mice and rats. Nat Protoc. 2008;3(9):1422-34.

103. Muller I, Vogl T, Pappritz K, Miteva K, Savvatis K, Rohde D, Most P, Lassner D, Pieske B, Kuhl U, Van Linthout S, Tschope C. Pathogenic Role of the Damage-Associated Molecular Patterns S100A8 and S100A9 in Coxsackievirus B3-Induced Myocarditis. Circ Heart Fail. 2017;10(11).

104. Radonic A, Thulke S, Mackay IM, Landt O, Siegert W, Nitsche A. Guideline to reference gene selection for quantitative real-time PCR. Biochem Biophys Res Commun. 2004;313(4):856-62.

105. Pappritz K, Savvatis K, Koschel A, Miteva K, Tschope C, Van Linthout S. Cardiac (myo)fibroblasts modulate the migration of monocyte subsets. Sci Rep. 2018;8(1):5575.

106. Nagamoto T, Eguchi G, Beebe DC. Alpha-smooth muscle actin expression in cultured lens epithelial cells. Invest Ophthalmol Vis Sci. 2000;41(5):1122-9.

107. Miteva K, Van Linthout S, Pappritz K, Muller I, Spillmann F, Haag M, Stachelscheid H, Ringe J, Sittinger M, Tschope C. Human Endomyocardial Biopsy Specimen-Derived Stromal Cells Modulate Angiotensin II-Induced Cardiac Remodeling. Stem Cells Transl Med. 2016;5(12):1707-18.

108. Ehrchen JM, Sunderkotter C, Foell D, Vogl T, Roth J. The endogenous Toll-like receptor 4 agonist S100A8/S100A9 (calprotectin) as innate amplifier of infection, autoimmunity, and cancer. J Leukoc Biol. 2009;86(3):557-66.

109. Borlaug BA, Paulus WJ. Heart failure with preserved ejection fraction: pathophysiology, diagnosis, and treatment. Eur Heart J. 2011;32(6):670-9.

110. Tschope C, Van Linthout S, Kherad B. Heart Failure with Preserved Ejection Fraction and Future Pharmacological Strategies: a Glance in the Crystal Ball. Curr Cardiol Rep. 2017;19(8):70.

111. Kiper C, Grimes B, Van Zant G, Satin J. Mouse strain determines cardiac growth potential. PLoS One. 2013;8(8):e70512.

112. Zhao W, Zhao T, Chen Y, Bhattacharya SK, Lu L, Sun Y. Differential Expression of Hypertensive Phenotypes in BXD Mouse Strains in Response to Angiotensin II. Am J Hypertens. 2017;31(1):108-14.

113. Rabin BS, Lyte M, Hamill E. The influence of mouse strain and housing on the immune response. J Neuroimmunol. 1987;17(1):11-6.

114. Laber K, Veatch LM, Lopez MF, Mulligan JK, Lathers DM. Effects of housing density on weight gain, immune function, behavior, and plasma corticosterone concentrations in BALB/c and C57BL/6 mice. J Am Assoc Lab Anim Sci. 2008;47(2):16-23.

115. Weber KT. Cardiac interstitium in health and disease: the fibrillar collagen network. J Am Coll Cardiol. 1989;13(7):1637-52.

116. Jugdutt BI. Ventricular remodeling after infarction and the extracellular collagen matrix: when is enough enough? Circulation. 2003;108(11):1395-403.

117. Kasner M, Westermann D, Lopez B, Gaub R, Escher F, Kuhl U, Schultheiss HP, Tschope C. Diastolic tissue Doppler indexes correlate with the degree of collagen expression and cross-linking in heart failure and normal ejection fraction. J Am Coll Cardiol. 2011;57(8):977-85.

118. Mohammed SF, Hussain S, Mirzoyev SA, Edwards WD, Maleszewski JJ, Redfield MM. Coronary microvascular rarefaction and myocardial fibrosis in heart failure with preserved ejection fraction. Circulation. 2015;131(6):550-9.

119. Ma ZG, Yuan YP, Wu HM, Zhang X, Tang QZ. Cardiac fibrosis: new insights into the pathogenesis. Int J Biol Sci. 2018;14(12):1645-57.

120. Desmouliere A, Geinoz A, Gabbiani F, Gabbiani G. Transforming growth factor-beta 1 induces alpha-smooth muscle actin expression in granulation tissue myofibroblasts and in quiescent and growing cultured fibroblasts. J Cell Biol. 1993;122(1):103-11.

121. Van Linthout S, Seeland U, Riad A, Eckhardt O, Hohl M, Dhayat N, Richter U, Fischer JW, Bohm M, Pauschinger M, Schultheiss HP, Tschope C. Reduced MMP-2 activity contributes to cardiac fibrosis in experimental diabetic cardiomyopathy. Basic Res Cardiol. 2008;103(4):319-27.

122. Heinzel FR, Hohendanner F, Jin G, Sedej S, Edelmann F. Myocardial hypertrophy and its role in heart failure with preserved ejection fraction. J Appl Physiol (1985). 2015;119(10):1233-42.

123. Peter AK, Rossi AC, Buvoli M, Ozeroff CD, Crocini C, Perry AR, Buvoli AE, Lee LA, Leinwand LA. Expression of Normally Repressed Myosin Heavy Chain 7b in the Mammalian Heart Induces Dilated Cardiomyopathy. J Am Heart Assoc. 2019;8(15):e013318.

124. Warkman AS, Whitman SA, Miller MK, Garriock RJ, Schwach CM, Gregorio CC, Krieg PA. Developmental expression and cardiac transcriptional regulation of Myh7b, a third myosin heavy chain in the vertebrate heart. Cytoskeleton (Hoboken). 2012;69(5):324-35.

125. Chen P, Li Z, Nie J, Wang H, Yu B, Wen Z, Sun Y, Shi X, Jin L, Wang DW. MYH7B variants cause hypertrophic cardiomyopathy by activating the CaMK-signaling pathway. Sci China Life Sci. 2020;63(9):1-16.

126. Stenzig J, Hirt MN, Loser A, Bartholdt LM, Hensel JT, Werner TR, Riemenschneider M, Indenbirken D, Guenther T, Muller C, Hubner N, Stoll M, Eschenhagen T. DNA methylation in an engineered heart tissue model of cardiac hypertrophy: common signatures and effects of DNA methylation inhibitors. Basic Res Cardiol. 2016;111(1):9.

127. Voelkl J, Castor T, Musculus K, Viereck R, Mia S, Feger M, Alesutan I, Lang F. SGK1-Sensitive Regulation of Cyclin-Dependent Kinase Inhibitor 1B (p27) in Cardiomyocyte Hypertrophy. Cell Physiol Biochem. 2015;37(2):603-14.

128. Crea F, Bairey Merz CN, Beltrame JF, Kaski JC, Ogawa H, Ong P, Sechtem U, Shimokawa H, Camici PG, Coronary Vasomotion Disorders International Study G. The parallel tales of microvascular angina and heart failure with preserved ejection fraction: a paradigm shift. Eur Heart J. 2017;38(7):473-7.

129. Ferrario CM. Cardiac remodelling and RAS inhibition. Ther Adv Cardiovasc Dis. 2016;10(3):162-71.

130. Van Linthout S, Tschope C. The Quest for Antiinflammatory and Immunomodulatory Strategies in Heart Failure. Clin Pharmacol Ther. 2019;106(6):1198-208.

131. Spillmann F, Van Linthout S, Miteva K, Lorenz M, Stangl V, Schultheiss HP, Tschope C. LXR agonism improves TNF-alpha-induced endothelial dysfunction in the absence of its cholesterol-modulating effects. Atherosclerosis. 2014;232(1):1-9.

132. Tall AR, Yvan-Charvet L. Cholesterol, inflammation and innate immunity. Nat Rev Immunol. 2015;15(2):104-16.

133. Lazzerini PE, Capecchi PL, Laghi-Pasini F. Systemic inflammation and arrhythmic risk: lessons from rheumatoid arthritis. Eur Heart J. 2017;38(22):1717-27.

134. Odeberg J, Freitag M, Forssell H, Vaara I, Persson ML, Odeberg H, Halling A, Rastam L, Lindblad U. Influence of pre-existing inflammation on the outcome of acute coronary syndrome: a cross-sectional study. BMJ Open. 2016;6(1):e009968.

135. Kindermann I, Kindermann M, Kandolf R, Klingel K, Bultmann B, Muller T, Lindinger A, Bohm M. Predictors of outcome in patients with suspected myocarditis. Circulation. 2008;118(6):639-48.

136. van Empel V, Brunner-La Rocca HP. Inflammation in HFpEF: Key or circumstantial? Int J Cardiol. 2015;189:259-63.

137. Paulus WJ, Tschope C. A novel paradigm for heart failure with preserved ejection fraction: comorbidities drive myocardial dysfunction and remodeling through coronary microvascular endothelial inflammation. J Am Coll Cardiol. 2013;62(4):263-71.

138. Volz HC, Laohachewin D, Seidel C, Lasitschka F, Keilbach K, Wienbrandt AR, Andrassy J, Bierhaus A, Kaya Z, Katus HA, Andrassy M. S100A8/A9 aggravates post-ischemic heart failure through activation of RAGE-dependent NF-kappaB signaling. Basic Res Cardiol. 2012;107(2):250.

139. Kerkhoff C, Nacken W, Benedyk M, Dagher MC, Sopalla C, Doussiere J. The arachidonic acid-binding protein S100A8/A9 promotes NADPH oxidase activation by interaction with p67phox and Rac-2. FASEB J. 2005;19(3):467-9.

140. Van Linthout S, Tschope C. Inflammation - Cause or Consequence of Heart Failure or Both? Curr Heart Fail Rep. 2017;14(4):251-65.

141. Tour O, Adams SR, Kerr RA, Meijer RM, Sejnowski TJ, Tsien RW, Tsien RY. Calcium Green FlAsH as a genetically targeted small-molecule calcium indicator. Nat Chem Biol. 2007;3(7):423-31.

142. Cotoi OS, Duner P, Ko N, Hedblad B, Nilsson J, Bjorkbacka H, Schiopu A. Plasma S100A8/A9 correlates with blood neutrophil counts, traditional risk factors, and cardiovascular disease in middle-aged healthy individuals. Arterioscler Thromb Vasc Biol. 2014;34(1):202-10.

143. Raphael R, Purushotham D, Gastonguay C, Chesnik MA, Kwok WM, Wu HE, Shah SJ, Mirza SP, Strande JL. Combining patient proteomics and in vitro cardiomyocyte phenotype testing to identify potential mediators of heart failure with preserved ejection fraction. J Transl Med. 2016;14:18.

144. Reche PA. The tertiary structure of gammac cytokines dictates receptor sharing. Cytokine. 2019;116:161-8.

145. Rozwarski DA, Gronenborn AM, Clore GM, Bazan JF, Bohm A, Wlodawer A, Hatada M, Karplus PA. Structural comparisons among the short-chain helical cytokines. Structure. 1994;2(3):159-73.

146. Seta Y, Shan K, Bozkurt B, Oral H, Mann DL. Basic mechanisms in heart failure: the cytokine hypothesis. J Card Fail. 1996;2(3):243-9.

147. Hulsmans M, Sager HB, Roh JD, Valero-Munoz M, Houstis NE, Iwamoto Y, Sun Y, Wilson RM, Wojtkiewicz G, Tricot B, Osborne MT, Hung J, Vinegoni C, Naxerova K, Sosnovik DE, Zile MR, Bradshaw AD, Liao R, Tawakol A, Weissleder R, Rosenzweig A, Swirski FK, Sam F, Nahrendorf M. Cardiac macrophages promote diastolic dysfunction. J Exp Med. 2018;215(2):423-40.

148. Dinarello CA. Biologic basis for interleukin-1 in disease. Blood. 1996;87(6):2095-147.

149. Frangogiannis NG, Entman ML. Targeting the chemokines in myocardial inflammation. Circulation. 2004;110(11):1341-2.

150. Palomino DC, Marti LC. Chemokines and immunity. Einstein (Sao Paulo, Brazil). 2015;13(3):469-73.

151. Batista AM, Alvarado-Arnez LE, Alves SM, Melo G, Pereira IR, Ruivo LAS, da Silva AA, Gibaldi D, da Silva T, de Lorena VMB, de Melo AS, de Araujo Soares AK, Barros MDS, Costa VMA, Cardoso CC, Pacheco AG, Carrazzone C, Oliveira W, Jr., Moraes MO, Lannes-Vieira J. Genetic Polymorphism at CCL5 Is Associated With Protection in Chagas' Heart Disease: Antagonistic Participation of CCR1(+) and CCR5(+) Cells in Chronic Chagasic Cardiomyopathy. Front Immunol. 2018;9:615.

152. Escher F, Vetter R, Kuhl U, Westermann D, Schultheiss HP, Tschope C. Fractalkine in human inflammatory cardiomyopathy. Heart (British Cardiac Society). 2011;97(9):733-9.

153. Husberg C, Nygard S, Finsen AV, Damas JK, Frigessi A, Oie E, Waehre A, Gullestad L, Aukrust P, Yndestad A, Christensen G. Cytokine expression profiling of the myocardium reveals a role for CX3CL1 (fractalkine) in heart failure. J Mol Cell Cardiol. 2008;45(2):261-9.

154. Chauvet C, Crespo K, Shi Y, Gelinas D, Duval F, L'Heureux N, Nattel S, Tardif JC, Deng AY. Unique quantitative trait loci in synergy permanently improve diastolic dysfunction. Can J Cardiol. 2013;29(10):1302-9.

155. Ma F, Feng J, Zhang C, Li Y, Qi G, Li H, Wu Y, Fu Y, Zhao Y, Chen H, Du J, Tang H. The requirement of CD8+ T cells to initiate and augment acute cardiac inflammatory response to high blood pressure. J Immunol. 2014;192(7):3365-73.

156. Tae Yu H, Youn JC, Lee J, Park S, Chi HS, Lee J, Choi C, Park S, Choi D, Ha JW, Shin EC. Characterization of CD8(+)CD57(+) T cells in patients with acute myocardial infarction. Cell Mol Immunol. 2015;12(4):466-73.

157. Karagoz A, Vural A, Gunaydin ZY, Bektas O, Gul M, Celik A, Uzunoglu E, Usta S, Saritas A, Elalmis OU. The role of neutrophil to lymphocyte ratio as a predictor of diastolic dysfunction in hypertensive patients. Eur Rev Med Pharmacol Sci. 2015;19(3):433-40.

158. Becher PM, Lindner D, Miteva K, Savvatis K, Zietsch C, Schmack B, Van Linthout S, Westermann D, Schultheiss HP, Tschope C. Role of heart rate reduction in the prevention of experimental heart failure: comparison between If-channel blockade and beta-receptor blockade. Hypertension. 2012;59(5):949-57.

159. Ha JW, Andersen OS, Smiseth OA. Diastolic Stress Test: Invasive and Noninvasive Testing. JACC Cardiovasc Imaging. 2020;13(1 Pt 2):272-82.

160. Nagueh SF, Smiseth OA, Appleton CP, Byrd BF, 3rd, Dokainish H, Edvardsen T, Flachskampf FA, Gillebert TC, Klein AL, Lancellotti P, Marino P, Oh JK, Alexandru Popescu B, Waggoner AD, Houston T, Oslo N, Phoenix A, Nashville T, Hamilton OC, Uppsala S, Ghent, Liege B, Cleveland O, Novara I, Rochester M, Bucharest R, St. Louis M. Recommendations for the Evaluation of Left Ventricular Diastolic Function by Echocardiography: An Update from the American Society of Echocardiography and the European Association of Cardiovascular Imaging. Eur Heart J Cardiovasc Imaging. 2016;17(12):1321-60.

161. Nagueh SF, Smiseth OA, Appleton CP, Byrd BF, 3rd, Dokainish H, Edvardsen T, Flachskampf FA, Gillebert TC, Klein AL, Lancellotti P, Marino P, Oh JK, Popescu BA, Waggoner AD. Recommendations for the Evaluation of Left Ventricular Diastolic Function by Echocardiography: An Update from the American Society of Echocardiography and the European Association of Cardiovascular Imaging. J Am Soc Echocardiogr. 2016;29(4):277-314.

162. Lancellotti P, Pellikka PA, Budts W, Chaudhry FA, Donal E, Dulgheru R, Edvardsen T, Garbi M, Ha JW, Kane GC, Kreeger J, Mertens L, Pibarot P, Picano E, Ryan T, Tsutsui JM, Varga A. The Clinical Use of Stress Echocardiography in Non-Ischaemic Heart Disease: Recommendations from the European Association of Cardiovascular Imaging and the American Society of Echocardiography. J Am Soc Echocardiogr. 2017;30(2):101-38.

163. Lancellotti P, Pellikka PA, Budts W, Chaudhry FA, Donal E, Dulgheru R, Edvardsen T, Garbi M, Ha JW, Kane GC, Kreeger J, Mertens L, Pibarot P, Picano E, Ryan T, Tsutsui JM,

Varga A. The clinical use of stress echocardiography in non-ischaemic heart disease: recommendations from the European Association of Cardiovascular Imaging and the American Society of Echocardiography. Eur Heart J Cardiovasc Imaging. 2016;17(11):1191-229.

164. Shah SJ. Matchmaking for the optimization of clinical trials of heart failure with preserved ejection fraction: no laughing matter. J Am Coll Cardiol. 2013;62(15):1339-42.

Eidesstattliche Versicherung

„Ich, **Chao Ma**, versichere an Eides statt durch meine eigenhändige Unterschrift, dass ich die vorgelegte Dissertation mit dem Thema: **Evaluation of mouse models of heart failure with preserved ejection fraction** selbstständig und ohne nicht offengelegte Hilfe Dritter verfasst und keine anderen als die angegebenen Quellen und Hilfsmittel genutzt habe.

Alle Stellen, die wörtlich oder dem Sinne nach auf Publikationen oder Vorträgen anderer Autoren/innen beruhen, sind als solche in korrekter Zitierung kenntlich gemacht. Die Abschnitte zu Methodik (insbesondere praktische Arbeiten, Laborbestimmungen, statistische Aufarbeitung) und Resultaten (insbesondere Abbildungen, Graphiken und Tabellen) werden von mir verantwortet.

Meine Anteile an etwaigen Publikationen zu dieser Dissertation entsprechen denen, die in der untenstehenden gemeinsamen Erklärung mit dem/der Erstbetreuer/in, angegeben sind. Für sämtliche im Rahmen der Dissertation entstandenen Publikationen wurden die Richtlinien des ICMJE (International Committee of Medical Journal Editors; www.icmje.og) zur Autorenschaft eingehalten. Ich erkläre ferner, dass ich mich zur Einhaltung der Satzung der Charité – Universitätsmedizin Berlin zur Sicherung Guter Wissenschaftlicher Praxis verpflichte.

Weiterhin versichere ich, dass ich diese Dissertation weder in gleicher noch in ähnlicher Form bereits an einer anderen Fakultät eingereicht habe.

Die Bedeutung dieser eidesstattlichen Versicherung und die strafrechtlichen Folgen einer unwahren eidesstattlichen Versicherung (§§156, 161 des Strafgesetzbuches) sind mir bekannt und bewusst.“

Datum Unterschrift:

Curriculum vitae

My curriculum vitae does not appear in the electronic version of my paper for reasons of data protection.

My curriculum vitae does not appear in the electronic version of my paper for reasons of data protection.

Publikationsliste

1. **Ma C**, Luo H, Liu B, Li F, Tschöpe C, Fa X. Long noncoding RNA s: A new player in the prevention and treatment of diabetic cardiomyopathy. Diabetes/metabolism research and reviews. 2018 Nov;34(8): e3056.

Acknowledgments

I want to express my heartfelt thanks to my supervisor, Prof. Dr. Carsten Tschöpe, for offering the great opportunity studying in Germany.

I want to extend my sincere gratitude to PD Dipl. Ing. Sophie Van Linthout, PhD, who guided me over my whole study period, inspired me to go bravely, when I was most vulnerable, and gave valuable comments helping to improve the quality of the present research.

I deeply appreciate the selfless assistance from Dr. rer. nat. Dipl.-Pharm. Kathleen Pappritz, Dr. rer. nat. Irene Müller, Dr. rer. nat. Dipl.-Biol. Muhammad El-Shafeey, Dr. Jie Lin, Dr. Fengquan Dong, Dr. Gang Huang, and Ahmed Elsanhoury throughout my entire research phase in Germany.

I am all grateful for the technical assistance provided by Kerstin Puhl, Dipl.-Ing. Annika Koschel, and Marzena Sosnowski.

Words cannot describe how thankful I am for my wife Huan Luo's accompany. I am genuinely grateful to my whole family supporting and encouraging me.

Finally, thanks to the China Scholarship Council (No. 201708410121), whose financial help allows me to complete my overseas research work smoothly and timely.